atmosphere

MDPI

Review

Carbon Dioxide Capture through Physical and Chemical Adsorption Using Porous Carbon Materials: A Review

Oneesha H. P. Gunawardene [1], Chamila A. Gunathilake [1,2,*], Kumar Vikrant [3] and Sumedha M. Amaraweera [4]

[1] Department of Chemical and Process Engineering, Faculty of Engineering, University of Peradeniya, Peradeniya 20400, Sri Lanka; hishendri1995@gmail.com
[2] Department of Nano Science Technology, Faculty of Technology, Wayamba University of Sri Lanka, Kuliyapitiya 60200, Sri Lanka
[3] Department of Civil and Environmental Engineering, Hanyang University, Seoul 04763, Korea; vikrant23@hanyang.ac.kr
[4] Department of Manufacturing and Industrial Engineering, Faculty of Engineering, University of Peradeniya, Peradeniya 20400, Sri Lanka; sumedha.sma@gmail.com
* Correspondence: chamila@wyb.ac.lk; Tel.: +94-777-651-127

Abstract: Due to rapid industrialization and urban development across the globe, the emission of carbon dioxide (CO_2) has been significantly increased, resulting in adverse effects on the climate and ecosystems. In this regard, carbon capture and storage (CCS) is considered to be a promising technology in reducing atmospheric CO_2 concentration. Among the CO_2 capture technologies, adsorption has grabbed significant attention owing to its advantageous characteristics discovered in recent years. Porous carbon-based materials have emerged as one of the most versatile CO_2 adsorbents. Numerous research activities have been conducted by synthesizing carbon-based adsorbents using different precursors to investigate their performances towards CCS. Additionally, amine-functionalized carbon-based adsorbents have exhibited remarkable potential for selective capturing of CO_2 in the presence of other gases and humidity conditions. The present review describes the CO_2 emission sources, health, and environmental impacts of CO_2 towards the human beings, options for CCS, and different CO_2 separation technologies. Apart from the above, different synthesis routes of carbon-based adsorbents using various precursors have been elucidated. The CO_2 adsorption selectivity, capacity, and reusability of the current and applied carbon materials have also been summarized. Furthermore, the critical factors controlling the adsorption performance (e.g., the effect of textural and functional properties) are comprehensively discussed. Finally, the current challenges and future research directions have also been summarized.

Keywords: porous carbon; amine functionalization; physisorption; chemisorption; CO_2 capture

check for updates

Citation: Gunawardene, O.H.P.; Gunathilake, C.A.; Vikrant, K.; Amaraweera, S.M. Carbon Dioxide Capture through Physical and Chemical Adsorption Using Porous Carbon Materials: A Review. *Atmosphere* **2022**, *13*, 397. https://doi.org/10.3390/atmos13030397

Academic Editor: Daiqi Ye

Received: 9 February 2022
Accepted: 24 February 2022
Published: 28 February 2022

1. Introduction

1.1. Physical and Chemical Properties of CO_2

Carbon dioxide (CO_2) is a triatomic gas under ambient conditions [1], which is abundant, non-toxic, recyclable, and economical [2]. Moreover, CO_2 sublimates from solid-state to gas at −78 °C under atmospheric pressure and is comparatively inert. As a commonly known fact, CO_2 gas that naturally occurs in the Earth's atmosphere is of paramount importance to photosynthesis [1]. From an economic point of view, CO_2 can be converted into high-value chemical products such as urea, carbonates, and acrylates [3] through catalytic conversion, mineralization, photochemical, or electrochemical reactions, and supercritical CO_2 can be also utilized in various industrial fields, including food beverages, refrigerants, transportation fuels, fire extinguishers, polymer synthesis, medical, and exploitation of heavy oil. Solid-state CO_2 can be used in artificial rainfall and concrete production [4,5].

1.2. Trend of Atmospheric CO_2 Concentration and Potential CO_2 Emissions Sources

Although the natural carbon cycle controls the CO_2 concentration level in the Earth's atmosphere [1], due to both anthropogenic activities and natural emissions, the current atmospheric CO_2 concentration reached around 416.5 ppm in mid-2020 [6], which is ~40% greater than the beginning of the industrial revolution (280 ppm) in 1750 [7–9], with an average growth rate of 2 ppm per year [9,10]. In other words, the global emission of CO_2 was estimated to be more than 36 MT in 2017, which is 18-fold greater than compared to the 1800s [11]. Although it is a consensus that the amount of atmospheric CO_2 should not exceed 350 ppm [12], according to the predictions by the International Panel on Climate Change (IPCC), it is expected to reach up to 570 ppm by 2100 [12–14]. It is identified that the main causes for the tremendous increase in such atmospheric CO_2 concentration are mainly associated with various anthropogenic activities, including vehicular emissions, fossil-fuel power plants, deforestation, chemical processes [15], and waste treatment [16], which have been growing steadily due to rapid industrialization and urban development [15,17]. The natural emission sources, including soil degradation processes and volcanic activities, are also responsible for supplying atmospheric CO_2 to some extent [18].

Figure 1 depicts the CO_2 emission sources across the globe with their percentage contributions. According to Figure 1, the emission of CO_2 is inevitable due to the rapid growth of the chemical, food, electronic, paper and pulp [19], and cement [17] industries, petroleum refineries, and metal/mineral production owing to fossil fuel combustion [20–22], which accounts for more than one-third of the worldwide CO_2 emission in the 40–70 °C range [23]. On the contrary, though natural gas (NG) is considered a clean energy source, high-pressure NG wells act as significant CO_2 emitters when vented into the atmosphere after gas purification [15,24,25]. Biogas upgradation also releases CO_2 into the atmosphere [25]. Nevertheless, according to the report from Pacific Institutes, bottling water plants also acted as CO_2 emission sources to pump more than 2.5 million MT of CO_2 in 2006 [6].

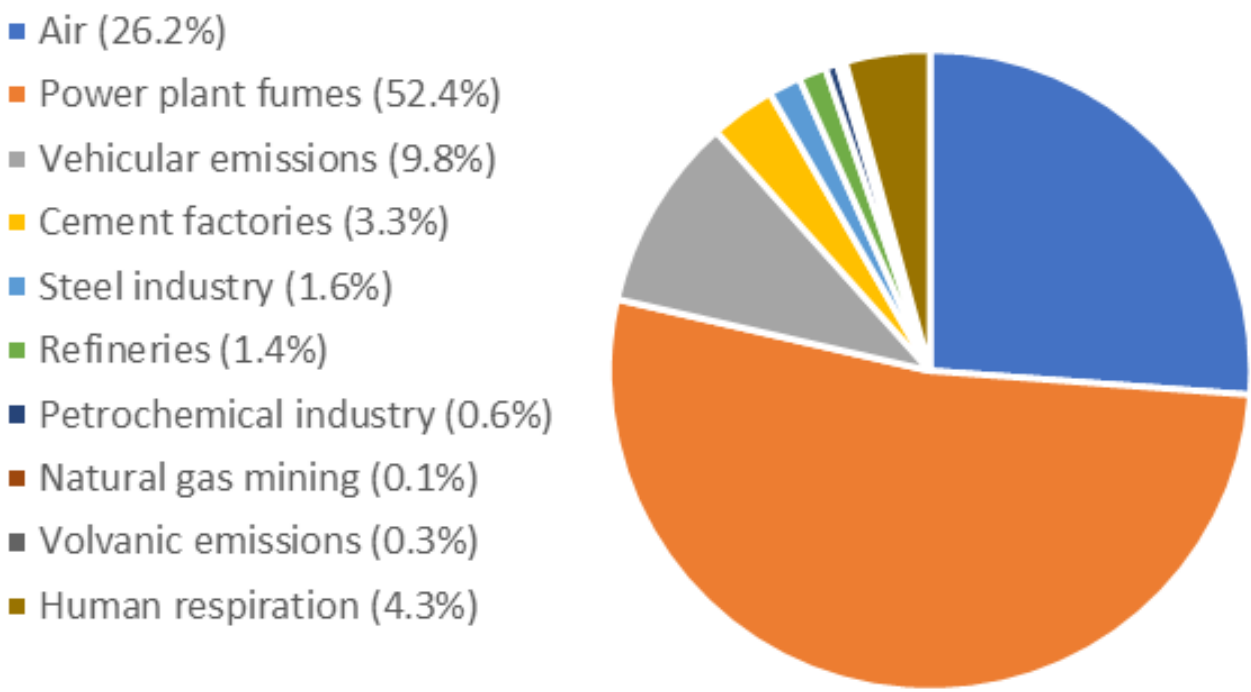

Figure 1. Contribution from different CO_2 emission sources towards the atmosphere across the globe (Reprinted with permission from ref. [26]).

1.3. Significant Outcomes Owing to the Trend of Increasing CO_2 Emissions

Unfortunately, the non-controllable anthropogenic activities have negatively affected human beings [27] and the entire ecosystem [3,6] by releasing greenhouse gases, including

CO_2, into the atmosphere. Among the greenhouse gases, CO_2 is considered as one of the primary sources, contributing to roughly 64% of the total greenhouse effect [14,28]. The progressive increase in atmospheric CO_2 concentration is responsible for climate change, which might adversely impact the global environmental processes, such as the long-term rise in global temperatures, changes in rainfall patterns, rising sea levels [29,30], ocean acidification [20], species extinction, melting of polar ice [9], shrinkage of snow covers [31], and severe weather events, ranging from flash floods [32], hurricanes, freezing winters, severe droughts [30], heat waves [33], urban smog [17], and cold streaks [34]. According to the predictions made by IPCC, the rise in sea level of 3.8 m [14,35] and rise in mean global temperature by 3.7 °C [36,37] are expected by 2100 [31]. Besides, the increasing trend of CO_2 in the air might cause various air-borne diseases, which will increase the risk of health complications [38]. The economic loss due to climate change is expected to be 5–20% of the global domestic production [12,35]. Therefore, extensive research projects are currently underway to reduce and control CO_2 emissions from power plants, industries, and transportation [39].

1.4. Approaches to Reduce Atmospheric CO_2 Concentration

Three feasible strategies to reduce CO_2 emissions are exhibited by the modified Kaya identity as expressed in equation (1) [35]. They are namely, (i) improving the energy efficiency of coal-fired plants [40,41], (ii) change of the fossil fuels to renewable and carbon-free energy resources [42], and (iii) utilization of carbon capture and storage (CCS) technologies [35,43,44].

$$CD = P\frac{GDP}{P}\frac{E}{GDP}\frac{C}{E} - S_{CO_2} \quad (1)$$

where CD: CO_2 emissions, P: Population, GDP: economic development in gross domestic production, E: energy production, C: carbon-based fuels used for energy production, and S_{CO2}: CO_2 sinks [35].

Apart from the above-mentioned three strategies, enhancing partial pressure in exhaust gas [43], geoengineering approaches including afforestation and reforestation [45], flue gas separation, and carbon mineralization [46] can also be considered. Among the different CO_2 mitigation options, IPCC has suggested CCS as a promising technology for achieving a 19% reduction of global CO_2 emissions by 2050 [41]. CCS can reduce CO_2 emissions (typically 85–90%) from significant stationary point sources such as power plants, cement kilns, and NG wells [25,47]. Nevertheless, CCS is considered a mid-term solution in reducing global warming, climate change, and simultaneously allowing humans to continue using fossil fuels until a renewable and clean energy source is discovered to replace them [41]. CCS is comprised of three significant steps, namely, (i) capture of emitted CO_2 from power plants and industrial processing without releasing them into the atmosphere, (ii) transportation of the captured and compressed CO_2, and (iii) underground storage of the captured CO_2 [33,48,49]. However, the process of CO_2 capture, which accounts for 70–80% of the total cost, has proven to be the major barrier for the deployment of CCS [25,50]. Interestingly, in recent years, carbon capture storage and utilization (CCSU) has grabbed significant attention compared to CCS owing to the convertibility of the captured CO_2 into commercial products [51,52]. The success of CCS and CCSU technologies are associated with the CO_2 adsorption efficiency, ease of handling, manufacturing cost, and renderability of the associated materials [30].

1.5. CO_2 Emission Sources

The CO_2 emission sources are the primary candidates for potential applications of CCS or CCSU technologies. Therefore, from a community and industrial point of view, CO_2 capture from typical gas streams, including flue gas, biogas, flare gas, syngas, and ambient air, has grabbed significant interest [53]. Table 1 depicts the summary of the compositions of different gas streams. According to Table 1, in all gas mentioned above, CO_2 is present

as an impurity in concentrations varying by about 35% in NG fired flue gas streams to about 38% in biogas, and thus, selective CO_2 capture from these sources could significantly reduce the CO_2 emissions and atmospheric CO_2 concentration [54]. Even though there has been a tremendous increase in the production of NG as a clean energy source [55], the presence of CO_2 in these gas streams notably reduces the heating value of NG. It causes corrosion problems in the transportation and storage systems [56,57], and hence the CCS or CCSU techniques are required on-site [58,59] to meet the gas quality before distribution [60]. Besides, low concentration CO_2 capture from confined spaces (<0.5%) [61] and CO_2 capture from atmospheric air, usually referred to as direct air capture from concentrated industrial sources, is of paramount importance in reducing the atmospheric CO_2 concentration [62].

Table 1. Compositions of different gas streams which act as potential CO_2 capture opportunities (Reprinted with permission from ref. [53,63]).

Component	Cement Rotary Kiln	Dry Atmospheric Air	Biogas Generated from Waste Water Treatment Plant Sludge	Natural Gas Fired Flue Gas	Coal-Fired Flue Gas
N_2	59 vol %	70 vol %	0–1 vol %	73–80 vol %	70–80 vol %
CO_2	19 vol %	410 ppm	19–33 vol %	3–8 vol %	11–15 vol %
H_2O	13 vol %	-	-	7–14.6 vol %	5–12 vol %
O_2	7 vol %	21 vol %	<0.5 vol %	4.5–15 vol %	3–6 vol %
SO_2	5–1200 ppm	-	-	<10 ppm	200–4000 ppm
SO_3	-	-	-	-	0–20 ppm
NO_X	100–1500 ppm	-	-	50–70 ppm	200–800 ppm
CO	-	-	-	-	50–100 ppm
H_2	-	0.5 vol %	-	5–300 ppm	5–20 g/m^3
Particulate matter	-	-	-	-	-
H_2S	-	-	100–4000 ppm	-	-
Ar	-	0.9 vol %	-	-	-
Xe	-	0.1 vol %	-	-	-
Ne	-	18 ppm	-	-	-
He	-	5.2 ppm	-	-	-
CH_4	-	1.6 vol %	60–75 vol %	-	-
Kr	-	1.1 vol %	-	-	-
N_2O	-	0.3 vol %	-	-	-

1.6. CO_2 Capture Technologies

Table 2 depicts the comparison of the leading carbon capture technologies. According to Table 2, carbon capture from power plants in industries can be classified as (i) pre-combustion capture, (ii) oxy-fuel combustion, and (iii) post-combustion capture [64] depending on the combustion method and composition of the gas stream [65]. The working conditions such as pressure and temperature differ for each technique [66]. The main factors impacting CO_2 capture efficiency are the gas composition, gas stream temperature, and energy penalty associated with regeneration [35].

Table 2. Comparison of the three main carbon capture technologies.

CO_2 Capture Technology	Advantages	Disadvantages
Pre-combustion capture	• The concentration of CO_2 produced within these processes range from ~15–60% which makes it easy to capture [66]	• When applying to new power plants, the technology is not yet commercialized and requires a high capital investment due to major alternatives to be done into boiler and flue gas systems [35] • Process of gasification and water gas shift reactions are expensive and quite challenging [66] • High energy penalty associated with regeneration of chemical solvents [67]
Oxy-fuel combustion	• Avoids the requirement of chemicals or other means of CO_2 separation from flue gas [67]	• Large energy penalty requirement for providing pure oxygen [68] • Absence of complete preparation methods [69] • Pure oxygen is expensive [67] • Limited knowledge regarding the technology [68] • Environmental impacts associated are higher due to energy intensive air separation process [67]
Post-combustion capture	• Readily applicable for large-scale in newly built and existing power plants without upgrading and reconstruction [70] • Repairing does not discontinue the procedure of the entire power plant and it can be regulated or managed easily [71] • Shorter time required for creation [72]	• Requirement of huge energy supplies for sorbent regeneration [68] • Requires the separation of impurities from captured CO_2 [73] • CO_2 in the flue gas is diluted with a concentration ranging from 10–15% which requires high recovery and capital costs and 25–35% additional energy for plant operation [35]

1.6.1. Pre-Combustion Capture

Pre-combustion capture is the technology used for capturing CO_2 before the combustion process. Pre-combustion capture could also refer to the capture of CO_2 generated as an undesired co-product of a process reaction [66]. Pre-combustion capture of CO_2 is widely utilized in integrated gasification combined cycles (IGCC) power plants to separate CO_2 from hydrogen (H_2) and carbon monoxide (CO) [74]. Besides, CO_2 should be removed during ammonia (NH_3) synthesis, which is produced as a co-product with H_2 during steam reforming. The pre-combustion technologies can be applied to power plants, fertilizer production plants, and NG wells [35,66].

1.6.2. Oxy-Fuel Capture

Oxy-fuel combustion involves the burning of a fuel in pure oxygen (O_2) environment to produce an effluent with high CO_2 concentration and free from nitrogen (N_2) and its compounds such as nitric oxide (NO) and nitrogen dioxide (NO_2). Oxy-fuel combustion can only be applied to fossil fuel power plants, cement, iron, and steel industries [75].

1.6.3. Post-Combustion Capture

Post-conversion capture, also known as post-combustion capture, involves separating CO_2 from waste gas streams after converting the carbon source to CO_2 [67]. According to Table 2, the post-combustion capture is considered to be the most promising near-term potential strategy [25] for CO_2 emission reduction since it can be applied to both the

existing and newly designed power stations, petrochemical and gas industries, biogas sweetening plants, ethylene oxide production plants, cement industries, fuel, iron, and steel industries [17,47,76]. Interestingly, Sask Power (Canada), which captures 1,000,000 MT of CO_2/year, and TMC Mongstad (Norway), which is capable of capturing 300,000 MT of CO_2/year, are examples for the applications of post-combustion capture technology [77].

1.7. Available CO_2 Sequestration Methods

CCS or CCSU is deployed for the sequestration of CO_2 by reducing the carbon footprint while simultaneously providing increased energy efficiency [78]. Of the CCS technologies mentioned above, CO_2 is separated from combustion flue gases in post-combustion capture by employing absorption, membrane technology, cryogenic distillation, micro-algal separation, chemical looping combustion, and hydrate-based separation [17,20,66]. Among the available CO_2 separation technologies, chemical looping combustion and hydrate-based separation technologies are still underdeveloped, with no large-scale operation experiences being available to date [67]. The cryogenic distillation process is associated with a considerable energy penalty. At the same time, micro-algal separation is inefficient due to the high sensitivity of microalgae to environmental conditions and gas stream impurities [68]. Moreover, membrane technology also faces problems associated with membrane regeneration, low purity of separated compounds, low fluxes, and frequent fouling [67]. The absorption approach utilizing liquid amine-based solvents (typically thirty hydro amines) [13,24], including ethanolamine, diethanolamine, diglycolamine, and monoethanolamine, has attracted widespread industrial attention [25,51] due to its high efficiency for capturing CO_2 through chemical reactions [59]. CO_2 absorption using amine-based solvents produces carbamate as the end product [79]. The amine-based absorption process has been extensively used since the 1970s, and it is considered a 1st generation technology for carbon capture [80]. Compared to the conventional CO_2 separation using amine-based solvents, separation of CO_2 via adsorption by solid materials is a more sustainable technology [81]. It is now widely adaptable due to its simplicity and effectiveness [82].

Table 3 demonstrates the comparison between the conventional amine-based CO_2 absorption and proposed adsorption processes. According to Table 3, ~30% of the energy produced from power plants is usually wasted for the regeneration of amine solvents which consumes 85 KJ/mol CO_2 while leading to a ~25% reduction of the overall energy production in the plant [78,83,84]. Interestingly, it is reported that the heat requirement for regeneration of amine solvents can be reduced by ~40% if the amine-based absorption is replaced by adsorption by solid materials [78]. Therefore, as can be seen from Table 3, adsorption of CO_2 using porous solid materials is an effective state-of-the-art technology for replacing the amine-based absorption process [46].

Table 3. Advantages and disadvantages of adsorption process and amine-based absorption processes.

Separation Technology	Advantages	Disadvantages
Adsorption using solid sorbents (proposed)	• Low energy conditions due to mild operation and easy regeneration [13,85] • Produces CO_2 streams with high purity with minimal pressure drop [68] • Applicability over a wide range of pressures and temperatures [68] • Low capital investment [81] • Easiness of scaling up [85] • No unfavorable byproducts [85]	• Low gas selectivity without surface modification [68] • Loss of sorption capacity over multiple cycles [68]

Table 3. *Cont.*

Separation Technology	Advantages	Disadvantages
Amine-based absorption (Liquid amine) (current)	• High absorption efficiency (>90%) [67] • Considered to be the most mature process [80] • High selectivity [2]	• High energy penalty associated with solvent regeneration [24,86] • Corrosive nature of amine solvents which reduces the service life of process equipment [32] • Flow problems caused by viscosity [87] • Secondary contaminations [88] • Production of hazardous wastes and byproducts [58] • Huge space requirement [89–91] • High operational cost [92] • Solvent loss due to amine degradation [15,93] • Exhibits low chemical stability and selectivity towards CO_2 in the presence of oxidizing gases such as NO_2, SO_2, and NO_X [94,95]

Several review articles have been published recently about CO_2 capture using carbon-based adsorption [33,66,68,86,95–98], along with research papers regarding the utilization of amine-functionalized carbon-based adsorbents for CO_2 capture [53,88,99]. Recent advances have prompted the present review on the adsorption of CO_2 onto different carbon-based solid adsorbents studied. The major contributions of the present review are to provide information regarding the CO_2 adsorption capacities by variety of carbon-based adsorbents derived from graphene, biomass, biopolymers, synthetic resins, synthetic polymers, fossil resources, and amine-functionalized carbons, along with their reusability, and gas selectivity. Finally, the technical challenges and practical implications that would hamper the implementation of carbon capture using porous carbons and the future research directions that might be beneficial in overcoming the possible challenges are also discussed in detail.

2. Solid Adsorbents for CO_2 Capture

2.1. Adsorption Process of CO_2

Adsorption is a surface phenomenon that highly depends on surface properties and functionalities [65]. Adsorption of CO_2 onto a material occurs through different types of interactions between the gas molecules and the adsorbent. Adsorption can be classified as (i) physisorption or (ii) chemisorption [100]. CO_2 adsorption is an exothermic process as reported elsewhere [92,101]. Figure 2 presents the schematic of the two adsorption processes, while Table 4 tabulates the differences between physisorption and chemisorption.

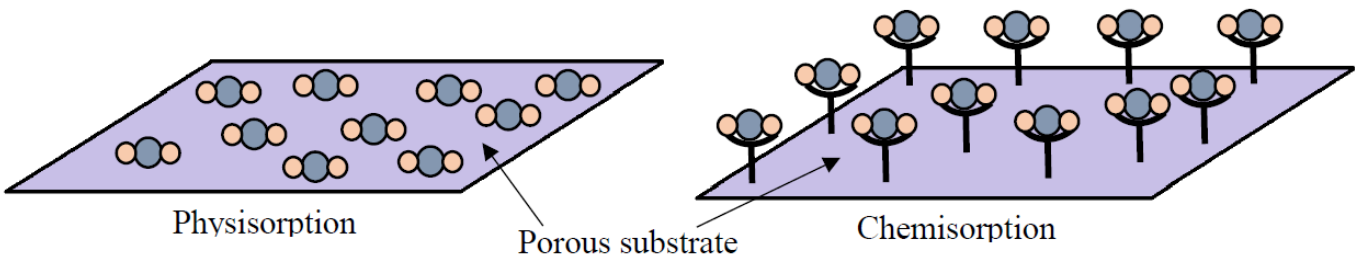

Figure 2. Schematic of the interactions between gas molecules and the adsorbent surface during physisorption and chemisorption (Reprinted with permission from ref. [26]).

Table 4. Comparison of the CO_2 physisorption and chemisorption processes.

Process	Advantages	Disadvantages
Physisorption	• More appropriate for high pressure applications [102] • Adsorbent is easily regenerated, and low energy is required for desorption [10] • Relatively stable even past 200 °C [10] • Low cost for adsorbent preparation [103]	• CO_2 capture capacity decreases with increasing temperature [15,104] • Low CO_2 uptake at low pressures [53] • Low CO_2 selectivity for combustion flue gas streams [48] • Adsorption capacity decreases in the presence of water [26]
Chemisorption	• High selectivity towards CO_2 due to strong interactions between basic species on the adsorbent surface and the acidic CO_2 molecule [48,105] • High adsorption capacity at low CO_2 partial pressures such as in the ambient air [48,106,107] • Enhanced adsorption capacity in the presence of water [103,108] • Comparatively higher mechanical stability [51]	• Slower than the physisorption process [109] • Functionalization of porous materials with amine groups decreases the CO_2 capture capacity due to pore blockage [105,110] • High energy requirement for regeneration of the adsorbent [99] • Low cyclic stability due to amine degradation [105]. Higher cost associated with adsorbent synthesis [103] • Chemisorbents can permanently bind to gases such as SO_2 to decrease the capacity of active sites for CO_2 capture [99] • Grafted amines volatilize and degrade above 120 °C due to instability at higher temperatures [99] • A corrosive environment could be produced during the regeneration of spent adsorbent due to the presence of amine groups [100]

2.1.1. Physisorption of CO_2 onto Adsorbents

During physisorption, the CO_2 molecules attach to the pore walls of the adsorbent primarily through the Van der Waals [111] and pole–pole interactions, as depicted in Figure 3 [112]. It is considered that the heat of adsorption values for the physisorption process is in the range of −25 to −40 kJ/mol [6], which is close to the heat of sublimation [99]. Physisorption is reversible where the adsorption and desorption of the gas molecules can be achieved under the influence of temperature and pressure [100]. The CO_2 adsorption at ambient temperature is primarily governed by physisorption [113], and the gas uptake is directly related to the porous texture of the adsorbent surface [114]. It has been reported that the narrow micropores (0.33–1 nm) are primarily responsible for the CO_2 adsorption performance [25]. However, the appropriate micropore size for CO_2 adsorption is highly dependent on the adsorption temperature and pressure [25].

2.1.2. Chemisorption of CO_2 onto Adsorbents

As shown in Table 4, to overcome the poor gas selectivity for CO_2 in physisorbents, chemical grafting or coating is widely performed on the surface of the porous materials by incorporating basic groups that effectively interact with the acidic CO_2 gas molecules [99,112,115]. Among different basic groups, the amine is a commonly used functionality for the surface modification of CO_2 adsorbents [111]. The CO_2 gas molecule forms a chemical bond with the adsorption sites in chemisorption, as demonstrated in Figure 2 [99]. Usually, CO_2 adsorption at elevated temperatures (above 140 °C) is primarily governed by chemisorption [94,113]. Both chemisorption and physisorption can occur in the temperature range of 25–140 °C. The heat of adsorption for chemisorbents can vary between −60 to −100 kJ/mol depending on the chemical functionality and bonding nature [99].

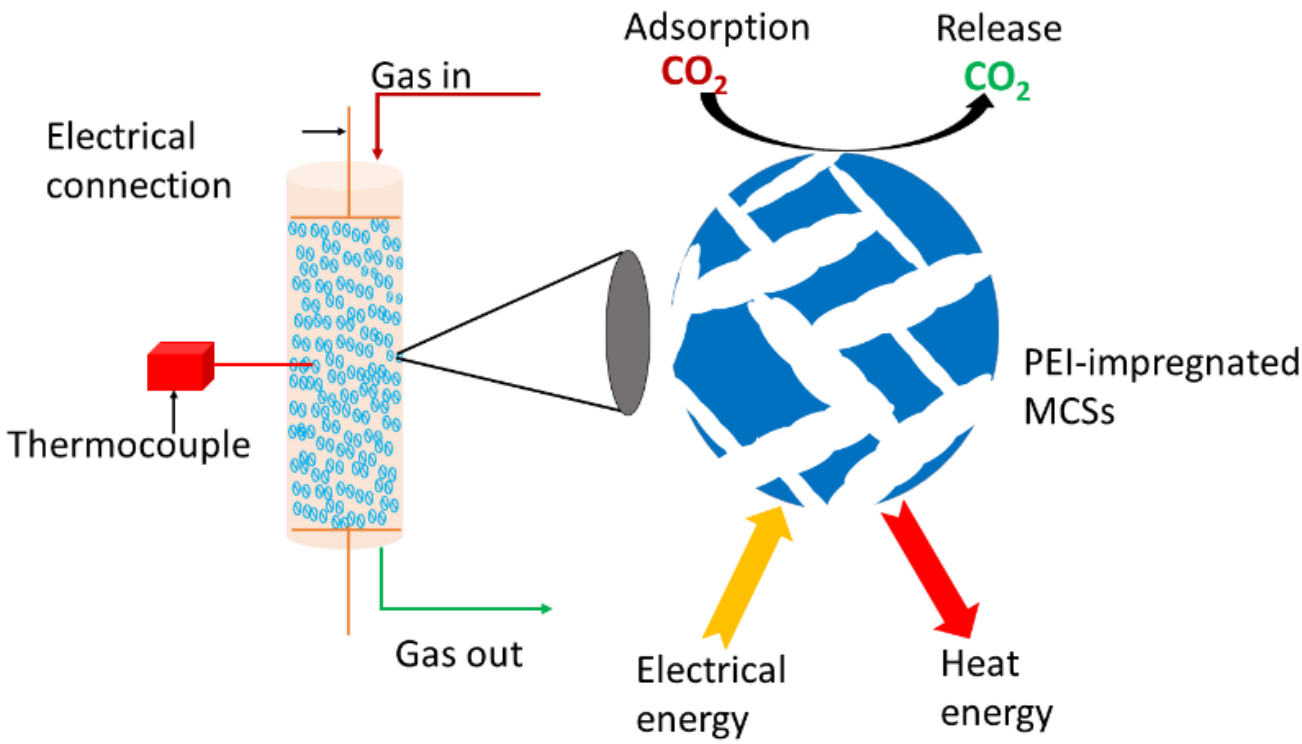

Figure 3. Schematic representation of the adsorption column for electric swing adsorption (Reprinted with permission from ref. [108]).

2.2. Different Regeneration Strategies

The attached CO_2 molecules onto the adsorbent surface could be regenerated through the (i) pressure swing adsorption (PSA), (ii) temperature swing adsorption (TSA), (iii) vacuum swing adsorption (VSA), (iv) pressure and vacuum swing adsorption (PVSA), and (v) electric swing adsorption (ESA) processes [33,35,116]. Table 5 shows the advantages and disadvantages of different regeneration strategies. The regeneration method depends on the chemical and structural properties of a given adsorbent [108]. Both TSA and PSA began to be used in the early 1960s [112]. Usually, TSA involves the adsorption at a low temperature (around 40 °C) followed by desorption by heating at around 120 °C [33,35]. The dominant regeneration strategy used for amine-functionalized adsorbents is the TSA owing to the simplicity of the process (Table 5). During PSA, the column pressure is lowered after adsorption to desorb the attached gas molecules. VSA involves adsorption at high pressure and lowering the pressure of the adsorption column to sub-atmospheric pressure after the adsorption step [112]. The ESA process is conducted by performing the adsorption–desorption cycle by varying the electrical supply [33]. Wang et al. [108] have proposed a schematic of the electric swing adsorption column, which is used to adsorb CO_2 gas molecules using polyethylenimine-impregnated millimeter-sized mesoporous carbon spheres illustrated in Figure 3. Usually, activated carbons, metal–organic frameworks (MOFs), zeolites, activated alumina, and silica gel are subjected to TSA and PSA. Although ESA is considered more economical than TSA and VSA, only conductive adsorbents are the potential candidates for ESA [35]. The cyclic PSA process has been estimated to be the most promising strategy to be applied in pre-combustion carbon capture since the gas stream is already pressurized after the conversion reactions [112].

Table 5. Comparison of different regeneration strategies.

Regeneration Strategy	Advantages	Disadvantages
Temperature swing adsorption (TSA)	• Simple in operation [108] • Can use low-grade heat from power plants [112]	• Long heating and cooling time periods [108] • Longer desorption time than PSA [35] • Higher energy requirement than PSA [35] • Rapid adsorbent deactivation due to coking at higher temperatures [35]
Pressure swing adsorption (PSA)	• Lower energy requirement than TSA [56] • Easy operation [56] • Low capital investment than TSA and VSA [56] • Applicability over a wide range of temperatures and pressures [117]	• Compression of the flue gas streams [108] • Dilute gas streams may result in intense energy consumptions during PSA [99]
Electric swing adsorption (ESA)	• More economical than TSA and PSA [35] • Independent purge gas flow [108] • Fast heating and cooling rates [108] • Low energy consumption [108]	• Further improvements are required before commercialization [35] • The adsorbents should have good electrical conductivity [108]
Vacuum swing adsorption (VSA)	• Applicability in large point sources [108]	• Energy intensive operation

2.3. Criteria for Selecting CO_2 Adsorbents

When synthesizing and selecting an effective CO_2 adsorbent, the material should be economical and operational simultaneously [112]. Therefore, a prospective CO_2 adsorbent should satisfy the following criteria (Table 6): (i) CO_2 adsorption capacity: The adsorption capacity plays a vital role since it determines the amount of adsorbent to be inserted into the adsorption column to attain the desired performance [118,119], (ii) Regenerability: The adsorbent should be fully regenerable and require relatively mild conditions for complete regeneration [119], (iii) CO_2 selectivity: The adsorbent should display substantially high selectivity for CO_2 in the co-presence of other species (e.g., N_2, methane (CH_4), sulfur dioxide (SO_2), hydrogen sulfide (H_2S), and moisture) [112,120,121], (iv) Adsorption/desorption kinetics: A rapid adsorption/desorption is required for swing adsorption to decrease the cycle time [112,116], (v) Thermal, chemical, and mechanical stability: During the cyclic regeneration process, the microstructure and morphology of the adsorbent should be retained. Moreover, the adsorbent should withstand harsh operating conditions, including vibration, high temperatures, pressures, and flow rates. Additionally, the amine-functionalized adsorbents should be resistant against oxidizing agents and contaminants such as sulfur oxides (SO_X), nitrogen oxides (NO_X), water vapor, and heavy metals [11,122], and (vi) Adsorbent cost: The adsorbent should be synthesized using cheap raw materials while adopting a cost-effective and energy-saving synthesis routes [26]. As shown in Table 6, it is considered that the cost valuing \$5/kg for an adsorbent is better from an economic point of view. In contrast, an adsorbent with a cost of \$15/kg is uneconomical. However, it is believed that the adsorbent cost of \$10/kg is optimum if the desired performance could be attained [112,123]. Apart from the above parameters, the adsorbent synthesis procedure should be straightforward, and the adsorbents should possess low heat capacities. The raw materials and the synthesis route should be environmentally friendly and not be harmful to human health [118,119].

Table 6. Threshold values of criteria for selecting an effective CO_2 adsorbent (Reprinted with permission from refs. [112,118]).

Parameter	Requirement
CO_2 adsorption capacity	3–4 mmol/g
Regenerability	>1000 cycles
CO_2 gas selectivity over other gases	>100
Adsorption/desorption kinetics	>1 mmol/g.min
Adsorbent cost	$5–15/kg sorbent

2.4. Different Adsorbents for CO_2 Capture

Numerous studies on CO_2 capture conducted in academic and industrial settings have developed promising adsorbents possessing the requirements demonstrated in Table 6 [70]. A variety of adsorbents have been discovered and synthesized, including MOFs, zeolites, activated carbons, zeolite imidazolate frameworks (ZIFs), grafted and impregnated polyamines [50], activated alumina, carbonized porous aromatic frameworks (PAFs), covalent organic frameworks (COFs) [124,125], porous organic polymers (POPs) [40], mesoporous silica, carbon nanotubes [126], metal oxides, ionic liquids [21], phosphates [35], and molecular sieves [5].

2.5. Importance of Carbon-Based Adsorbents for Effective CO_2 Capture

Of the previously mentioned CO_2 adsorbents, though zeolites and well-ordered frameworks exhibit high CO_2 adsorption capacities at relatively lower pressures [46], the CO_2 adsorption performance gradually decreases in the co-presence of moisture [41,127]. Similarly, molecular sieves and silica gel also demonstrate decreased CO_2 adsorption performance in the co-presence of moisture [5]. Additionally, the usage of MOFs has been severely limited due to structural collapse upon vacuum treatments [41], contact with acid gases, thermal regeneration [126], and their complex and expensive synthesis procedures [127]. The ionic liquids are also unfavorable for practical applications due to their relatively high operational costs and high viscosity, leading to corrosion-related problems [60].

On the other hand, the application of carbon materials in the day-to-day lives of human beings can be traced back to more than 5000 years when the early humans discovered charcoal formed through the incomplete combustion of wood. Interestingly, many carbon materials have been discovered, such as graphene, fullerene, activated carbons, graphite, carbon foams, biochar carbon nanotubes, and carbon aerogels [96]. The carbon-based materials can be used as appropriate candidates in catalysis, electronics, fuel cells, biology, metal recovery, and gas storage and separation [34,96,128].

Among the aforementioned wide range of applications, carbon-based porous materials can serve as appropriate candidates for CO_2 capture due to their advantageous, including low production cost [34], competitive CO_2 adsorption performance at a given pressure [46,78], easy synthesis, ease of scaling up [96], wide availability, controllable pore structure, high thermal stability [15], good chemical resistance against alkaline and acidic media [129], fast adsorption kinetics [50], lower regeneration energy requirements [127], high apparent density (0.3 g/cm^3) [130,131], high surface area [132,133], environmental benignity [21], favorable surface chemistry [134], selectivity [105], and flexibility for heteroatom doping or surface functionalization [135]. Additionally, the high thermal and chemical conductivity of carbon-based materials can be exploited for thermal, electric, and pressure swing adsorption strategies [130].

3. CO_2 Capture Using Porous Carbon Materials: Physisorption

3.1. Synthesis of Physisorbents

3.1.1. General Introduction

Carbon-based adsorbents can be prepared via direct carbonization [64], carbonization followed by activation [42], sol–gel process, and nanocasting [42,64,136]. In general, a raw material containing high amounts of volatile organic compounds, carbon content, and low ash content makes for a better candidate for porous carbon preparation [56]. Among the synthesis processes mentioned above, numerous studies have conducted post-synthesis activation to create enhanced surface areas and porosity in the final material [134]. Chemical activation is conducted in the presence of chemical agents including KOH, NaOH, H_3PO_4, K_2CO_3, Na_2CO_3, $AlCl_3$, $ZnCl_2$ [23,137–139], $CaCl_2$ [25], H_3PO_3 [116], H_2SO_4, H_2O_2, formamide [46], Na_2SiO_3, K_3PO_4, $C_6H_5K_3O_7$ [23,46], whereas the physical activation process is conducted using mild oxidizing gases such as CO_2 [101], steam [86], air [138], water vapor [140], humidified N_2 [141], or their mixture at elevated temperatures [142]. Ultrasound treatment has also been recently adopted as an alternative to high-temperature physical activation, which opens up the clogged pores, cleans the adsorbent surface, and removes mineral matter [65].

Carbonization can be categorized into three major categories depending on the pyrolysis conditions: (i) slow pyrolysis (temperatures < 300 °C with slow heating rates for long time durations), (ii) moderate pyrolysis (temperatures < 300–500 °C), and (iii) fast pyrolysis (temperatures > 500 °C). Usually, the carbonization temperature affects the textural properties, surface functional groups, and elemental composition of the final material, and 500–800 °C is considered the optimum temperature range for carbonization during the preparation of carbon-based adsorbents [65]. The carbonized materials produced at higher temperatures exhibit better thermal stability [143], whereas those produced at lower carbonization temperatures display better mechanical integrity [58]. During carbonization, the carbon precursor decomposes while reducing its density and increasing the porosity [25,138]. However, direct carbonization is reported to be time-consuming and requires a higher amount of energy [42].

Carbon-based adsorbent synthesis via physical activation demonstrates advantages over chemical activation such as the elimination of additional expenses for the processes such as impregnation, washing [140], recovery of the chemical activators [11], being cleaner and more straightforward, capable of preserving the original macroscopic structure of the final product [144], eco-friendliness [68,140], economical [68], avoiding the usage of harmful substances such as NaOH, KOH, $ZnCl_2$, and H_3PO_3 [117]. Nevertheless, the chemical activation process also offers some advantages. For example, the usage of $ZnCl_2$ as the chemical activating agent restricts tar formation [25]. Additionally, lower temperatures are needed for chemical activation compared to physical activation. Thus, the former is more favorable in terms of energy-saving [17], higher yield [142], less time requirement, a considerable number of pore generation, decreased pre-oxidation temperature, and higher production rate [34].

The carbon-based adsorbents for CO_2 capture can be prepared in the forms of foams, membranes, sheets, fibers, spheres, monoliths, particles, or aerogels [53]. Among different macro shapes of the adsorbents, the spherical shape has grabbed significant attention owing to its high surface-to-volume ratio, better structural stability, low regeneration energy requirement [145], reduced flow resistance, abrasion in the packed bed, larger specific surface area, and better moisture and thermal stability [90].

Of the porous carbon synthesis routes mentioned above, the nanocasting technique is considered the most effective method for developing the textural properties [42,64], which involves infiltration of the precursor into the pores of the rigid template and subsequent carbonization and template removal [104]. Apart from the above-discussed synthesis processes, one-step carbonization and activation, which is performed simultaneously in the presence of the activating agent, offers advantageous properties over the conventional route as such processes offer simplicity, reduction of the operational time, cost, energy

consumption, manpower, and avoids liquid discharge requiring effluent treatment [84,141]. Interestingly, microwave treatment has been extensively used to replace conventional furnace heating since microwave heating can reduce the impregnation time and lead to better surface area and porosity development [142]. The properties of the final carbon-based adsorbent largely depend on the activation conditions, synthesis routes, and, most importantly, the chemistry of the carbon precursor [52,146,147].

A few studies have carried out a cost estimation regarding adsorbent preparation. For instance, a study reported that the total adsorbent preparation cost associated with pine wood-derived porous carbon was about 1.93 US$/kg, which is comparatively lower than the commercially available activated carbons (2–5 US$/kg) [17].

3.1.2. Porous Carbon Synthesis Using Different Precursors

The porous carbon materials can be effectively categorized based on the type of precursor utilized for their synthesis (Figure 4):

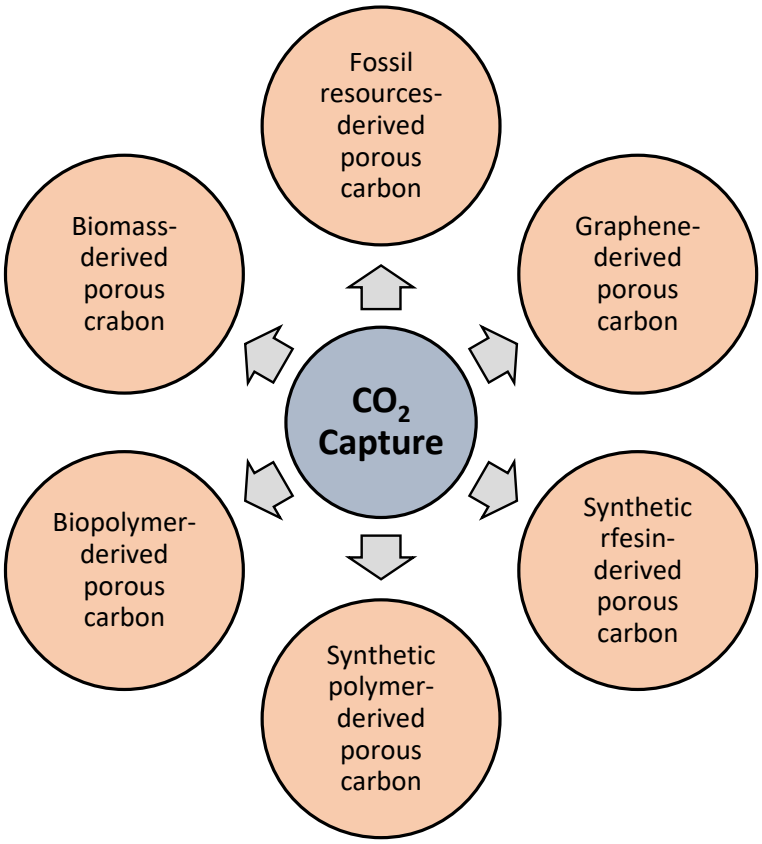

Figure 4. Various precursor-derived porous carbon materials for CO_2 adsorption.

(i) Fossil resources-derived porous carbons: Conversion of cheap and abundant wastes or the byproducts of petroleum industry into porous carbons is of paramount importance since it creates a path for high-value utilization of these materials at a large-scale [148]. Petroleum coke, one of the waste residues of heavy oil upgrading, is considered a good candidate for porous carbon preparation. It contains a large amount of fixed carbon with reasonably low volatile organic and ash content [10,81]. Moreover, asphaltene, usually recovered from the deposits in oil wells during crude oil distillation contains C, H, S, N, O, and other heteroatoms, including V and Ni, making it a good candidate for the production of heteroatom-rich porous carbons [7,89,148,149]. Besides, oil-based pitches, petroleum tar, and coal–tar pitches can also be utilized as precursors for CO_2 adsorbent preparation.

(ii) Graphene-derived porous carbons: Graphene has captured significant attention as a precursor for porous carbon preparation owing to its unique molecular structure,

lightweight, high flexibility, high chemical stability, large surface area, tunable porosity, favorable planar geometry for functionalization, hardness, high thermal conductivity (which makes it highly favorable for TSA) [21], high mechanical strength, and robustness, and can withstand hot, humid conditions, and other impurities such as SO_x, O_2, and NO_X [21,150]. On the contrary, graphene oxide, which is the functionalized graphene derived via oxidation of graphite in the presence of strong oxidizing agents [94,151], can also be used as a precursor for CO_2 adsorbent preparation due to its chemical stability, flexibility, high surface area, porosity [152], and advantageous electronic and electrochemical properties [94].

(iii) Synthetic resin-derived porous carbons: Synthetic resin-derived porous carbons can be prepared using the organic polycondensation method [107]. At present, phenolic resins are preferred over resorcinol-based resins due to favorable cost economics [153].

(iv) Synthetic polymer-derived porous carbons: Most polymeric wastes are non-degradable [23,65], and can be used for porous carbon preparation [154,155]. Interestingly, the utilization of plastic wastes as carbon precursors solves two problems simultaneously, namely, (i) reducing plastic waste accumulation across the globe, and (ii) reducing atmospheric CO_2 via carbon capture [154]. Polyethylene terephthalate (PET) [23], polyurethane foam (PUF; one of the most important thermosetting polymers) [156], polyaniline (PAN; cheap polymer containing a large amount of readily available carbon with high mechanical stability) [34], and optical discs produced from polycarbonates [154] are the most widely used carbon precursors for carbon-based adsorbent synthesis. PET is the most widely used carbon precursor among these polymers due to its wide availability and high carbon content [3]. Poly-ionic liquids (PIL) are also being actively utilized as a potential polymer-based carbon precursor for synthesizing adsorbents [157,158]. The PILs possess high thermal stability (even up to 400 °C), are rich in heteroatoms (e.g., nitrogen), and produce a higher yield of the adsorbent compared to other polymeric precursors [157–159].

(v) Biopolymer-derived porous carbons: The literature reveals that the natural biopolymers such as chitosan, an inexpensive renewable material [88], lignin, one of the most abundant biopolymers [160,161] composed of aromatic alcohols, and cellulose, the primary component of vegetal biomass (abundant on earth) [162], are excellent precursors for the preparation of porous carbon-based adsorbents due to their biocompatibility, biodegradability, high thermal and mechanical stability, low cost, non-toxicity, high surface reactivity [48], renewability, and low density [51]. Chitin is the second most abundant natural biopolymer after cellulose [52] and has been extensively utilized as a carbon precursor during porous carbon preparation. Furthermore, enzymatically hydrolyzed lignin (EHL), a byproduct formed during bio-ethanol production, has also been used to prepare CO_2 adsorbents owing to its abundance, low cost, high carbon content, and renewable nature [141]. Pigskin collagen is also a good candidate for porous carbon fabrication since it contains about 41.6 wt % carbon and several amino acids [163]. Apart from the above, waste wool has also been used as a precursor for CO_2 adsorbent synthesis [164].

(vi) Biomass-derived porous carbons: It is well-known that biomass is widely abundant and well distributed globally [96]. The conversion of biomass into porous carbon materials has become a common practice due to their heterogeneous texture and complicated chemical composition, which strongly affects the development of textural properties [76]. Waste materials and byproducts can be effectively utilized from the practical perspective to minimize the overall cost of porous carbon fabrication. In this context, biomass serves as the best candidate [15,47,165]. In the reported literature, scientists have used cork dust, bio-tar, date seed, coconut shells, rice husk, lotus stalk, mangosteen peel, poplar catkin, sugarcane bagasse, pinewood, peanut shell, walnut shell, algae, chars derived from biomass gasifiers, palm kernel shells, paper mill sludge, pine sawdust, sucrose, solid bamboo residues, and hazelnut shells to produce porous carbon-based materials for CO_2 gas capture.

Different types of porous carbon synthesis methods have been adopted by different research groups, as depicted in Table 7. Table 7 also lists the synthesis routes used for different precursors to prepare porous carbons for effective CO_2 gas capture.

Table 7. Summary of different synthesis routes adopted for porous carbon preparation.

Synthesis Route	Carbon Precursor					
	Biomass-Derived Porous Carbon	**Biopolymer-Derived Porous Carbon**	**Fossil–Resources-Derived Porous Carbon**	**Graphene-Derived Porous Carbon**	**Synthetic Polymer-Derived Porous Carbon**	**Synthetic Resin-Derived Porous Carbon**
Carbonization followed by KOH activation	Biomass cork dust [76], Bio-tar [24], Date seeds [141], Coconut shells [81], Rice husk [50], Mangosteel peel [15]	Starch [32,46,49,138], Chitin [52], Waste wool [165], Chitosan [88], Lignin [161]	Anthracene oil-based pitch [166], Petroleum coke [10,81,146], Asphalt [89,167], Iranian asphaltene [7], Petroleum tar pitch [168], Coal particles [169]	Graphene oxide [170], Graphene [91]	PAN [34,58], Polypyrrole [135,171], Triazine-based hyper cross-linked polymer [172], PET [3,12,101], Waste CDs and DVDs [154], PUF [156]	Commercial phenolic resin [173], Urea–formaldehyde [17,42]
Carbonization followed by $ZnCl_2$ activation	Biomass cork dust [76], Poplar catkin [101]	-	-	-	Triazine-based hyper cross-linked polymer [172]	-
Thio-urea modification of the carbonized product followed by KOH activation	Hazelnut shells [174]	-	-	-	-	-
Carbonization followed by NaOH activation	Waste sugarcane bagasse [47]	Chitosan [88]	-	-	PAN [34], PET [101]	-
Post nitridation of the carbonized product using melamine followed by KOH activation	Water caltrop shells [175]	-	-	-	-	-
Single step KOH activation	Pine wood [17], *Taihu* blue algae [176], Peanut shell [17], Chars derived from biomass gasifiers [25], Walnut shell [17], *N-Salina* algae [62]	EHL [141]	-	-	Main-chain PIL [157]	Commercial phenolic resin [177]
$ZnCl_2$ activation	Chars derived from biomass gasifiers [25]	-	-	-	Polypyrrole [130]	-
Carbonization followed by steam activation	Paper mill sludge [54], Palm kernel shell [59], Pine sawdust [54]	-	-	Reduced graphene oxide [144]	-	-
Carbonization followed by CO_2 activation	Sucrose [55], Rice husk [90], Bamboo solid residue [11], Waste sugarcane bagasse [47]	Starch [145]	-	Graphene/Glucose composite [61]	Polyvinylidene fluoride [155], Polypyrrole [140], Waste CDs and DVDs [162]	Phenolic resin [178]
Carbonization flowed by NH_3 activation	-	-	-	-	-	Phenolic resin [179]
Carbonization followed by air activation	Waste sugarcane bagasse [47]	-	-	-	-	-
Carbonization followed by H_3PO_3 activation	Waste sugarcane bagasse [47]	-	-	-	-	-
Carbonization followed by potassium acetate activation	Waste sugarcane bagasse [47]	-	-	-	-	-

Table 7. *Cont.*

Synthesis Route	Carbon Precursor					
	Biomass-Derived Porous Carbon	**Biopolymer-Derived Porous Carbon**	**Fossil–Resources-Derived Porous Carbon**	**Graphene-Derived Porous Carbon**	**Synthetic Polymer-Derived Porous Carbon**	**Synthetic Resin-Derived Porous Carbon**
Single step CO_2 activation	Palm kernel shell [86]	Cellulose [117,180]	Petroleum coke [179]	Reduced graphene oxide [150]	-	-
Single step low temperature $NaNH_2$ activation	Hazelnut shell [181], Lotus stalk [182], Lotus leaf [183]	-	-	-	-	-
Carbonization followed by $NaNH_2$ activation	Water chestnut shells [184]	-	-	-	-	Phenolic resin [185]
Carbonization followed by $FeCl_3$ activation	-	-	Coal tar pitch [186]	-	Polypyrrole [172]	-
Direct carbonization	-	-	-	-	-	Resorcinol–formaldehyde [4]
Electrospinning followed by carbonization	-	-	-	-	-	Phenolic resin [153]
Nanocasting	-	-	-	-	-	Urea–formaldehyde [36,42], Resorcinol–formaldehyde [45], Phenol–formaldehyde [66], Hexamethoxymethylmelamine (HMMM) [105]
In-situ activation using potassium organic salt during precursor synthesis followed by carbonization	-	-	-	-	-	Resorcinol–formaldehyde [135]
Carbonization followed by $K_2C_2O_4$ activation	-	Corn starch [46]	-	-	-	-
Carbonization followed by K_2CO_3 activation	-	Corn starch [46]	-	-	-	-
Carbonization followed by KOH and Urea activation	-	Chitosan [187]	-	-	-	-
One step carbonization/activation with N_2	-	Cellulose [116]	-	-	-	-
Carbonization followed by alkali metal carbonate activation	-	Chitosan [188]	-	-	-	-
Carbonization followed by potassium citrate activation	-	Chitosan [189]	-	-	-	-
Carbonization followed by $CaCO_3$ activation	-	Pigskin collagen [163]	-	-	-	-
Carbonization followed by CH_4 activation	-	Starch [145]	-	-		-
Carbonization followed by H_2 activation	-	Starch [145]	-	-	-	-

Table 7. *Cont.*

Synthesis Route	Carbon Precursor					
	Biomass-Derived Porous Carbon	Biopolymer-Derived Porous Carbon	Fossil–Resources-Derived Porous Carbon	Graphene-Derived Porous Carbon	Synthetic Polymer-Derived Porous Carbon	Synthetic Resin-Derived Porous Carbon
Microwave treatment	-	-	-	-	Polyacrylonitrile [142]	-
Spheroidization, oxidation, cross-linking and KOH activation	-	-	-	-	PVC [190]	-
Cross-linking, pre-oxidation and carbonization	-	-	-	-	PAN [143]	-
Spheroidization followed by alkaline activation	-	-	-	-	PVC [61]	-
C_3N_4 nanosheets as sacrificial template	-	-	-	-	PIL [159]	-
Carbonization followed by Fe-Based template removal	-	-	-	-	PIL [158]	-
Reduction-induced self-assembly process of graphene oxide nano platelets in aqueous dispersion at 45–90 °C	-	-	-	Graphene [191]	-	-
Sol–gel method	-	-	-	Magnesium oxide nanoparticle fabricated on graphene oxide [94]	-	-
Polyol-mediated self-assembly and subsequent thermal annealing treatment	-	-	-	Reduced graphene oxide and nanocrystalline composite [192]	-	-
Electrospinning process followed by physical activation	-	-	-	Activated carbon fibers/graphene nanocomposite [39]	-	-

3.1.3. The Effect of Synthesis Procedures on the Development of Textural Properties

A hierarchically porous structure is generally more favorable for adsorbing the CO_2 molecules [158]. Although the narrow micropores are more beneficial than large-sized micropores for CO_2 adsorption (stronger adsorbate–adsorbent interactions) [4,101,188], the mesoporous and microporous structure in a particular adsorbent plays a vital role in improving the mass transfer of CO_2 molecules. The mesopores also act as a passage for the CO_2 molecules to reach the micropores [25,135,144,158]. Besides, the fraction of micropore volume, shape, and size distribution are the critical factors to be controlled during the synthesis of carbon-based adsorbents [25,146].

The carbonization temperature has a powerful effect on pore development. Lower carbonization temperatures are responsible for forming meso and macropores, whereas the higher carbonization temperatures result in producing micropores [50]. The activation temperatures also give rise to similar phenomena [36,42]. The surface area and porosity are lower at lower activation temperatures and time durations for the activation [140,144], whereas the increased activation temperatures could narrow the micropore distribution while forming smaller micropores [150]. According to previously published literature, steam activation is favorable for generating high porosity and increasing the specific surface area while maintaining the three-dimensional (3D) macroscopic structure [144]. The specific surface area of the adsorbent generally increases during steam activation if the temperature is in the 600–800 °C range. The specific surface area of the adsorbent decreases for temperatures beyond 1000 °C. The product yield is also relatively low at higher temperatures [59]. If the CO_2 activation strategy is employed, the formation of micropores becomes dominant [11]. However, it is reported that the pyrolysis temperatures in the range of 700–800 °C decrease the specific surface area and total pore volume due to structural ordering and merging of pores [65].

It has been reported that chemically activated samples generally exhibit higher pore volumes than the physically activated carbons [47,144]. During KOH activation, the development of micro and mesopores could be observed in the 400–800 °C range. At 800 °C, the formation of macro and mesopores begins due to the strong etching behavior of the K species (K_2O). Additionally, the specific surface area and total pore volume increase with a reduction in the micropore volume with the temperature increment (>800 °C). Moreover, it could be observed that high KOH loadings could widen the micropores [76]. Furthermore, at lower KOH loadings, the micropore formation contributes to the increment of the total pore volume. Mesopore formation is responsible for increasing the total pore volume at higher KOH loadings [76,177]. Similar observations were reported for both NaOH and $ZnCl_2$ activation [3,12,76,81,88,101,134,193].

On the contrary, $NaNH_2$ activation has proven an effective activator during porous carbon preparation [182–185]. The reaction mechanism of sodium amide during pore formation in carbon structure contains three major steps; namely, (i) Generation of pores during the reaction of $NaNH_2$ and oxygen-containing groups on carbon precursor while simultaneously incorporating N into carbon skeleton, (ii) Redox reaction between carbon and previously formed NaOH and/or Na_2O, and (iii) Further etching of carbon surface by released gaseous NH_3 and H_2 [182,183,185]. Additionally, the porous carbons prepared at higher activation temperatures and higher $NaNH_2$ loadings possess better textural properties [182,184]. Nevertheless, smaller $NaNH_2$ dosages create narrow micropores [181,182].

3.2. CO_2 Adsorption Capacities of Carbon-Based Physisorbents

The adsorption rate and the capacity of the porous carbon materials are highly dependent on their pore structures, diffusion processes, and the available surface area [5]. Besides, adsorption kinetics plays a significant role during practical applications since faster kinetics are beneficial to shorten the cycle time [21,173,181] and determine the adsorbent mass be loaded into the fixed bed (column length) [150]. Moreover, a higher dynamic CO_2 adsorption capacity reflects the better capacity of a particular adsorbent to capture CO_2 from activated flue gas [181]. The equilibrium adsorption capacity is always more significant

than the dynamic adsorption capacity, critical during practical applications [10]. Furthermore, the time required to switch a particular adsorbent bed from adsorption to desorption is called the breakthrough time. It is considered one of the most critical parameters from a practical perspective [194]. Apart from the above, the value of the diffusion time constant of a particular adsorbent also plays a vital role where a high CO_2 diffusion rate indicates a reduced adsorption cycle time, which is beneficial during industrial applications [185].

Table 8 elucidates the CO_2 adsorption capacities of porous carbon materials. In the case of CO_2 physisorption by porous carbon materials, the adsorption capacity decreases with increasing temperature [114], and the adsorbate–adsorbent interactions primarily comprise weak Van der Waals forces [86,114,150]. The previously reported literature can evidence the favorable adsorption of CO_2 at lower temperatures. For instance, Chang et al. [101] and Li et al. [143] reported a decrease in the CO_2 adsorption capacity from 6.22 to 4.05 mmol/g and from 6.4 to 4.36 mmol/g (see Table 8) when the temperature increased from 0–25 °C at 1 bar for $ZnCl_2$ activated poplar catkin, and KOH activated date sheets, respectively. Moreover, when the temperature was increased from 25 to 50 °C at 1 bar, the CO_2 uptake capacity reduced from 2.45 to 1.64 mmol/g for a graphene oxide-derived porous carbon [150]. Furthermore, a notable reduction in adsorption capacity from 1.34 to 0.6 mmol/g was also reported by Tiwari et al. [103] for a temperature increment from 30 to 100 °C. Nevertheless, Ludwinowicz et al. [134] have revealed that the decrease in CO_2 adsorption capacity was more prominent at low pressures.

Apart from the temperature, the behavior of the CO_2 uptake capacities with the pressure changes was also studied by several researchers. Both Li et al. [145] and Liu et al. [173] reported that the CO_2 adsorption capacity increased with adsorption pressure while not leveling off, even at the highest test pressure valuing 20 bar. Additionally, at 25 °C and 1 bar, the CO_2 uptake was reported to be in the range of 2.4–3.01 mmol/g for asphalt-derived porous carbon, and the capacity increased about 5 mmol/g when the pressure was increased to 3.8 bar [148]. Similar observations were noted by Nan, Liu, and Ma, [153] where the CO_2 adsorption capacity increased from 0.44 to 1.06 mmol/g when the pressure was increased from 40 to 150 mbar (low-pressure region).

Besides the temperature and pressure, the CO_2 concentration in the feed gas stream also regulates the CO_2 capture performance of a particular adsorbent. Li and Xiao [92] observed an increase in CO_2 capture capacity at both 25 and 50 °C with the increment in CO_2 concentration, and this behavior was ascribed to the increase in CO_2 partial pressure with the increase in CO_2 concentration [92] and due to the higher driving force at elevated concentrations [3,13,42,104]. For instance, the PET-derived porous carbon and urea–formaldehyde resin-derived porous carbon displayed an increase in the CO_2 uptake capacity from 0.63 to 2.31 mmol/g and 0.48 to 2.43 mmol/g at 30 °C, respectively, when the CO_2 concentration was increased from 6 to 100% [3,13]. The increment in CO_2 uptake capacity from 0.36 to 0.676 mmol/g for HMMM-derived porous adsorbent [105], from 0.62 to 1.4 mmol/g for urea–formaldehyde-derived porous carbon [42], from 0.78–1.25 mmol/g for phenol–formaldehyde-derived porous carbon [66], and from 0.25 to 0.94 mmol/g for melamine–formaldehyde resin-derived porous carbons were observed when the CO_2 concentration was increased from 5 to 12.5%.

From a practical point of view, numerous research groups have examined the breakthrough time durations and the dynamic adsorption capacities. For example, Wang et al. [176] reported the breakthrough time as 192.5 s for a feed gas containing 10% CO_2 and 90% N_2 gas for an algae-derived porous carbon. Besides, a breakthrough time of 8 min for lotus leaf-derived porous carbon [183] and $NaNH_2$ activated water chestnut shells-derived porous carbon [184], 9.5 min for lotus stalk-based activated carbon [182], and 6 min for KOH activated phenolic resins [177] were reported by previous researchers for a gas mixture containing 10% CO_2 and 90% N_2 gas. Furthermore, for a gas mixture containing 98% CO_2 and 2% H_2O, the CO_2 adsorption front travels faster through the sorbent bed compared to that of moisture, and the breakthrough time for CO_2 gas molecules was reported to be approximately 4.5 min, whereas, for H_2O molecules, the breakthrough time

was 127 min. Additionally, it was noted that the presence of moisture did not affect the breakthrough time of CO_2. However, in the presence of a gas stream that contains 84% N_2, 14% CO_2, and 2% H_2O, the breakthrough time of CO_2 gas of 4.5 min (for the gas mixture containing 98% CO_2 and 2% H_2O) decreased due to the initially adsorbed higher amount of moisture content [195].

On the contrary, several research teams reported the dynamic CO_2 adsorption capacities as 0.98 mmol/g for commercial phenolic resin-derived porous carbon at 25 °C [196], 1 mmol/g for coconut shell-derived carbon at 25 °C [81], 0.97 mmol/g for lotus stalk-derived porous carbon [182], 0.82 mmol/g for lotus leaf-based activated carbon [183], 0.96 mmol/g for KOH activated phenolic resin-derived porous carbon [177], 0.94 mmol/g for sodium amide activated phenolic-resin [185], 0.96 mmol/g for water chestnut shells-derived porous carbon [184], 1.31 mmol/g for waste sugar cane bagasse-based sorbent [47], 1 mmol/g for hazelnut-derived carbon [178], 0.95 and 0.66 mmol/g for petroleum coke-derived porous carbons [127,180], 1.45 mmol/g for polypyrrole-based sorbent at 25 °C [135], 2.1 mmol/g for activated carbon fibers/graphene nanocomposite at 25 °C [197], and 1.04 mmol/g for a commercial phenolic resin-derived porous carbon at 25 °C [173] for a feed gas stream containing 10% CO_2 and 90% N_2 gas. Interestingly, it is reported that the obtained dynamic CO_2 adsorption capacities via experiments are consistent with the saturation adsorption data at a partial pressure of 0.1 bar [184]. Furthermore, a similar dynamic adsorption capacity of 0.36 mmol/g for both CO_2 and H_2O was observed for biochar developed from olive stones in the presence of a gas stream containing 2% H_2O, 84% N_2, and 14% CO_2 while demonstrating a reduction of 13% of original CO_2 gas capture capacity from a pure CO_2 gas stream, 22% reduction of H_2O adsorption capacity from a 100% moisture stream, and a reduction of 37% of original N_2 gas capture capacity from a 100% N_2 gas stream [195].

Apart from the facts mentioned above, some researchers have noted that rapid CO_2 adsorption kinetics could be beneficial for practical applications. For instance, hazelnut shell-derived porous carbons have demonstrated 90% adsorption saturation within 6 min [181], and 92 and 98% CO_2 were adsorbed after 1 and 3 min, respectively, by a nanocellulose-based carbon [117]. Additionally, very fast CO_2 adsorption rates of 95% adsorption saturation after 4 min for commercial phenolic resin-based porous carbons [173], 90% of saturation within 3 min by $NaNH_2$ activated lotus stalk [182], and 3.5 min by KOH activated commercial phenolic resin-derived porous carbon [177], adsorption saturation at 6 min for $NaNH_2$ activated lotus leaves-based porous carbons [183], 5 min for $NaNH_2$ activated water chestnut shells-derived carbon [184], and a 95% adsorption saturation around 4 min were exhibited at 25 °C in the presence of a 10/90 CO_2/N_2 (*v/v*) feed gas mixture. On the contrary, according to Wang et al. [185], the value for diffusion time constant is 0.053 min^{-1} for $NaNH_2$ activated phenolic resin-derived porous carbon. It is stated that such a relatively high value is capable of reducing the adsorption cycle time, which is beneficial during practical applications. Most importantly, according to Plaza et al. [195], it was reported that the effective diffusivity of H_2O molecules is smaller compared to CO_2 gas molecules due to the higher isosteric heat of adsorption of moisture, and this phenomenon is beneficial during practical applications.

Table 8. Comparison of the CO_2 physisorption capacities of porous carbon materials.

Porous Carbon Material	S_{BET} (m^2/g)	V_t (cm^3/g)	V_{mic} (cm^3/g)	V_{mes} (cm^3/g)	S_{mic} (m^2/g)	S_{mes} (m^2/g)	Average Pore Size (nm)	CO_2 Capture Conditions for Pure CO_2 Gas Flow	CO_2 Capture Capacity (mmol/g)	Reference
KOH activated carbon nanoflakes	2010	0.82	0.718	0.102	-	-	-	0 °C and 1 bar 25 °C and 1 bar	7.82 4.27	[64]
Mesoporous carbon synthesized using 3D silica KIT-6 as the hard template	740	0.88	-	-	-	-	1.7 8.7	0 °C and 1.2 bar 25 °C and 0.01 bar	2.29 1.62	[114]
KOH activated biotar	2595	1.296	-	-	-	-	2.5	0 °C and 1 bar	5.35	[24]
$ZnCl_2$ activated Poplar cat skin-derived porous carbon	1005.4	0.41	0.34	-	867.6	137.8	-	0 °C and 0.15 bar 25 °C and 0.15 bar	1.94 1.13	[23]
KOH activated date sheets	2367	1.48	0.834	-	2059	-	-	0 °C and 1 bar 25 °C and 1 bar	6.4 4.36	[143]
$NaNH_2$ activated lotus stalk	1113	0.41	-	-	-	-	-	0 °C and 1 bar 25 °C and 1 bar	3.88 5.45	[182]
$NaNH_2$ activated lotus leaf	1087	0.45	-	-	-	-	-	0 °C and 1 bar 25 °C and 1 bar	3.50 5.04	[183]
KOH activated coconut shells	1172	0.58	0.44	-	-	-	-	0 °C and 1 bar 25 °C and 1 bar	6.04 4.23	[81]
NaOH activated sugarcane bagasse	1149	1.73	0.08	-	-	-	6.02	25 °C and 1 bar	4.28	[47]
$NaNH_2$ activated water chestnut shells	1416	0.53	-	-	-	-	-	0 °C and 1 bar 25 °C and 1 bar	4.50 6.04	[183]
CO_2 activated bamboo	953	0.4	0.51	0.04	-	-	-	25 °C and 1 bar	3.4	[11]
CO_2 activated solid residue	1316	0.55	0.54	0.07	-	-	-	25 °C and 1 bar	3.4	[11]
KOH activated pinewood	900.76	0.38	0.33 (87%)	0.05 (13%)	-	-	1.69	25 °C and 1bar	3.92	[17]
Steam activated pine sawdust	581.74	0.25	-	-	-	-	2.24	25 °C and 1 bar	2.498	[54]
CO_2 activated palm kernel shell	367.8	0.2199	-	-	-	-	-	25 °C and 1 bar	2.13	[84]

Table 8. *Cont.*

Porous Carbon Material	S_{BET} (m^2/g)	V_t (cm^3/g)	V_{mic} (cm^3/g)	V_{mes} (cm^3/g)	S_{mic} (m^2/g)	S_{mes} (m^2/g)	Average Pore Size (nm)	CO_2 Capture Conditions for Pure CO_2 Gas Flow	CO_2 Capture Capacity (mmol/g)	Reference
KOH activated blue algae	1018.55	-	0.46	-	-	-	2.09	0 °C and 1 bar 25 °C and 1 bar	4.88 2.76	[176]
Carbonized mangosteen peel	1270	0.55	0.51	-	-	-	-	0 °C and 1 bar 25 °C and 1 bar 45 °C and 1 bar	6.93 4.77 3.35	[15]
$NaNH_2$ activated hazelnut shells	1099	0.45	-	-	-	-	-	0 °C and 1 bar 25 °C and 1 bar	6.06 4.23	[151]
Chemically activated rice husk with prior compaction	1190	0.777	0.422	0.175	-	-	-	25 °C and 15 kPa	1.9	[50]
KOH activated algae	1247.2	-	0.69	-	1192.4	39.4	-	0 °C and 1 bar 25 °C and 1 bar	5.7 3.9	[57]
Potassium acetate activated sucrose	1917	0.85	-	71%	78.8%	-	-	25 °C and 1 bar	4.82	[78]
Urea activated MOF-5-derived porous carbon	1161	1.31	0.25	1.06	554	607	-	25 °C and 1 bar	2.44	[198]
Cu-BTC framework-derived porous carbon	1364	0.65	0.59 (91%)	-	-	-	-	25 °C and 1 bar	4.51	[22]
ZIF-8-derived porous carbon	948	0.73	0.39	0.34	826	122	-	25 °C and 1 bar	3.7	[199]
KOH activated graphite oxide	3240	2.23	-	-	-	-	2.75	25 °C and 20 bar	21.1	[170]
KOH activated graphene	716	0.66	-	-	-	-	3.7	25 °C and 1 bar	3.13	[42]
CO_2 activated graphene	1315.98	1.07	0.21	-	-	-	-	0 °C and 1 bar	3.36	[150]
MgO nanoparticles fabricated on Graphene oxide	12	0.1	<0.01	-	-	-	-	25 °C and 1 bar	0.16	[94]
Urea and KOH activated graphene oxide	1032	0.61	0.59	-	-	-	-	25 °C and 1 bar	2.4	[21]

Table 8. *Cont.*

Porous Carbon Material	S_{BET} (m^2/g)	V_t (cm^3/g)	V_{mic} (cm^3/g)	V_{mes} (cm^3/g)	S_{mic} (m^2/g)	S_{mes} (m^2/g)	Average Pore Size (nm)	CO_2 Capture Conditions for Pure CO_2 Gas Flow	CO_2 Capture Capacity (mmol/g)	Reference
KOH activated petroleum coke	1445	0.52	-	-	-	-		0 °C and 1 bar 25 °C and 1 bar	6.41 4.57	[127]
Urea modified and KOH activated petroleum coke	1394	0.52	-	-	-	-	-	25 °C and 1 bar	4.4	[193]
KOH activated petroleum coke	1433	0.6	-	-	-	-	-	25 °C and 1 bar	3.68	[10]
$NaNH_2$ activated petroleum coke	1666	0.66	-	-	-	-	-	0 °C and 1 bar 25 °C and 1 bar	5.93 3.84	[180]
KOH activated petroleum coke	1470	0.6	-	-	-	-	-	0 °C and 1 bar 25 °C and 1 bar 50 °C and 1 bar	6.7 4.17 2.45	[146]
KOH activated asphalt	4200	2.4	-	-	-	-	2.4	25 °C and 54 bar	35	[130]
KOH activated Iranian asphalt	2186	1.3	0.25	1.05	-	-	2.37	25 °C and 1 bar 35 °C and 1 bar	11.37 38.49	[7]
KOH activated carbon fibers from anthracene oil-based pitch	1294	0.6	-	-	-	-	-	25 °C and 1 bar	3.5	[166]
Phenolic resin electrospun carbon fibers	650	0.277	0.249	-	-	-	-	25 °C and 1 bar	2.92	[153]
CO_2 activated Resorcinol–formaldehyde-derived carbon	1458	0.647	-	-	-	-	-	25 °C and 1 bar	4.54	[178]
KOH activated phenolic resin spheres	2130	1.1	0.78 (71%)	-	-	-	-	0 °C and 1 bar	6.6	[134]
Urea modified and KOH activated phenolic resin-derived carbon	1404	0.53	-	-	-	-	-	25 °C and 1 bar	4.61	[196]
KOH activated commercial phenolic resin	1040	0.37	-	-	-	-	-	0 °C and 1 bar 25 °C and 1 bar	4.12 5.66	[177]
KOH activated resorcinol–formaldehyde spheres	1235	0.67	0.52	1084	-	-	-	25 °C and 1 bar	4.83	[4]

Table 8. *Cont.*

Porous Carbon Material	S_{BET} (m^2/g)	V_t (cm^3/g)	V_{mic} (cm^3/g)	V_{mes} (cm^3/g)	S_{mic} (m^2/g)	S_{mes} (m^2/g)	Average Pore Size (nm)	CO_2 Capture Conditions for Pure CO_2 Gas Flow	CO_2 Capture Capacity (mmol/g)	Reference
$NaNH_2$ activated phenolic resin	1924	0.71	-	-	-	-	-	0 °C and 1 bar 25 °C and 1 bar	4.57 7.13	[185]
Urea modified and KOH activated phenolic resin-derived carbon	1482	0.56	-	-	-	-	-	25 °C and 1 bar	5.01	[173]
CO_2 activated cellulose	1249	0.53	0.4	-	-	-	-	0 °C and 0.15 bar 0 °C and 1 bar	1.96 5.52	[117]
KOH activated chitosan	1746	-	-	-	-	-	-	0 °C and 1 bar 25 °C and 1 bar	6.37 3.91	[187]
KOH activated chitosan	3226	1.35	-	-	-	-	3.91	0 °C and 1 bar	8.3	[88]
Potassium citrate activated chitosan	2278	1	63%	-	-	-	0.56 0.73	0 °C and 30 bar	22	[189]
Potassium citrate activated chitosan	1784	0.78	74%	-	-	-	0.56 0.66	0 °C and 1 bar	6.1	[189]
CO_2 activated carbon aerogel by cellulose	1364	1.43	0.37	-	-	-	-	25 °C and 1 bar	3.42	[179]
KOH activated lignin	1788	0.91	0.49	-	-	-	-	0 °C and 1 bar 25 °C and 1 bar	8.2 4.8	[161]
KOH activated EHL	2870	2.02	0.7	1.32	1000	-	2.8	30 °C and 1 bar	1.31	[141]
KOH activated starch-based packing peanut	1354	0.551	0.539	-	1235	-	-	0 °C and 1 bar 25 °C and 1 bar 50 °C and 1 bar	6.51 4.07 2.35	[138]
KOH activated waste wool	1352	0.78	0.54	-	-	-	-	25 °C and 1 bar	2.78	[164]
KOH activated starch	1636	0.51	-	-	-	-	-	0 °C and 1 bar 25 °C and 1 bar	7.49 3.84	[49]
CO_2 activated starch	3350	1.75	1.67	-	3281	-	-	25 °C and 20 bar	1.2	[145]
KOH activated chitin aerogel	521	0.19	-	-	-	-	-	0 °C and 1 bar 25 °C and 1 bar	5.02 3.44	[52]
KOH activated polypyrrole	941	-	0.34	-	-	-	-	25 °C and 0.1 bar 25 °C and 1 bar	1.42 4.5	[135]

Table 8. *Cont.*

Porous Carbon Material	S_{BET} (m^2/g)	V_t (cm^3/g)	V_{mic} (cm^3/g)	V_{mes} (cm^3/g)	S_{mic} (m^2/g)	S_{mes} (m^2/g)	Average Pore Size (nm)	CO_2 Capture Conditions for Pure CO_2 Gas Flow	CO_2 Capture Capacity (mmol/g)	Reference
KOH activated waste CDs and DVDs	2710	1.27	91%	-	-	-	-	0 °C and 1 bar 25 °C and 1 bar	5.8 3.3	[154]
PILs as the precursor and C_3N_4 nanosheets	1120	2.28	-	-	-	-	-	0 °C and 1 bar	4.37	[159]
KOH activated PIL	1742	1.415	1.078	-	1392	-	-	0 °C and 1 bar 25 °C and 1 bar	6.2 4.5	[157]
Chitosan grafted graphene oxide aerogel	33.32	0.129	-	-	-	-	-	25 °C and 1 bar	0.2579	[152]

(Note: S_{BET}; Specific surface area, V_t; Total pore volume, V_{mic}; Micropore volume, V_{mes}: Mesopore volume, S_{mic}; Micropore volume, S_{mes}; Mesoporous volume).

3.3. Importance of Textural Properties in CO_2 Capture by Carbon-Based Adsorbents

During physisorption, the textural properties, including the size of the micropores, micropore fraction, total pore volume, pore size distribution, and the surface area, play critical roles in attaching the CO_2 molecules onto the adsorbent surface. Various studies have shown the importance of textural properties in controlling the adsorption process.

The majority of previous studies have reported that microporosity is the primary governing factor for effective CO_2 adsorption. On the contrary, it is also believed that the physical textural properties, including open 3D mesoporous and microporous interconnected structure, are favorable for the rapid diffusion of the CO_2 gas molecules and faster mass transfer rates [15,50,141] while improving the accessibility of micropores in the adsorbent [50,96]. Most of the studies have revealed that the narrow micropore volume provides a greater contribution in the CO_2 capture performance [21,32,34,76,81,130,157,166,178,186,196]. Besides, some of the research groups have proven that the combined effects of surface area and microporous structure [3,24,25,34,39,62,78,140,143,145,146,161,179,188], ultramicropore volume, and narrow pore size distribution [50], surface area/pore volume, and ultramicroporous surface area/volume [101], pores size distribution and surface area [49,161], specific surface area along with pore size and pore volume [49,142,146,150,153,157,159,172,189,192], surface area, pore volume, and void fraction [24], microporous fraction, pore size, and pore size distribution [151,180], surface area along with both micropores and mesopores [179], and large mesopores and narrow pore size distribution peaks [56] are responsible for the high CO_2 gas capture performances.

The researchers have also stated that the presence of fine micropores below 1 nm is responsible for CO_2 adsorption on porous carbon materials [15,76,88,101,134,141,153,163,187] since the pores in the range of two or three times larger than the kinetic diameter of CO_2 molecules are the most suitable candidates for adsorption of CO_2 gas molecules onto pores [143].

Several studies have conducted mathematical modelling and further research work to determine the exact micropore size that plays the dominant role in capturing the CO_2 gas molecules. For instance, the micropores in the range of 0.43–0.78 nm [88], pore widths less than 0.86 and 0.7 nm [76,156], pores in the range of 0.5–0.7 nm [143], micropores with 0.5 nm size [49,55,91], small micropores below 0.7 nm [161,171], pore sizes less than 0.8 nm [10,146,155], narrow micropores centered at 0.52 and 0.84 nm [164], pore size with 0.97 nm [46], ultramicropore sizing 0.5–0.63 nm which is approximately 2 times greater than that of the kinetic diameter of CO_2 gas molecules (0.3 nm) [153], pore sizes ranging from 0.6–0.9 nm [101], pores in the range of 0.48–0.79 nm [34], and ultramicropores smaller than 0.44 nm [50].

Apart from the above, several studies have also examined the textural properties responsible for adsorbing CO_2 gas molecules onto sorbent at specified pressures and temperatures. For instance, Rao et al. [182], Liu et al. [183], Rao et al. [184], and Liu et al. [177] have stated that the synergetic effect of a large number of narrow micropores and narrow pore size distribution is responsible for better CO_2 gas capture performance at 1 bar and 25 °C. Kamran, Choi, and Park [34] have reported that the ultramicropores below 0.7 nm provide effective active sites for CO_2 adsorption below 1 bar. In contrast, the results have indicated that the micropores are the better indicators for CO_2 sorption at room temperature and ambient pressure [48,173]. Moreover, the remarkable CO_2 adsorption capacities at 0 and 25 °C were attributed to the most significant micropore volume of the sorbent materials [4]. In contrast, the small micropores govern the CO_2 capture performances at 0 °C and 800 mmHg and 25 °C and 850 mmHg [154]. Furthermore, the research groups have also claimed that small micropores contribute mainly to CO_2 capture at high temperature and low pressure, total pore volume is responsible for CO_2 adsorption capacity at 50 bar [156], the micropores in the range of 0.7–0.9 nm are favorable for CO_2 capture at low pressure [143], micropores/small mesoporous specific surface area is a better indicator for low pressure CO_2 capture [56,117], mesopores are found to play a major role in high pressure CO_2 gas adsorption [7,101], micropores with pore width less than 0.86 nm are

favorable for CO_2 capture at 0 °C and 1 bar, while pore width less than 0.7 nm provides greater contribution for carbon capture at 25 °C [76,156], volume of the narrow micropores are good candidates for carbon capture at 0 °C and 1 bar [32], micropore contribution is the major factor controlling the CO_2 adsorption at 0.15 bar [78], high specific surface area plays a prominent role for high pressure CO_2 gas capture [145], the pores of 0.8 nm are slightly higher than twice the CO_2 gas kinetic dimeter, which governs the CO_2 adsorption capacity of the sorbents at 101.3 kPa [101], pores with diameters smaller than 4 nm contribute mainly for carbon capture at 25 °C and 30 bar, the ultramicropores less than 0.5 nm play a vital role for CO_2 adsorption capacity at 0 °C and 0.1 bar. A similar contribution was found for a notable CO_2 gas capture performance at 25 °C and 0.1 bar with pore sizes of 0.37 nm and 0.83 nm [59], both the pore size and pore size distribution determine the CO_2 gas adsorption capacity for porous carbons at 25 °C and 1 bar [180], both the specific surface area, and the total pore volume is eligible for CO_2 gas molecules capture at 0 °C [172]. On the contrary, the CO_2 adsorption capacity of some of the porous carbon sorbents is said to be directly related to the specific surface area [73,142,143,158,189].

3.4. Selectivity of CO_2 over Other Gases and Moisture

Numerous studies have explored the selectivity of CO_2 over other gases such as N_2, CO, and CH_4, and the selectivity values of previous studies are summarized in Table 9. According to the previous studies, both the textural properties and the surface functional groups are responsible for better selectivity of CO_2 over other gases [4,55,58,88,117,135,158,172,200].

Table 10 enumerates the physical properties related to gas molecules associated with the selective adsorption of CO_2. It is reported that the ultramicropores centered at 0.34–0.39 nm are the best candidates for selective CO_2 adsorption due to the contribution of the molecule sieve effect. As the kinetic diameter of the CO_2 molecule is the most minor compared to other gases (Table 10) [57], it is easier for it to access the porous structure [25,54,57,59,88,164]. Furthermore, the better CO_2 separability can also be attributed to the higher polarizability and quadrupole moments of CO_2 than other gas components, as enumerated in Table 10. Such a process can induce more vital Van der Waals forces between the carbon chain of the adsorbent surface and the gas molecules [4,25,34,46,86,146,164,191].

The CO_2/N_2 selectivity could be enhanced by self-doped nitrogen functionalities on the adsorbent surface [24,55,62,88,135]. Strong interactions between the acidic CO_2 (Lewis acid) molecules and the basic N-containing functional groups [21,114,127,181,193] are expected. The oxygen-containing functionalities such as carboxylic and hydroxyl groups could also lead to strong H-bonding and electrostatic interactions with the CO_2 molecules [4,45,47,55,181]. Apart from the CO_2/N_2 selectivity, the N-containing functional groups also play critical roles in separating CO_2/CH_4 mixtures [125]. When sulfur exists in the oxidized form (-SO or -SO_2), the negatively charged oxygen also possesses a high affinity towards CO_2 gas molecules, and thus, the CO_2 separability is enhanced [10].

Several research groups have investigated the effect of CO_2 capture behavior in water vapor and impurity gases, including NO_2, SO_2, and NO. Polypyrrole-derived porous adsorbent demonstrated a CO_2 adsorption capacity of 0.71 and 0.54 mmol/g at 50 °C under dry and humid conditions, respectively. Interestingly, the authors also explored the capture capacity under simulated flue gas conditions, and a 14% reduction of CO_2 uptake was observed compared to the pure CO_2 adsorption capacity [135]. Furthermore, Park et al. [155] have stated that the reduction in CO_2 uptake capacity compared to dry CO_2 is due to the competitive adsorption of H_2O onto the adsorbent surface. Wang et al. [185] have investigated the influence of moisture on CO_2 gas capture performance by flowing the gas stream through a bottle of water to achieve a moist gas mixture with a relative humidity of 28% at room temperature. According to the experimental data, a negative impact on CO_2 adsorption capacity was observed in the presence of water valuing 0.94 mmol/g (under humid conditions) and 0.86 mmol/g (under dry conditions), and such reduction in CO_2 capture capacity was ascribed to the competitive adsorption between CO_2 gas and H_2O [185].

Table 9. The selectivity of CO_2 gas over other gases for various carbon adsorbents.

Porous Carbon Material	Gas Mixture	Selectivity Value	Pressure (Bar)	Temperature (°C)	Reference
Biomass-derived porous carbon					
Cork dust-derived porous carbon	CO_2/N_2 (15/85 *v/v*%) gas mixture	7	1	25	[76]
KOH activated starch-based sorbent		16	1	25	[32]
Algae-derived porous carbon		69.7	Ambient	Ambient	[62]
$ZnCl_2$ activated poplar catkin		22	1	25	[101]
Date sheets-derived porous carbon		41.53	1	25	[143]
Coconut shell-based activated carbon	CO_2/N_2 (10/90 *v/v*%) gas mixture	22	1	25	[81]
Rise husk-derived activated carbon		63	Ambient	Ambient	[50]
Rise husk-derived activated carbon		7.6	1	25	[92]
Taihu blue algae-derived porous carbon		39.3	1	25	[176]
Mangosteen peel-based activated carbon		12	1	25	[165]
Hazelnut shell-based porous carbon		17	1	25	[181]
Lotus leaf-derived activated carbon		21	1	25	[183]
Lotus stalk-derived activated carbon		22	1	23	[182]
Water chestnut shells-derived activated carbon		23	1	25	[184]
Pine sawdust-based sorbent		26.7	Ambient	Ambient	[55]
Palm kernel shell-derived activated carbon		7	Ambient	Ambient	[86]
N-saline algae-derived porous carbon	CO_2/CH_4 (50/50 *v/v*%) gas mixture	5.5	Ambient	Ambient	[61]
Palm kernel shell-derived activated carbon		1.7–2.5	0–1.1	25	[59]
Biopolymer-derived porous carbon					
Cellulose-derived porous carbon	CO_2/N_2 (15/85 *v/v*%) gas mixture	41.8	1	25	[117]
Starch-based peanut packaging-derived activated carbon		15–38	1	25	[138]
Cornstarch-based activated carbon		59–135	0–1	0	[46]
Waste wool-activated carbon		16	1	25	[164]

Table 9. *Cont.*

Porous Carbon Material	Gas Mixture	Selectivity Value	Pressure (Bar)	Temperature (°C)	Reference
Chitosan-derived porous carbon	CO_2/N_2 (10/90 *v/v*%) gas mixture	12–25	1	25	[187]
Chitosan-derived porous carbon		17–69	1	25	[88]
Lignin-derived porous carbon		21.8	1	25	[161]
Starch-derived porous carbon		98	1	25	[49]
Fossil resources-derived porous carbon					
Petroleum coke-derived porous carbon	CO_2/N_2 (10/90 *v/v*%) gas mixture	17	1	25	[180]
Petroleum coke-derived porous carbon		25	1	25	[193]
Petroleum coke-derived porous carbon		22	1	25	[127]
Coal tar pitch-based sorbent		23.8	1	25	[186]
Tar pitch and coal powder-derived porous carbon		5.94	1	25	[168]
Petroleum coke-derived porous carbon	CO_2/N_2 (15/85 *v/v*%) gas mixture	13.7	1	25	[10]
Iranian asphaltene-derived porous carbon		22.74	1	25	[7]
Graphene-derived porous carbon					
Graphene oxide-based porous carbon	CO_2/N_2 (10/90 *v/v*%) gas mixture	12	1	25	[32]
Graphene-based sorbent		53	1.03	25	[191]
Graphene oxide-derived porous carbon	-	162	Simulated flue gas conditions		[150]
	-	253	Natural gas fired power plant		
Synthetic resin-derived porous carbon					
Commercial phenolic resin-derived porous carbon	CO_2/N_2 (10/90 *v/v*%) gas mixture	48	1	25	[196]
Phenolic resin-derived activated carbon		17	1	25	[177]
Phenolic resin-derived activated carbon		14	1	25	[185]
Phenolic resin-derived porous carbon		19	1	25	[173]
Resorcinol–formaldehyde-derived porous carbon	CO_2/N_2 (15/85 *v/v*%) gas mixture	45	1	25	[4]
Phenol–formaldehyde-based porous sorbent		16.4	1	25	[201]

Table 9. *Cont.*

Porous Carbon Material	Gas Mixture	Selectivity Value	Pressure (Bar)	Temperature (°C)	Reference
Synthetic polymer-derived porous carbon					
Polypyrrole-derived porous carbon	CO_2/N_2 (10/90 *v/v*%) gas mixture	194	1	50	[135]
PIL-derived porous carbon		14	1	25	[157]
PIL-derived porous carbon		44	1	0	[197]
PVC-based sorbent		6.9	1	25	[61]
Triazine-based hyper cross-linked polymer-derived porous carbon		8.9–42.6	1	25	[172]
K_2CO_3 activated polyacrylonitrile-based sorbent material		33.6	1	0	[34]
PIL-derived porous carbon		43.69	1	25	[158]
Pyrrole-derived porous carbon		35	1.01	0	[171]
NaOH activated PET-derived porous carbon	CO_2/N_2 (15/85 *v/v*%) gas mixture	13.3–31.1	0–1	50	[23]
KOH activated PET-derived porous carbon	CO_2/CO gas mixture	9.09–18.94	0–1	50	[23]
Polyaniline-derived porous carbon	CO_2/CH_4 (10/90 *v/v*%) gas mixture	14.3	1	25	[58]

Table 10. Critical physical properties of gas molecules associated with the selective adsorption of CO_2 (Reprinted with permission from refs. [57,112,202]).

Gas Molecule	Kinetic Diameter (Å)	Dipole Moment ($\times 10^{-19}$ esu^{-1} cm^{-1})	Quadrupole Moment ($\times 10^{-26}$ esu.cm^2)	Polarizability ($\times 10^{25}$ cm^3)
CO_2	3.3	0	4.3	29.1
N_2	3.64	0	1.52	17.6
CO	3.76	1.1	-	19.5
CH_4	3.8	0	0	25.9

On the contrary, Plaza et al. [195] have noted that the maximum adsorption capacity of H_2O molecules is relatively lower in biochar developed from olive stones by air oxidation compared to zeolites and commercially available activated carbons. This behavior is beneficial for practical applications due to the lower moisture hold up during CO_2 capture operations. Apart from the above-mentioned facts, according to the breakthrough curves obtained for the ternary mixture of N_2, CO_2, and H_2O, it was observed that the adsorbent was initially saturated with H_2O, and this behavior confirmed that the adsorption of H_2O molecules is little influenced in the presence of CO_2 gas. However, the CO_2 adsorption capacity decreased with initially adsorbed H_2O. This behavior reflects that the CO_2 adsorption capacity of biochar derived from olive stones is highly influenced by the relative humidity of the gas stream. Additionally, a 64% reduction in CO_2 capture performance was observed under a gas stream with a relative humidity of 95% [195]. However, You and Liu [203] have stated that the absence of CO_2 gas and moisture slightly affect each other's adsorption performance on activated carbon.

On the other hand, according to Plaza et al. [204], it was stated that the biochar produced via single-step oxidation could preferentially adsorb CO_2 gas molecules over N_2 gas in both humid conditions and dry conditions. Interestingly, according to their observations, despite biochar adsorbing moisture, there was no significant decrease in CO_2 gas capture performance in humid conditions in the short time scale. Such behavior is due to the delayed adsorption of H_2O molecules [204].

3.5. Regeneration and Cyclic Stability of Porous Carbon Materials

Easy regeneration and long-term cyclic stability are of great importance for practical applications of a solid adsorbent [86,150]. The isosteric heat of adsorption (Q_{st}) demonstrates the strength between adsorbent–adsorbate interactions and reflects the energy required for adsorbent regeneration [21,181]. Q_{st} values that are too low are not favorable for CO_2 adsorption, whereas a Q_{st} that is too high is not beneficial during regeneration of the adsorbent. Therefore, a moderate Q_{st} value is preferred for effective CO_2 capture and an easy regeneration process for a particular adsorbent [21].

The research groups have adopted different types of regeneration procedures. For instance, Chang et al. [101], Rashidi, and Yusup, [86], Yu et al. [186], Politakos et al. [191], and Ganesan and Shaijumon et al. [170] have used pressure swing adsorption technology wherein the porous carbons were prepared via polyaniline. Coconut shells, polyaniline, petroleum coke, and hazelnut shells were heated at 200 °C for 6 h in a vacuum before the subsequent CO_2 adsorption cycle [59,81,88,180,181,191,205]. Additionally, the desorption tests for mangosteen peel-derived porous carbons were performed at 25 °C under 1 bar [15]. Furthermore, Xu et al. [117] have evaluated the desorption behavior via VSA and TSA strategies. In contrast, for chitosan-derived porous carbons, EHL-derived porous sorbents, PET-derived porous carbons, urea–formaldehyde, and resorcinol–formaldehyde resin-based porous carbon materials were degassed by mild heating at around 100–200 °C [3,42,134,141,189]. On the contrary, starch-based peanut packaging-derived porous carbons and petroleum coke-derived sorbents were quickly regenerated by alternatively switching the flowing gas stream to N_2 at 25 °C and 1 atm [11,138,146]. Moreover, An et al. [21] and Guo et al. [158] have carried out the desorption tests by heating the sorbent bed at 150 °C for 2 h in a vacuum to remove the previously adsorbed CO_2 gas. Apart from the above procedures, urea–formaldehyde [42,45] and resorcinol–formaldehyde [36] resin-derived porous carbons were degassed by raising the temperature of the sorbent sample to 200 °C and maintaining a purge nitrogen stream until the adsorbent was successfully regenerated.

Some of the previous studies have reported the stability of the prepared porous carbon materials up to several consecutive cycles. For instance, Zhang et al. [76] have stated that biomass cork dust-derived porous carbon material was stable up to 15 cycles, and 3D-ordered mesoporous carbon [114], bio tar-derived sorbent [24], coal tar pitch-derived porous carbon [186], petroleum coke-derived porous materials [127,193], EHL-derived sorbent [141], PIL-derived porous carbon [158], graphene-based monolith [191], polyurethane foam-derived porous carbon [156], cornstarch-based carbon sorbent [46], $NaNH_2$ activated lotus stalk-derived porous carbon [182], and KOH activated commercial phenolic resin-based carbon [177] were stable up to 5 adsorption–desorption cycles. The CO_2 uptake amount was almost unchanged, even at the eighth cycle for the poplar catkin-derived porous carbon [23], asphaltene-based sorbent [89,180], chitosan-derived porous carbons [88,164], and waste wool-derived carbon sorbent [164]. Date sheet-derived sorbent material [143], PET-derived porous carbon [3], polyacrylonitrile-based sorbent [34], urea–formaldehyde, melamine–formaldehyde, and resorcinol–formaldehyde resins-derived carbon sorbent [13,36,45,103] were stable up to four consecutive cycles. A cyclic stability of up to 10 cycles for starch-based packaging material-derived activated carbon [138], petroleum coke-derived porous carbon [146], biochar-derived porous carbon [25], palm kernel shell-based activated carbon [86], graphene oxide-based porous carbon [150], PET-derived porous carbons [23], microporous carbon fibers [197], polypyrrole-derived sor-

bent [135], graphene-based sorbent material [157], and PIL-based porous carbons [157,159] was reported. Cyclic stability of up to seven cycles for petroleum coke-derived sorbent [10] was reported. It is reported that graphene oxide/magnesium oxide nanoparticle composite could withstand up to 16 consecutive adsorption–desorption cycles [192]. The cyclic stability of synthetic polymer-based sorbent [205] and triazine-based hyper crosslinked polymer-derived porous carbon [172] were noted up to six cycles. The cyclic stability of phenolic resin-derived porous carbon was only up to three consecutive cycles [153]. Besides, Yang et al. [81], Wang et al. [176], Liu et al. [181], Tehrani et al. [7], and Rao et al. [180] have reported only a loss of original CO_2 capture capacity by 2.4, 6, 5, 1.08, and 7.95% after 10, 7, 5, 4, and 5 consecutive runs, respectively. Moreover, a CO_2 adsorption capacity loss of 4 [196] and 5% [21] were reported for commercial phenolic resin-derived porous carbon at the fifth cycle. Apart from the above, for cellulose-derived porous carbon materials, the CO_2 capture capacity was reported to be stable up to 10 cycles during PSA cyclic adsorption tests. In contrast, the cyclic stability was maintained for the TSA process up to 11 cycles [117]. Furthermore, according to Wang et al. [185], the sodium amide-activated phenolic resin-derived porous carbon was stable up to 8 consecutive cycles with a loss of 5.4%. In contrast, a loss of 5% in the original CO_2 gas capture capacity at the 5th adsorption–desorption cycle was reported by Rao et al. [184].

Besides, Plaza et al. [195] and Plaza et al. [204] have reported that the low H_2O adsorption capacity at relatively lower pressures for biochar prepared from olive stones is advantageous from an economic point of view during operation, since a relatively smaller reduction in pressure during PSA or a small increase in the temperature during TSA processes causes a notable reduction in relative humidity of the gas stream which is capable of reducing the equilibrium adsorption capacity of H_2O molecules [195]. On the other hand, a simulation study to investigate the effect of humidity on the amount of CO_2 recovery during regeneration studies was conducted by You and Liu [203]. According to their observations, the CO_2 recovery rate declined with the increase of relative humidity of the feed gas conditions. The trend of decrease is more minor at lower relative humidity values. In contrast, a notable decrease in CO_2 recovery rate was observed under high relative humidity values. Based on the simulations, it was recommended to maintain the relative humidity of the feed gas stream in the range of 40.00% and 50.00% while maintaining the feed gas temperature in between 313 and 333 K in order to achieve a CO_2 recovery rate in the range of 82.29% and 97.08%. Moreover, the simulation studies have also recommended maintaining the feed gas temperature below 333 K when the H_2O concentration in the feed gas stream is 10.50% (high moisture concentration) and below 323 K when the moisture composition in the feed gas stream is 4.6% (under low H_2O concentration), where high recovery rates of 81.36% and 90.92% could be obtained, respectively. Additionally, a significant inhibitory effect on the CO_2 adsorption and recovery rates was observed at high humidity conditions [203].

Interestingly, it was reported by Politakos et al. [191] that the mechanical stability and the morphological structure of the graphene-based carbon monolith were well retained, even after five cycles. Nevertheless, PIL-derived carbon sorbent exhibited a loss of 8% of the original capture capacity. This loss was attributed to the blocked particles of common high boiling point impurities, such as water [157].

Even though the estimation of cost or energy associated with adsorbent regeneration is of paramount importance from a cost and practicality point of view, a minimal number of studies have reported the estimated cost and energy requirements. For example, the energy required for degassing 1 kg of CO_2 from KOH activated PET-derived porous carbon was estimated to be 1.21 MJ [3], while for resorcinol–formaldehyde-derived porous carbons, the energy associated with CO_2 desorption was noted as 1.82 MJ/kgCO_2 [45]. Furthermore, Tiwari, Bhunia, and Bajpai [42] have also estimated that the energy required to desorb 1.26 mol/g of adsorbed CO_2 is 0.073 MJ.

4. CO_2 Chemisorption Using Amine-Functionalized Porous Carbon Materials

4.1. Importance of Chemisorbents

Even though porous carbon-based materials which adsorb CO_2 molecules via physisorption exhibit remarkable CO_2 capture capacities and easy regenerability, the selectivity of CO_2 over other gas molecules is poor, and the presence of moisture hinders the CO_2 capture performance [57,206]. To overcome these significant drawbacks, research groups have suggested increasing the basic nature of the adsorbent surface to make the capture of acidic CO_2 molecules relatively easier [57]. Therefore, the amine-functionalization of porous carbon materials has become a common practice to enhance the basicity of adsorbents [57,118,207]. Such a process could enhance the separability of CO_2 in the presence of other gases owing to the highly favorable CO_2–amine interactions [111]. Generally, amine-functionalized porous carbon materials can be categorized into two major types based on their preparation methods [208,209]: (i) amine-impregnated porous sorbents where the amine groups and the carbon support interact via Van der Waals forces [53,111,208] and (ii) amine-grafted porous supports where the amine species and the support are covalently bonded [118,207].

Interestingly, amine functionalization on porous carbon supports offers some advantages over absorption of CO_2 using alkanolamines, such as reduced corrosion problems due to decreased contact between amines and the equipment [209], solids being easy to handle, and most importantly, reduced energy consumption for regeneration due to the lower heat capacity of solid sorbents compared to that of water [57,206,210,211].

Of the different carbon-based porous supports, graphene and carbon nanotubes (CNTs) are receiving much attention owing to their remarkable properties such as unique molecular structure, huge specific surface area, tunable textural properties, better thermal and mechanical stability, good thermal conductivity, and most importantly, better accessibility to surface functionalization [38]. Chemical functionalization of CNTs can be categorized into two major divisions: (i) functionalization from inside and (ii) functionalization from outside [9].

Alkanolamines can be divided into three major types, namely, (i) primary amines, (ii) secondary amines, and (iii) tertiary amines [57,95]. The amine reactivity follows the order of primary > secondary > tertiary. This order reflects the critical role of the number of protons attached to the N atom in determining the amine reactivity towards the acidic CO_2 molecules [57,212]. It is a well-known fact that the CO_2 molecules possess acidic nature, and thus, they undergo acid-base interactions with the amine functional groups. The zwitterion mechanism was initially proposed by Caplow, followed by reintroduction by Danckwerts [87,112,113,211]. The Zwitterion mechanism is often used to explain the reaction between CO_2 molecules and primary/secondary amines [2,87,112,211]. Such a mechanism generally involves two primary steps: (i) formation of an intermediate zwitterion where the lone electron pair of amines first attaches to the carbon atom of the CO_2 molecule, and (ii) deprotonation of the zwitterion by the base to produce ammonium carbamate [82,104,112,211–214]. The two steps involved in the zwitterion mechanism are presented in Figure 5.

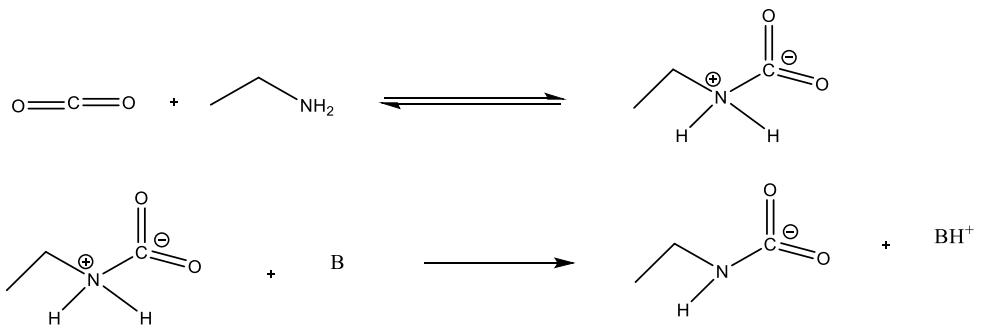

Figure 5. Reaction steps involved during zwitterion formation (Reprinted with permission from ref. [107]).

The tertiary amines react with CO_2 gas molecules differently in the presence of moisture, where the reaction mechanism involves base-catalyzed hydration of CO_2 to yield bicarbonates [104,113,213,214]. The overall reactions between CO_2 gas molecules and primary amines (Reaction (2)), secondary amines (Reaction (3)) at anhydrous conditions, and tertiary amines (Reaction (4)) are as follows, where R_1, R_2, and R_3 are aryl/alkyl groups [115,118].

$$CO_2 + 2R_1NH_2 \leftrightarrow R_1NH_3{}^+ + R_1NHCOO^- \quad (2)$$

$$CO_2 + 2R_1R_2NH \leftrightarrow R_1R_2NH^+ + R_1R_2NCOO^- \quad (3)$$

$$CO_2 + R_1R_2R_3N + H_2O \leftrightarrow R_1R_2NH^+ + HCO_3{}^- \quad (4)$$

According to the stoichiometry of the above reactions, only one mole of CO_2 can react with two moles of amine in dry conditions, while under humid conditions, one mole of CO_2 can adequately be chemisorbed to one mole of amine [48,82,112,113]. On the other hand, the amount of chemisorbed CO_2 gas molecules is enhanced in the presence of moisture due to the formation of bicarbonates [37]. Apart from the above, from an industrial point of view, amine efficiency is vital to determining the deployment of a particular sorbent material for CO_2 capture [195]. Usually, the amine efficiency is defined as the normalized capacity of adsorbed CO_2 gas per N content (mmol CO_2/mmol N) [195,207]. Moreover, the maximum theoretical amine efficiency at anhydrous conditions is 0.5 mol CO_2/mol (primary/secondary) amine [213], and it is reported to be improved to 1 mol CO_2/mol (primary/secondary) amine under humid conditions [48,207,213].

4.2. CO_2 Capture by Amine-Impregnated Carbon-Based Adsorbents

During amine impregnation, the sorbent material is prepared by physically loading any kind and amount of amine species onto or into support surfaces [112,118]. However, amine loading is limited by the available pore volume [118]. The type of amine species to be impregnated depends on the amine molecule size, molecular weight of the amine, sorbent dimensions including pore volume, pore size distribution, and regeneration conditions [214]. Among the available amine species, polyethyleneimine (PEI) is the primary functionalization agent being used by numerous researchers [118]. In contrast, the wet impregnation method has been widely used during amine impregnated porous carbon synthesis due to several advantages, such as accessible synthesis routes under mild synthesis conditions [215]. Amine-impregnated sorbent materials have been suggested to be used at temperatures between 60–70 °C. At the same time, it is also reported that the regeneration temperature should be kept below 250 °C since, if the amine decomposition occurs, the adsorbent cannot be reused [216].

The type of carbon support is a significant factor that should be considered during the preparation of amine impregnated sorbents. According to the literature, it is stated that mesoporous carbon supports are the better candidates for amine impregnation since they are capable of providing a large surface area to accommodate a large number of amines [110,217]. In contrast, if microporous supports are used, it may cause diffusion limitations owing to pore blockage by chemical species [26,218]. On the contrary, 2D materials are the most promising candidates for the synthesis of amine-functionalized solid sorbents as the amine loading is limited in solid sorbents that possess cylindrical or slit-like pores [219]. Overall, it is reported that the large pore width is helpful for amine dispersion, while higher pore volume is required to maximize the amine loading [210].

From an industrial point of view, amine-impregnated sorbents possess distinct advantages over amine-grafted sorbents owing to their easy synthesis [220], easy implementation on a large scale [207,219], decreased corrosion problems [85], and the possibility to synthesize adsorbents with high amine capacities [205,207,210,219].

Figure 6 demonstrates the pore structure before amine loading and the occurred pore blockage after amine loading. Despite their advantages, the amine-impregnated porous carbons exhibit several disadvantages, including pore blockage without penetrating the amine species into internal deeper pore spaces as illustrated in Figure 6b [206,217,218,221–223],

limited CO_2 gas diffusion [210,217], amine leaching during adsorption and regeneration processes which hinders the reusability of the adsorbents [212,224], amine volatilization/emissions [37,225], and long term stirring during amine impregnation, which destroys the macroporous structure of the carbon support [37] and limits their applications.

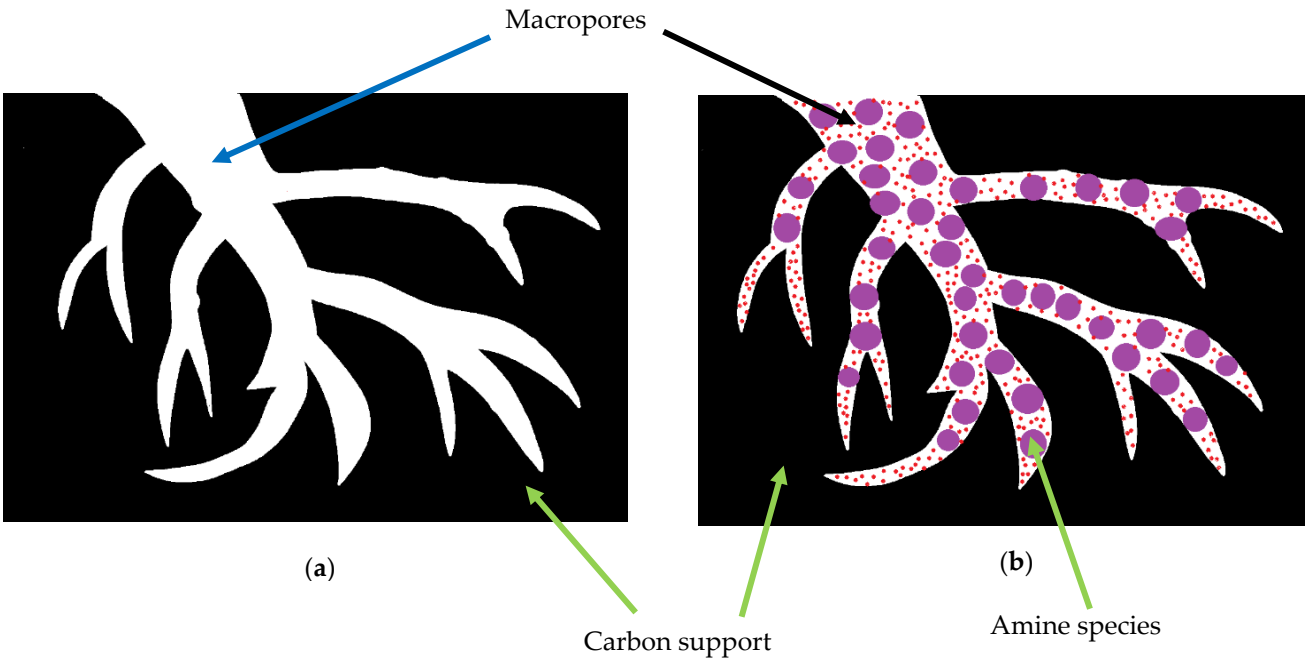

Figure 6. Pore structure of (**a**) non-impregnated porous carbon support and (**b**) amine-functionalized carbon with blocked pores (Reprinted with permission from ref. [226]).

4.2.1. Synthesis of Amine-Impregnated Porous Carbon Adsorbents

The chemical structures of the amines used to functionalize carbon supports are depicted in Figure 7.

During the synthesis of amine-impregnated porous carbon adsorbents, the use of the wet impregnation method has been extensively reported by several researchers for monoethanolamide (MEA), Piperazine (PZ), and 2-amino-2-methyl-1-propanol (AMP) impregnated sea mango-derived activated carbon [226]. Monoethanolamine (MEA) and diethanolamine (DEA) impregnated $ZnCl_2$ activated green coconut shell-derived porous carbon [206]. EDA and triethylenetetramine (TETA) impregnated mesoporous carbon [110], pentaethylenehexamine (PEHA) loaded chitosan-derived mesoporous carbon [210], tetraethylenepentamine (TEPA), monoethanolamine (MEA), diethanolamine (DEA), PEI and diethylenetriamine (DETA) impregnated wood ash [70], triethanolamine (TEA) functionalized KOH activated Jatropha curcas shell-based activated carbon [224], MEA impregnated corn and potato starch-derived porous carbon sorbents [227], DEA impregnated activated carbon [211], PEI impregnated mesoporous carbon microparticles and mesoporous carbon nanospheres (as shown in Figure 8a) [207], PEI functionalized graphitic carbon nitride [228], MEA and DEA impregnated activated carbon [216], DEA and MEA incorporated $ZnCl_2$ activated fresh green coconut shell-derived activated carbon [87], TEPA functionalized semi coke [228], EDA, DEA, TETA, and branched PEI impregnated porous carbon [218], PEI-functionalized MWCNTs [217], TEPA impregnated on MOF-derived carbon monolith [93], porous silica-coated MWCNTs prepared via nanocasting and PEI impregnation [223], branched PEI impregnated on graphene oxide [229], TEPA impregnated onto graphene and silica containing aerogel [194], and TEPA impregnated carbon aerogels prepared via sol–gel process [215]. The structure of amine-functionalized mesoporous carbons synthesized via physical impregnation of PEI is demonstrated in Figure 8a.

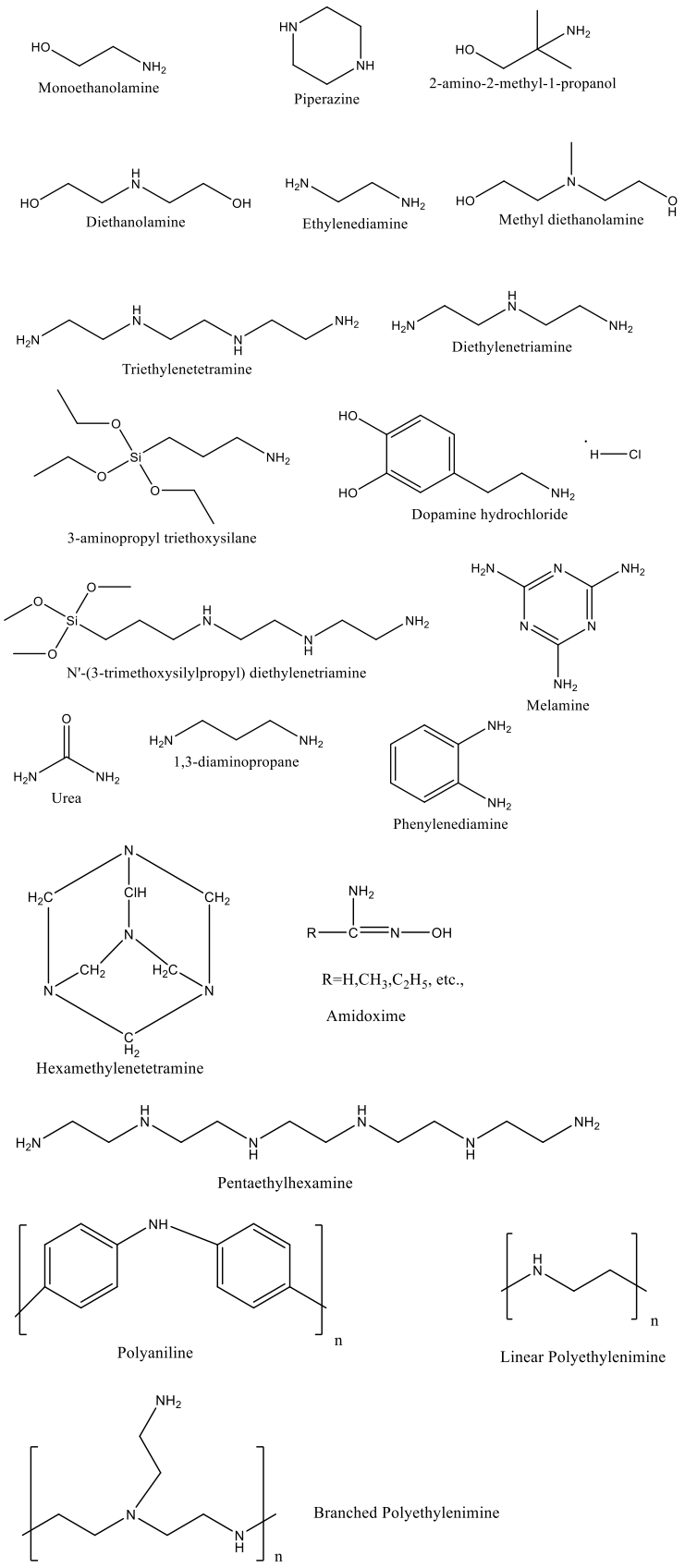

Figure 7. Chemical structures of the amine species used for functionalizing the porous carbon materials.

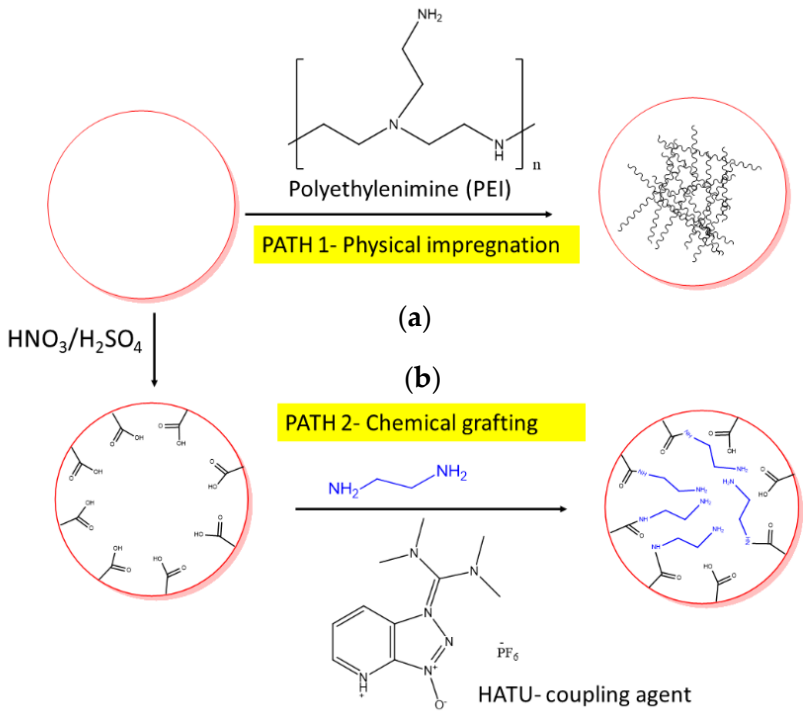

Figure 8. The structure of amine functionalized mesoporous carbons by (**a**) Physical impregnation of PEI, and (**b**) Chemical grafting of EDA (Reprinted with permission from ref. [206]).

Apart from the above, several other synthesis procedures are as follows. Activated methyl diethanolamine was impregnated onto mesoporous supports using a soft template [230]. The urea–KOH method was used to fabricate amine-impregnated sugarcane bagasse [44]. A suspension polymerization assisted sol–gel method, involving colloidal silica as the hard template, can be used to synthesize the PEI-functionalized mesoporous carbon spheres [108]. Wang et al. [62] prepared PEI impregnated mesoporous carbon via a combination of hard templating and sol–gel methods. The EDA-functionalized graphene oxide was synthesized through simultaneous self-assembly and reduction of graphene oxide in an aqueous solution which contains EDA via a low-temperature hydrothermal method, and 3D graphene aerogels were also fabricated by adopting a one-step approach which involves modification with EDA and gelation by hydrothermal reduction, followed by subsequent lyophilization [231].

4.2.2. CO_2 Adsorption Capacities of Amine-Impregnated Porous Carbon Materials

The comparison of CO_2 adsorption capacities of amine-functionalized materials is presented in Table 11. The behavior of CO_2 adsorption capacities of amine-impregnated porous carbon supports with the variation of temperature, pressure, CO_2 feed gas concentration, and amine loading has been extensively studied by various research teams. Even though Alhassan et al. [224] could observe an increase in CO_2 adsorption capacity with the increase in amine loading for a TEA-impregnated Jatropha curcas shell-derived activated carbon, Chai [232], Faisal et al. [110], and Shin, Rhee, and Park, [229] have reported a decline in CO_2 adsorption capacity with the increase of amine loading since the bare surface of the porous carbon support might be clogged by extra amine species, resulting in more diffusional resistance while reducing the accessibility of CO_2 molecules towards the chemisorption sites [207,229]. Moreover, the results of the study carried out by Faisal et al. [110] have suggested that the optimum TETA loading of 30 wt % could exhibit remarkable CO_2 capture capacities with minimum pore blockage. Besides, according to Ali et al. [226], it has been stated that the CO_2 capture capacity of both diamines and sterically hindered amines are more significant compared to that of alkanolamines. Such a behavior can be attributed to the two N-atoms in diamine, which could double the CO_2 uptake.

Table 11. CO_2 adsorption capacities of the amine-functionalized porous carbon materials.

Support	Amine Attaching Method	Amine Type	CO_2 Capture Conditions for Pure CO_2 Gas Flow		CO_2 Capture Capacity (mmol/g)	Reference
			Temperature (°C)	Pressure (bar)		
Sea mango activated carbon	Impregnation	Monoethanolamine	25	1	0.52	[226]
	Impregnation	Piperazine	25	1	0.66	
	Impregnation	2-amino-2-methyl-1-propanol	25	1	0.25	
Green coconut shell-based activated carbon	Impregnation	Monoathanolamine	25	1	0.84	[206]
	Impregnation	Diethanolamine	25	1	0.46	
Mesoporous carbon	Impregnation	Ethylenediamine	27	1	19.68	[110]
	Impregnation	Triethylenetetramine	27	1	11.24	
Carbon nanotubes	Grafting	Polyaniline	17	1	6.3	[233]
Chitosan-derived mesoporous carbon	Impregnation	Pentaethylhexamine	100	1	3.27	[210]
Mesoporous carbon	Impregnation	Methyl diethanolamine	27	0.07	2.63	[230]
Sugarcane bagasse	Grafting	Ethylenediamine	25	1	2.2	[225]
	Grafting	Diethylenetriamine	25	1	2.08	
	Grafting	Tetraethylenepentamine	25	1	2.79	
	Grafting	Triethylenetetramine	25	1	2.68	
Activated carbon	Impregnation	NH_2-Cl	0	1	3.069	[222]
			25	1	1.95	
	Impregnation	3-aminopropyl triethoxysilane	0	1	2.433	
			25	1	1.762	
	Impregnation	Dopamine hydrochloride	0	1	0.429	
			25	1	0.389	
Mesoporous carbon microparticles	Grafting	Ethylenediamine	30	1	0.75	[207]
			75	1	0.37	
	Impregnation	Polyethylenimine	30	1	0.82	
			75	1	0.40	

Table 11. *Cont.*

Support	Amine Attaching Method	Amine Type	CO_2 Capture Conditions for Pure CO_2 Gas Flow		CO_2 Capture Capacity (mmol/g)	Reference
			Temperature (°C)	Pressure (bar)		
Multiwalled carbon nanotubes/Cd-nanozeolite composite	Impregnation	Polyethylenimine	25	1	5.7	[2]
Graphite carbon nitride	Impregnation	Polyethylenimine	100	1	3.77	[229]
Waste tea activated mesoporous carbon	Grafting	Diethanolamine	30	1	33.57	[82]
KOH activated broom sorghum stalk-derived activated carbon	Grafting	Diethanolamine	25	1	2.13	[57]
Activated carbon	Impregnation	Monoethanolamine	40	1.01325	1.79	[216]
			50	1.01325	1.99	
			60	1.01325	2.19	
			70	1.01325	2.36	
	Impregnation	Diethanolamine	40	1.01325	2.11	
			50	1.01325	2.36	
			60	1.01325	2.57	
			70	1.01325	2.81	
Multiwalled carbon nanotube	Grafting	N′-(3-trimethoxysilylpropyl) diethylenetriamine	120	1	0.48	[234]
Activated carbon derived from ordos coal	Impregnation	Tetraethylenepentamine	60	1.01325	3.24	[228]
Biochar derived from rice straw	Impregnation	Tetraethylenepentamine	25	1	5.7	[111]
Phosphoric acid activated risk husk	Impregnation	Melamine	30	1	6.877	[221]
			45	1	6.518	
			60	1	6.113	

Table 11. *Cont.*

Support	Amine Attaching Method	Amine Type	CO_2 Capture Conditions for Pure CO_2 Gas Flow		CO_2 Capture Capacity (mmol/g)	Reference
			Temperature (°C)	Pressure (bar)		
Microporous activated carbon	Impregnation	Triethylenetetramine	75	1	1.05	[218]
	Impregnation	Polyethylenimine	75	1	1.85	
Mesoporous activated carbon	Impregnation	Polyethylenimine	75	1	1.4	
Polyaniline	Grafting	Melamine	25	0.15	1.3	[235]
			25	1.01325	4.6	
Multiwalled carbon nanotubes	Impregnation	Polyethylenimine	25	1	2.14	[217]
MOF-derived carbon monolith	Impregnation	Tetraethylenepentamine	25	0.15	5.6	[93]
Pinecone-based activated carbon	Grafting	Polyaniline	25	1	3.16	[79]
Multiwalled carbon nanotubes	Grafting	3-aminopropyl triethoxysilane	25	1	5.76	[109]
Carbon nanotubes	Grafting	Polyethylenimine	50	1	2.9	[37]
Multiwalled carbon nanotubes	Impregnation	Polyethylenimine	25	1	1.41	[223]
Sugarcane bagasse	Impregnation	Urea	25	1	4.8	[44]
Multiwalled carbon nanotubes	Grafting	Phenylenediamine	25	2	0.21	[80]
Carbon nanotubes	Grafting	1,3-diaminopropane	30	17.3	2.11	[80]
Multiwalled carbon nanotubes	Grafting	3-aminopropyl triethoxysilane	0	1	1.32	[38]
Graphene oxide	Impregnation	Tetraethylenepentamine	70	50	4.26	[232]
Graphene oxide	Impregnation	Polyethylenimine	25	1	1.91	[229]
Graphene oxide aerogel	Impregnation	Ethylenediamine	25	1	1.1	[231]
Graphene oxide	Grafting	Tetraethylenepentamine	70	0.1	1.2	[151]
Biochar	Grafting	Aminopropyl triethoxysilane	25	1.01325	3.7	[90]
Porous carbon	Grafting	Ethylenediamine	25	0.15	1.1	[236]
Hierarchical microporous carbon	Grafting	Melamine	0	1	3.82	[237]
			25	1	2.69	

Table 11. *Cont.*

Support	Amine Attaching Method	Amine Type	CO_2 Capture Conditions for Pure CO_2 Gas Flow		CO_2 Capture Capacity (mmol/g)	Reference
			Temperature (°C)	Pressure (bar)		
Porous carbon	Grafting	Melamine	30	1	1.12	[238]
	Grafting	Ethylenediamine	30	1	2.84	
	Grafting	Hexamethylenetetramine	30	1	1.40	
Porous carbon	Grafting	Phenylenediamine	25	5	4.65	[171]
Nanocrystalline cellulose	Grafting	Amidoxime	120	1.01325	5.54	[51]
			25	1.2159	1.11	
Microcrystalline cellulose	Grafting	Amidoxime	120	1.01325	3.85	[48]
			25	1.2159	1.27	
Wheat bran husk-derived carbon	Grafting	Polyethylenimine	75	1	0.43	[165]
Sugar cane bagasse	Impregnation	Melamine	25	1	3.34	[239]

The amine efficiency of PEHA functionalized chitosan-derived mesoporous carbon was 0.18 mol/mol at 100 °C with a PEI loading of 3.9 g/g, suggesting a moderate utilization of amine species during the CO_2 adsorption process [210]. The theoretical amine efficiency for PEI-impregnated graphitic carbon nitride composite was observed to be 0.15–0.27 mol/mol at 100 °C by assuming that the reaction stoichiometry between primary/secondary amine groups and CO_2 gas molecules is 2:1 [219]. Furthermore, the maximum CO_2 uptake capacity for TEPA-impregnated biomass-derived wood ash was reported to be 1.76 mmol/g, which corresponds to an amine efficiency of 0.3 mol/mol. Amine efficiency decreased from 0.36 to 0.8 mol/mol was observed with the increased amine loading [70].

Apart from the above observations, both Yaumi, Bakar, and Hamed [221] and Wang et al. [108] have noted an increase in CO_2 capture performance with CO_2 concentration in the feed gas stream. For instance, the melamine-impregnated rice husk-derived mesoporous carbon displayed an increase in the CO_2 capture performance from 4.41 to 5.43 mmol/g with the increase of CO_2 concentration from 10 to 20% in the feed gas stream at 30 °C and 1 bar [221]. The PEI-functionalized mesoporous carbon adsorbent demonstrated an increasing trend from 2.55 to 4.53 mmol/g when the CO_2 concentration in the feed gas mixture was increased from 55 to 60% [108]. Such behavior was ascribable to the enhanced driving force between the adsorbent surface and bulk adsorbate concentration, resulting in better diffusion and mass transfer [221].

On the other hand, a sharp increase in the CO_2 capture performance was demonstrated by PEI-impregnated hollow fibers [240], DEA-functionalized activated carbon [216], and activated carbon/polyaniline composites [79] at any given temperature when the pressure was increased. The increase in CO_2 adsorption capacity with pressure is due to the enhanced reactivity between amine species and CO_2 molecules via chemisorption [79]. Additionally, Keller et al. [240] have stated that an amine-functionalized porous carbon adsorbent that possesses a remarkable CO_2 adsorption capacity of 1.07 mmol/g at a very low pressure of 350 ppm acts as a promising candidate for CO_2 capture from the air with a CO_2 concentration about 400 ppm.

Several researchers have extensively studied the CO_2 capture behavior with temperature change. For instance, Wang et al. [62] had observed a slight increase in the adsorbed CO_2 amount when the temperature was increased from 25 to 75 °C, whereas a sharp decrease from 75 to 110 °C for PEI-impregnated mesoporous carbon. TEA-functionalized activated carbon has exhibited a sharp decline of CO_2 adsorption amount as the temperature was increased from 20 to 60 °C [224]. An increase in the adsorption capacity was observed with a temperature rise from 25 to 60 °C for TEPA-loaded CNTs, while the maximum adsorption capacity was obtained at 60 °C [14]. A decrease in CO_2 capture capacity was observed for melamine-impregnated rise husk-derived mesoporous carbon from 4.41 to 3.56 mmol/g as the temperature was increased from 30 to 75 °C [221]. An initial rise in the CO_2 adsorption amount with the rise of temperature from 25 to 90 °C and a sharp decline from 90 to 120 °C [194], an increase from 40 to 50 °C, whereas a decrease with further increase in temperature [214] was also reported. The researchers have attributed the improvement of CO_2 capture performance at low temperature to the increased CO_2 diffusion to available reactive sites. In contrast, the sharp decrease in CO_2 capture capacity at elevated temperatures is suggested to be associated with the combined effect of the exothermic nature of the chemisorption process and the loss of amine sites available via amine degradation at temperatures higher than 100 °C [60,214].

Several research groups have also conducted CO_2 adsorption experiments to determine the optimum parameters associated with adsorbent beds. Alhassan et al. [224] reported an increment in CO_2 adsorption performance from 0.82 to 1.5 mmol/g when the bed height was increased from 2.7 to 5.4 cm. This increment was ascribed to the increased interactions between the active sites of the adsorbent and CO_2 molecules. Exciting results were generated by Das et al. [213], indicating a reduction in CO_2 removal efficiency (%) with the increase in CO_2 feed gas velocity due to decreased gas diffusion for DEA-functionalized

activated carbon. An increasing trend of CO_2 removal efficiency with the increase of CO_2 feed gas flow rate and weir height was observed, which could be attributed to enhanced gas–solid interactions. Similar observations were also noted by Das and Meikap [87] and Ali et al. [226]. Furthermore, Das et al. [211] have stated that the maximum CO_2 removal efficiency of 80% was achieved under a low CO_2 flow rate of 0.188 m/s, highest adsorbent flow rate of 4.12 kg/h, and a high weir height of 50 mm.

Apart from the above results, a few researchers have generated kinetic CO_2 adsorption behaviors. A breakthrough capacity of 2.17 mmol/g was exhibited by PEI-impregnated mesoporous carbon at a PEI loading of 60%. The breakthrough and saturation adsorption capacities were reduced as the PEI loading was increased to 70% [62]. Moreover, an adsorption rate of 0.23 mmol/min at the breakthrough stage was observed by [228] for TEPA-modified activated semi-coke. On the contrary, a decline in breakthrough time with the increase of inlet gas flow rate from 30 to 60 mL/min at 30 °C [221] and an increase in breakthrough time with the increase of carbon adsorbent dosage [226] was observed by the researchers.

4.2.3. Regeneration and Cyclic Stability of Amine-Impregnated Porous Carbon Materials

The researchers have adopted different regeneration strategies to evaluate the cyclic stability of the adsorbent materials. For example, Peng et al. [210] and Pen et al. [218] used the concentration swing adsorption to regenerate PEHA-loaded chitosan-derived mesoporous carbon and PEI-grafted graphitic nitride. Temperature swing adsorption was used for TEA-impregnated activated carbon and biochar, PEI-modified CNTs and mesoporous carbon spheres, MEA functionalized activated carbon, and melamine loaded rise husk-derived activated carbon [63,108,111,216,221,224,240]. The pressure swing adsorption was used for PEI-functionalized micro- and nanosized mesoporous carbon [207]. Several research groups have reported the regeneration capabilities of various carbon adsorbents. For instance, a 16% reduction in CO_2 capture capacity for PEHA-loaded mesoporous carbons was observed after 10 consecutive cycles [210]. The regeneration conversions of 92.6%, 83.1%, 69.8%, 90.2%, and 86.2% were observed after 5 adsorption/desorption cycles for TEPA, MEA, DEA, PEI, and diethylenetriamine impregnated biomass-derived wood ash, respectively [70]. Good cyclic stability was maintained for up to 7 cycles for TEA-impregnated activated carbon [224]. A stable reversible capacity of up to 10 cycles with a small reduction of 5% compared to the original adsorption capacity for PEI-functionalized graphitic carbon nitride was observed [219]. Overall, 47% CO_2 capture reduction after 19 cycles for PEI-impregnated micro- and nanosized mesoporous carbon [207], 1% reduction after 10 regeneration cycles for PEI-modified CNTs [240], regeneration capability up to 10 consecutive cycles for PEI-impregnated mesoporous carbon [108] and PEI-functionalized MWCNTs (multi-walled carbon nanotubes) [217], reduction of 20% of the original CO_2 capture performance after 10 cycles for TETA-impregnated CNTs [14], 7.7% reduction after 10 adsorption/desorption cycles for TEPA-modified semi coke [217], better reusability up to 5 cycles for TEPA-modified biochar [111], and PEI-impregnated silica coated MWCNT [79], 8.8% reduction of initial CO_2 adsorption amount after 12 cyclic tests for melamine-impregnated mesoporous carbon [223], a loss of 6% of the original capture performance after 20 cycles and a loss of 40% at the 50th cycle for TEPA-loaded MOF-derived carbon monolith [93], 14% reduction of CO_2 desorption capacity after 15 regeneration cycles for DEA-impregnated activated carbon [60,214], regenerability up to 10 cycles for amine-functionalized graphene/silica aerogel [187], and amine-modified sugar cane bagasse [44], 3% drop in CO_2 adsorption capacity after 10 cycles for PEI-impregnated mesoporous carbon [62], and an original capture capacity reduction by 20% after 8 consecutive cycles for TEPA-impregnated carbon aerogels [8] were reported.

A weakening of adsorbent regeneration performance could be observed for TEPA-impregnated biomass-derived wood ash due to the formation of byproducts, including sulfur or nitrogen adducts and nitrosamine compounds in the presence of SO_2, NO_X, HCl, and other acid impurities [70]. On the other hand, the significant loss of CO_2 capture

performance during adsorbent regeneration experiments was ascribed to the degradation and evaporation of amines [93,111,216,227], thermal instability of amine species [31,152], or amine leaching from the carbon support [93,215,218], pore blockage after repeated cycles which cause CO_2 inner diffusion resistance [108,221,227], and oxidative degradation during both adsorption and desorption processes where some of the active sites are occupied by O_2 via an irreversible reaction [108]. Furthermore, a 7% decrease of original CO_2 capture capacity after the second cycle for PEI-impregnated millimeter-sized mesoporous carbon spheres was also reported in the presence of dry O_2 containing gas mixture (15% CO_2, 5% O_2, and 80% N_2) during the regeneration process. On the contrary, Liu et al. [241] conducted the CO_2 regeneration studies for TEPA-impregnated MWCNTs in the presence of SO_2 gas. During the cyclic adsorption–desorption experiments, the adsorbent was exposed to a feed gas flow rate of 50 cm^3/min, which contains an SO_2 concentration of 1000 ppm. At the first cycle, a remarkable decrease with a CO_2 capacity loss of 23.48% was observed, whereas a CO_2 capture loss of 53.56% was exhibited at the fifth consecutive cycle in the presence of SO_2 gas. This sharp CO_2 capture drop is attributed to reducing the number of active adsorption sites. The pore blockage occurred through the reactions between SO_2 and amine species to hinder the CO_2 diffusion into active sites [241].

Apart from the above, a few studies have explored the regeneration energies associated with the adsorbent regeneration process. The regeneration energies associated with TEPA, MEA, DEA, PEI, and diethylenetriamine impregnated biomass-derived wood ash was found to be 92.68, 147.38, 146.69, 92.64, and 106.25 kJ/molCO_2, respectively, which are notably less compared to that of the parasitic regeneration energy load (197.91 kJ/mol CO_2) associated with aqueous amine scrubbing technique, which uses 30% MEA. Additionally, it is stated that both TEPA and PEI-impregnated biomass-derived wood ash demonstrated the minimum energy requirement for CO_2 degassing. The discrepancy in the energy loads is due to the difference in the number of amine groups and the structure of amine species [70].

4.3. CO_2 Capture by Amine-Grafted Porous Carbon Adsorbents

Amine grafting has grabbed significant attention as a more stable alternative to the physical impregnation of amines [218]. The available specific surface area decides the maximum amine content that can be covalently bonded onto the porous support [118]. Even though previous research groups have noted that the grafting of amines onto porous carbon materials has greatly improved the thermal stability [53,210] and reusability [53,104,112], there are some disadvantages associated with amine-grafting, such as complicated synthesis routes [210] and the reduced amine loading onto the support compared to the amine-impregnation process [207].

4.3.1. Synthesis of Amine-Grafted Porous Carbon Adsorbents

Various synthesis methods have been developed to synthesize amine-grafted porous carbon adsorbents for carbon capture effectively. For instance, TETA was incorporated into the sugar cane bagasse matrix fiber via graft copolymerization [225]. Polyaniline-functionalized pinecone-based activated carbons were prepared through nitric acid oxidation, followed by subsequent amine anchoring [79]. Tetraethylenepentamine (TEPA)-functionalized graphene oxide was fabricated using a sonochemical activation method with ultrasound irradiation [151]. PEI-modified CNTs were fabricated by spirally wrapping each CNT using PEI chains [37]. MWCNTs were modified by 1,3-Diaminopropane via two steps. Initially, a mixture of H_2SO_4/HNO_3 was used. Then, a subsequent modification step was employed using 1,3-Diaminopropane [9]. Covalent functionalization of ethylenediamine (EDA) through condensation and nucleophilic substitution of semi-coke and graphene was also reported [242]. Melamine-grafted carbon was prepared using monodispersed polymer microspheres as the template following the self-assembly of the template with calcination [237]. Laponite RD was modified using aminopropyl triethoxysilane (APTES) to fabricate a ternary composite aerogel comprising graphene oxide/Laponite RD/chitosan through the electrostatic self-assembly method [243]. According to the Schiff reaction, PEI

was functionalized onto wheat bran husks without biomass carbonization [165]. Microcrystalline cellulose/silica and nanocrystalline cellulose/silica composites attached with amidoxime groups were fabricated via the evaporation-induced self-assembly (EISA) [48,51]. Melamine, EDA, and hexamethylenetetramine-functionalized porous carbon adsorbents were synthesized via a template-free method [238]. Melamine and urea were incorporated into asphaltene using three different synthesis routes: soft-template synthesis, self-assembly synthesis, and molten-salt syntheses [5]. The structure of EDA functionalized nanosized mesoporous carbons is demonstrated in Figure 8b. Additionally, the mechanism for the functionalization of acid treated MWCNTs with APTES is illustrated in Figure 9.

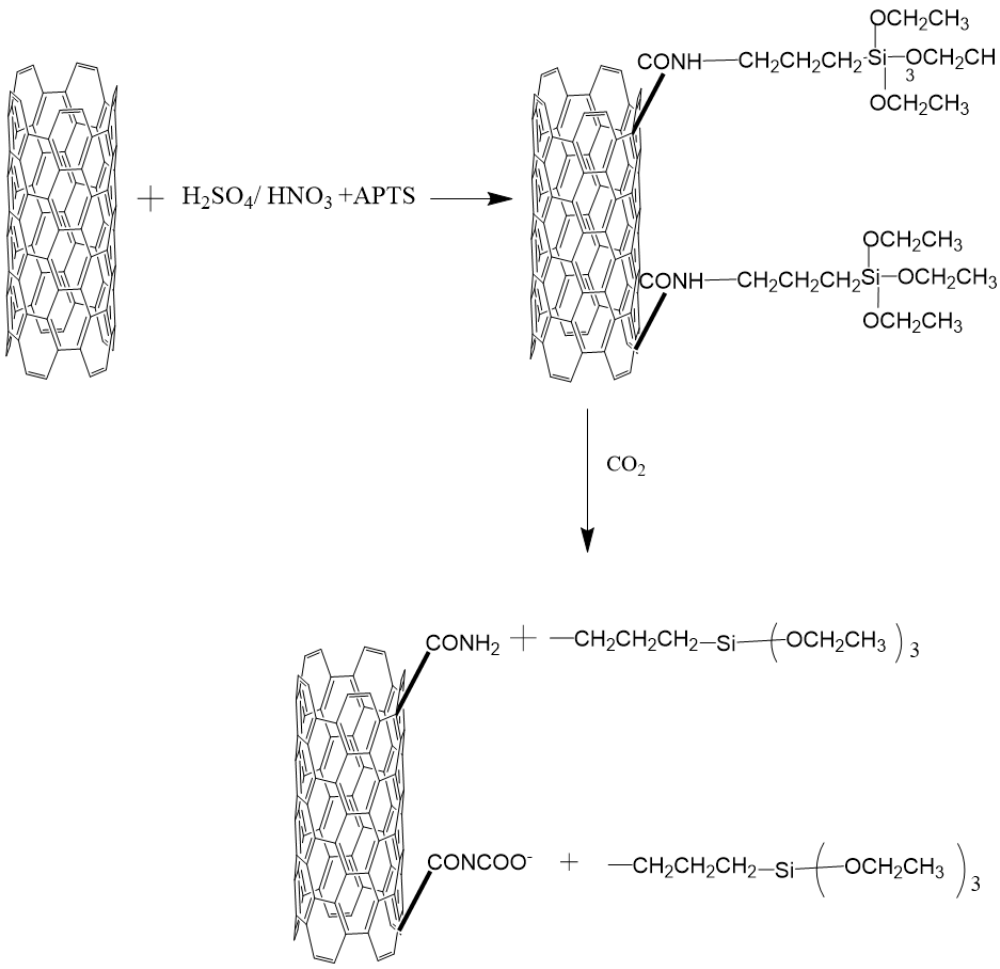

Figure 9. The mechanism for functionalization of acid treated MWCNTs with 3-aminopropyltrietheoxysilane (APTES) (Reprinted with permission from ref. [109]).

Gunathilake et al. [48] reported that the total production cost of amidoxime-functionalized microcrystalline cellulose/mesoporous silica composites to be less than 8 US$ to make their production economically feasible.

4.3.2. CO_2 Adsorption Capacities of Amine-Grafted Porous Carbon Materials

Previous studies have reported that the CO_2 adsorption capacity of amine-grafted sugar cane bagasse depends on the amine content and hydrophobicity of the matrix fiber since the presence of hydroxyl groups in the carbon support enhances CO_2 chemisorption via changing the mechanism into a more favorable route, requiring less activation energy. Additionally, it was noted that the amine-grafted carbon supports with mild alkalinity could exhibit higher CO_2 adsorption capacities [225]. Deng and Park [37] reported that the PEI-grafted CNT demonstrates enhanced CO_2 capture performance using spacers containing an optimal or moderate chain length. Furthermore, Gunathilake et al. [48]

reported that the CO_2 uptake increased from 2.84 to 3.85 mmol/g when the amidoxime content was increased from 10 to 40% at 120 °C. Similar observations were reported by Zhodi et al. [202] for amine-grafted CNT/hollow silica particle composites. It was also reported that the CO_2 adsorption capacity decreases with increased grafted amine loading due to pore blockage by larger amine groups that prevent effective CO_2 diffusion at low temperatures [90].

Furthermore, it was revealed that the CO_2 adsorption in low molecular weight amine-functionalized carbon supports is higher than in the high molecular weight amine-functionalized porous carbons [60]. When the CO_2 concentration in the feed gas stream increased from 5 to 20%, the CO_2 capture capacity also increased from 2.32 to 3.35 mmol/g. The amine efficiency also increased from 32.535 to 46.98% [225]. Moreover, Auta et al. [82] have suggested the optimized conditions for CO_2 adsorption for waste tea activated diethanolamine (DEA)-grafted adsorbent material as 30 °C (temperature), 10% (CO_2 feed gas concentration), 90 mL/min (inlet flow rate of the gas stream), and 3 g of adsorbent dosage with 1–2 mm particle sizes [82]. Shafeeyan et al. [116] have noted that the CO_2 adsorption performance of NH_3-grafted activated carbon increased with increasing pressure. Besides, the adsorbed CO_2 amount of amine-grafted CNTs increased from 0.42 to 0.48 mmol/g with the rise of temperature from 293.15 to 303.15 K. In contrast, the CO_2 capture performance of non-functionalized CNTs declined with the temperature increment [80].

Apart from the adsorption capacities, several research teams have published data on adsorption kinetics. For instance, Luo et al. [225] have observed faster kinetics for amine-grafted sugar cane bagasse under high CO_2 feed concentrations. In contrast, Auta et al. [82] have reported the adsorption capacity to be 0.45, 1.22, and 1.47 mmol/g at the adsorbent column loadings of 2, 3, and 4 g, and the breakthrough time durations of 240, 900, and 970 s, respectively. Apart from the above, Andredi et al. [244] have noted that the CO_2 adsorption kinetics is mainly affected by the curvature of the porous carbon support. For example, the rate of CO_2 adsorption exhibited an increasing trend with increasing curvature of the support [244].

4.3.3. Regeneration and Cyclic Stability of Amine-Grafted Porous Carbon Materials

The regeneration of the adsorbents is of paramount importance from a practical and economical point of view for long-term usage [151]. The cyclic stability of the amine-grafted porous carbon adsorbents has been investigated via different regeneration procedures. For instance, Lourenco et al. [234] have carried out the desorption process at 80 °C under vacuum and temperature–vacuum swing adsorption (TVSA) [9,242]. The spent adsorbent can also be regenerated by exposing it to 303 K [203] or 378 K [151] in a He atmosphere [51,90,236]. PSA can also be utilized for regenerating the spent adsorbents [236].

According to the previous studies, the cyclic stability has been reported as recyclability up to 10 cycles [5,51,225,234], 5 cycles [235], 4 cycles [9,60], 8 cycles [242], 50 cycles [37], 3 cycles [202], and 6 cycles [238] without a noticeable CO_2 capture drop. A decline of 2% of original CO_2 capture capacity for phenylenediamine-functionalized MWCNTs after 4 consecutive cycles [80], 1% loss in adsorption capacity after 10 cycles for TEPA-grafter graphene oxide [151], 20% decrease after the tenth cycle for APTES-modified biochar [90], and a stability of up to 11 cycles with a drop of 2% for amidoxime-functionalized microcrystalline cellulose/mesoporous silica composite has been reported [48].

4.4. CO_2 Selectivity of Amine-Functionalized Porous Carbons

As mentioned in Section 4.1, the selectivity of CO_2 over other gases present in the feed is more excellent for amine-functionalized materials than that of physisorbents. Iqbal et al. [233] obtained CO_2/N_2 selectivity for amine-functionalized CNT as 78 at 25 °C and 1 bar, while the IAST selectivity for melamine loaded polyaniline was 75 [235]. Moreover, the CO_2 adsorption capacity of 1.27 mmol/g and an N_2 capture capacity of 0.15 mmol/g was reported by Gunathilake et al. [48] at 1.2 atm and 25 °C. On the other hand, according to Khalza et al. [79], it was observed that, although the CO_2/N_2 selectivity decreased

with increasing the pressure and N_2 mole fraction in the gas mixture, the selectivity of polyaniline-modified activated carbon was much greater than the pristine activated carbon. Furthermore, increased CO_2/N_2 selectivity was exhibited when the polyaniline loading was increased, whereas, for a gas mixture containing CO_2/N_2 (15/85) at 298 K and 1 bar, the selectivity value was noted as 18.97 [79]. A reduction in CO_2/N_2 selectivity with the increase of pressure was also observed by Wang et al. [171], and this behavior was attributed to enhanced physical adsorption of N_2 at higher pressures. Melamine-loaded carbon has exhibited a notable CO_2/N_2 separability of 158 at 25 °C, and 100 kPa for a gas mixture containing 10% of CO_2 and when the CO_2/N_2 (1/9 *v/v*) gas stream flowed over a packed bed which contains the melamine-loaded porous carbon as the adsorbent material with a total flow rate of 5 mL/min at 25 °C, the CO_2/N_2 selectivity was reported to be 145 [237].

Apart from the above, for amine-impregnated porous carbon adsorbents, selectivity values in the range of 412–4110, which is 21–206 times higher than that of pristine adsorbent, were exhibited by pentaethylhexamine (PEHA) loaded chitosan-derive mesoporous carbon [210], 18.7 for amine-modified activated carbon at 298 K [234], selectivity values in the range of 2257–6588 for PEI-impregnated graphitic carbon nitride at 25 °C and 1 bar [219], selectivity value of 22 for amine-impregnated sugar cane bagasse [44], 196 for PEI-impregnated CNT [240], and a CO_2/N_2 selectivity of 37.13 for PEI-impregnated graphene oxide-derived porous carbon at 298 K and 1 bar [229] were observed for a gas mixture with 15% CO_2 and 85% N_2.

Several researchers have reported remarkable CH_4/CO_2 separability for diethanolamine (DEA) impregnated palm shell-derived activated carbon [216], DEA functionalized broom sorghum-based activated carbon [56], amine-functionalized MWCNT/hollow silica nanocomposite [202], amine-functionalized asphalt-derived porous carbon nanosheets [5], and amine-functionalized graphene-based semi-coke porous carbon [244]. According to Kongnoo et al. [216], under atmospheric pressure, the CO_2/CH_4 selectivity was more pronounced owing to the higher steric hindrance for CH_4 than CO_2, making it difficult for the CH_4 molecules to reach the active sites. Additionally, the active sites favor CO_2 adsorption due to amine modification [57,202,216]. Besides, for amine-functionalized graphene-based porous carbon materials, the secondary amine groups play a prominent role in achieving better selectivity performance of CO_2/CH_4. In contrast, the interlayer spacing of 0.362 nm in the hierarchical sandwich-like structure of the porous material only allows the CO_2 molecules to pass through due to the larger kinetic diameter of CH_4 compared to CO_2 (Table 10). Similar results were observed for the selectivity of CO_2/N_2 [231]. Moreover, a selectivity value for CO_2/CH_4 of 6.83 was noted by Mehrrarz, Ghoreyshi, and Jahanshahi [56] at 308 K and 1 bar, while the selectivity increased with the temperature increment.

Liu et al. [241] have carried out experiments to examine the effect on CO_2 gas adsorption performance of TEPA-impregnated MWCNTs in the presence of SO_2 gas. The sorbent exhibited a reduction in CO_2 capture capacity from 2.765 to 2.642 mmol/g when the SO_2 concentration in the feed gas stream was increased from 100 to 2000 ppm. Additionally, the research group was able to explore the effect of temperature at a constant SO_2 concentration of 1000 ppm in the feed gas stream. The results of this study indicated an initial increment of CO_2 adsorption capacity from 2.109 to 2.732 mmol/g when the temperature was increased from 293 to 333 K, respectively. In contrast, a reduction of the CO_2 capture capacity valuing 2.543 mmol/g was also demonstrated at 353 K. This behavior confirmed that the CO_2 adsorption capacity declines more significantly at elevated temperatures in the presence of SO_2 gas [241].

4.5. Importance of Amine-Functionalization for Effective CO_2 Capture

It is a well-known fact that the CO_2 adsorption capacity predominantly depends on chemisorption by amine-functionalized porous carbon materials. Lourenco et al. [234], Kwan et al. [165], Shafeeyan et al. [116], Gibson et al. [218], and Shin, Rhee, and Park [229] have claimed that the notable CO_2 adsorption capacities of the amine-modified carbon

supports compared to the pristine materials is due to the enhanced acid–base interactions between the basic functional groups such as EDA, PEI, TETA, AMP, PZ, MEA, and amidoxime as illustrated in Figure 10 on the carbon support surface and acidic CO_2 molecules. It has been reported that the more significant CO_2 capture performance at low temperatures and 1 bar is also due to the favorable interactions between the basic NH_2 groups and acidic CO_2 molecules [233]. The sharp increase in CO_2 uptake at low pressures was attributed to the dominant chemisorption behavior between the NH_2 groups in polyphenylenediamine and APTESi and the CO_2 molecules, respectively [171,243]. Additionally, according to Wang et al. [171], the increase in CO_2 adsorption capacity from 4.1 to 6.5 mmol/g when the temperature and phthalimide loading were increased from 25–85 °C and 0.5–1.5%, respectively, was due to a more significant affinity of the NH_2 groups in phthalimide and these interactions enhanced with the temperature increment. Similar observations were reported by Peng et al. [210] for PEHA incorporated mesoporous carbon, Pen et al. [219] for DEA-modified palm shell-derived activated carbon, and Kongnoo et al. [216] for PEI-functionalized graphitic carbon nitride. Khalza et al. [79] have claimed that the amine polymerization of activated carbon could decrease the number of carboxylic groups while increasing the basic sites on the support surface, which is beneficial for improving the CO_2 capture performance. Moreover, functionalization of porous carbon using ethylenediamine was reported to be useful since it could enhance the CO_2 adsorption capacity via acid–base interactions while preserving the original structure of the adsorbent [238]. The amidoxime functionalization has been proven effective for CO_2 capture at elevated temperatures [51].

4.6. Importance of Moisture in the Effective Capture of CO_2 by Amine-Functionalized Porous Carbon Adsorbents

The presence of moisture plays a dominant role in determining the CO_2 adsorption performance of amine-functionalized porous carbon materials. Moisture is ubiquitous in the flue gas and ambient air [8,14,62,108]. The possible reactions occurring between the CO_2 molecules and the primary, secondary, and tertiary amines under dry and moist conditions are presented in Table 12.

Table 12. Reactions of CO_2 with primary, secondary, and tertiary amines under (a) dry and (b) moist conditions (Reprinted with permission from ref. [26]).

Dry Conditions (Carbamate Formation)	Humid Conditions (Bicarbonate Formation)
Primary amines	
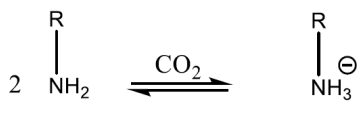	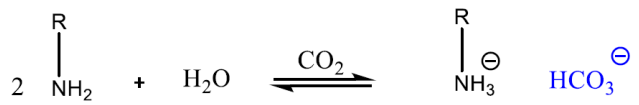
Secondary amines	
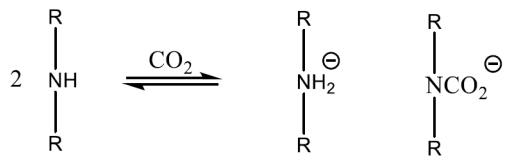	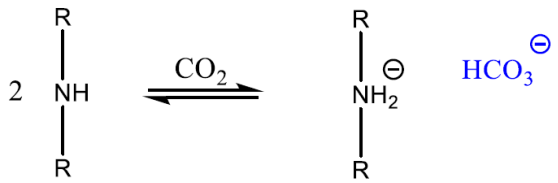
Tertiary amines	
No carbamate formation	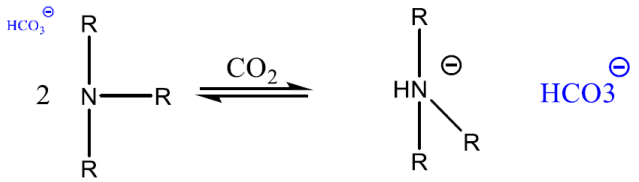

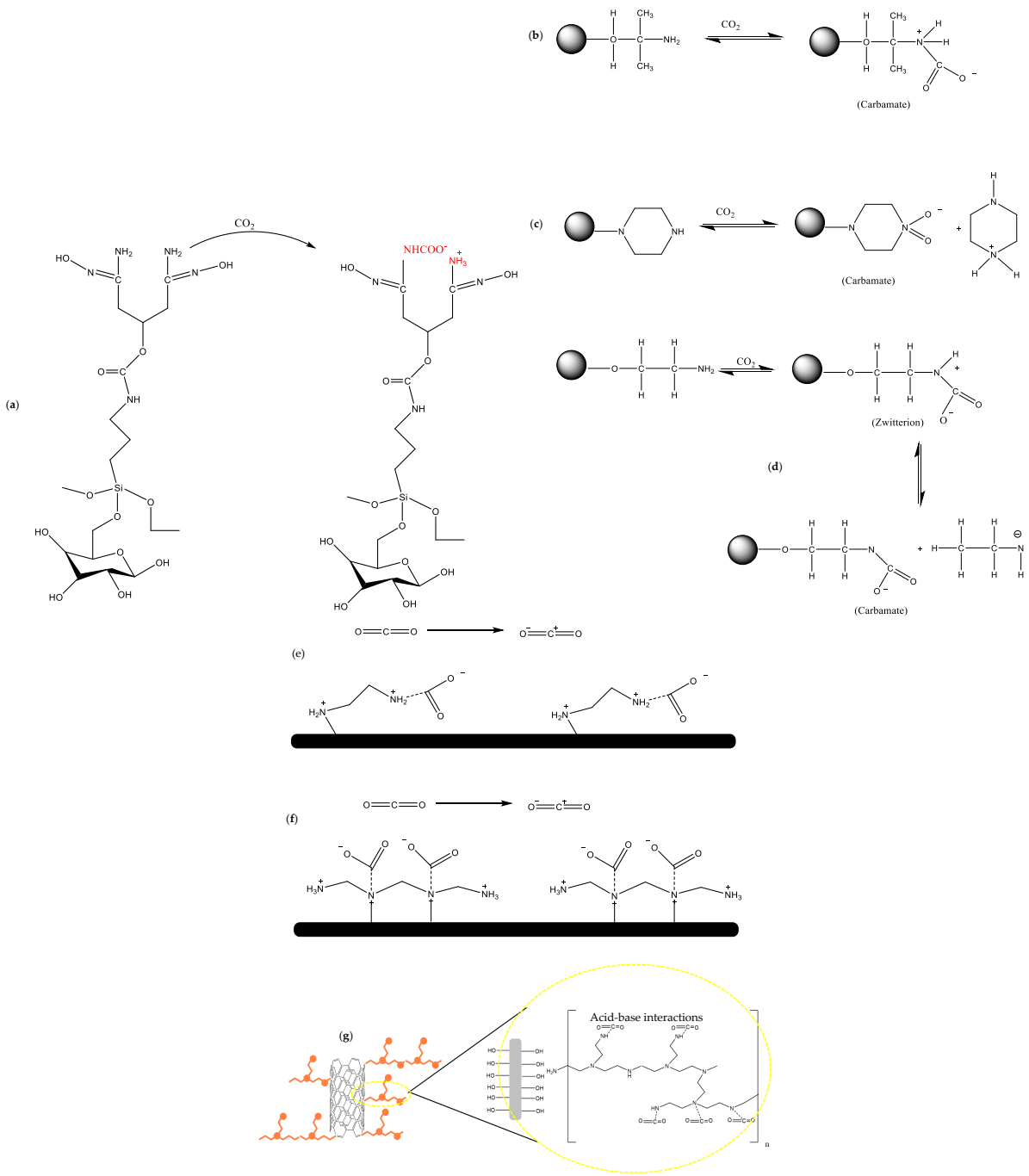

Figure 10. Reactions between the CO_2 molecules and (**a**) amidoxime, (**b**) AMP, (**c**) PZ, (**d**) MEA, (**e**) EDA, (**f**) TETA, and (**g**) PEI functionalities (Reprinted with permission from refs. [51,110,215,222,226]).

As mentioned in Section 4.1, 1 mol of amine groups react with 0.5 mol of CO_2 molecules to form carbamates in dry conditions. In contrast, in moist conditions, 1 mol of amine groups react with 1 mol of CO_2 molecules to form bicarbonate and carbonate species (Table 12) [14,62,210,234]. The moisture in the CO_2 feed gas streams must be utilized to enhance the CO_2 capture performance of amine-modified carbon supports [14,210]. For the reaction between tertiary amine groups and CO_2 molecules, moisture plays a prominent role, as depicted in Table 12. Additionally, moisture adsorption onto porous supports is reportedly relatively slower than the chemisorption of CO_2 molecules onto the amine species. Additionally, the desorption of water molecules is slower than the moisture adsorption process [234]. Andredi, Cullum, and Barron [244] have claimed

that moisture was not adsorbed with CO_2 gas molecules on PEI-modified nanocarbon at high temperatures.

An enhanced CO_2 capture performance by amine-functionalized porous carbon adsorbents in the presence of water has been extensively reported in the literature. According to Wang et al. [108], the CO_2 adsorption capacity sharply increases with relative humidity (RH). The maximum adsorption capacity of 4.26 mmol/g is obtained at an RH of 60% for PEI-impregnated mesoporous carbon spheres. A remarkable increase in the CO_2 capture capacity for PEHA-loaded mesoporous carbon from 3.31 mmol/g (under dehydrated conditions) to 4.49 mmol/g (under humidified conditions) at 75 °C was reported by Peng et al. [210]. Additionally, according to Luo et al. [225], a sharp increase in CO_2 adsorption capacity from 0.5 to 2.79 mmol/g was observed for TETA-functionalized sugarcane bagasse in the presence of a moist environment, and such behavior was attributed to the enhancement of chemical adsorption of alkylamino groups for CO_2 gas molecules. Nevertheless, Wang et al. [171] have observed that the phthalimide-loaded cellulosic nanofibers could exhibit the highest CO_2 adsorption capacity of 5.5 mmol/g at 95% RH at ambient pressure. This remarkable capture performance at high moisture levels was attributed to the easy dissolution of non-polar CO_2 molecules in water, improving CO_2 adsorption [8]. Furthermore, an increase in breakthrough time, both equilibrium and breakthrough adsorption capacities for TEPA-functionalized activated semi-coke in the presence of water vapor [228], enhanced CO_2 uptake capacity in the presence of 4.5% water [234], negligible effect on the adsorbed amount of CO_2 gas onto PEI-modified graphitic carbon nitride [219] and PEI-grafted graphene oxide [244], and enhanced CO_2 uptake at 80% RH compared to that of dry conditions [62] have been reported.

However, Irani et al. [14] reported that even though the adsorbed CO_2 level increased by 56% with 1 vol %; of moisture into the feed gas stream, the CO_2 capture capacity declined with a further increment of moisture content beyond 1%. This reduction could be ascribed to the occupation of available adsorption sites in the adsorbent material by the H_2O molecules competing with CO_2 [14,62]. Similar observations were reported by Gholidoust et al. [214] that the CO_2 adsorption capacity of DEA-functionalized activated carbon increased gradually up to 20% RH and then declined. The increase in capture capacity up to 20% RH was due to the catalytic effect of H_2O on the reaction between amine species and CO_2 molecules. Additionally, it was stated that when the moisture amount is less than the CO_2 gas concentration, it leads to enhanced CO_2 capture performance and vice versa [214]. On the contrary, a reduction in CO_2 capture capacity from 2.02 to 1.71 mmol/g was noted when the adsorbents were exposed to gas steam containing 5% CO_2 and 5% H_2O in the presence of acidic impurities. A reduction in amine efficiency from 0.19 to 0.16 mol/mol was also reported [70]. Apart from the above observations, though an initial rise in adsorption capacity from 2.97 to 3.88 mmol/g for TEPA-impregnated CNTs was observed as the water vapor amount was increased from 0 to 2%, a notable decrease from 3.88 to 2.67 mmol/g was exhibited by the adsorbent when the water vapor was increased from 2 to 7% at 298 K [245].

Moreover, a reduction in CO_2 capture performance from 2.765 to 2.579 mmol/g was noted by Liu et al. [241] for TEPA-impregnated MWCNTs when the RH was increased from 0 to 100% at 323 K. Such a reduction in capture capacity was ascribed to the formation of water vapor into a thin layer of a water film which hinders the CO_2 mass transfer, pore blockage occurred through the reactions between bicarbonate/carbonate and CO_2/H_2O/TEPA, and due to the capillary condensation occurring with the increase of water vapor content which resulted in micropore blockage [241].

Apart from the above, the presence of moisture affects the cyclic performances of amine-functionalized porous carbon materials. For instance, the CO_2 capture decreased from 2.02 to 1.94 mmol/g within 10 consecutive cycles when the adsorbent was exposed to a gas mixture containing 5% CO_2 and 5% H_2O [70]. A rapid decrease in the cyclic CO_2 capture capacity at 60% RH in the presence of SO_2, NO, and NO_2 were observed. This adverse effect was attributed to the high solubility of the gases such as SO_2, NO, and NO_2 in

water, which caused enhanced adsorption of these impurity gases compared to CO_2 [108]. Preferential adsorption of CO_2 when in the co-presence of water vapor pressure (>3.2 kPa) at the third cycle was also reported [234]. Besides, Wang et al. [108] have reported an increase in cyclic performance from 97 to 98.6% at dry conditions and 60% RH, respectively. This exciting observation was due to the inhibition of the formation of urea-linkages in the presence of moisture, which is considered an irreversible by-product of the reaction between amine species and CO_2 molecules.

5. Contactors for CO_2 Adsorption Using Porous Carbon Materials

The wise choice of a suitable contactor system plays a vital role in better utilization of the sorbent material, improving the overall process sufficiency, and cost reduction [246–248]. When choosing a contactor configuration, the other parameters, including the ease of retrofitting into existing plants, affordability, flexibility during operation, and effectiveness towards the global technology, should also be considered [248–250]. In this context, the proposed reactor configurations for CO_2 adsorption include the (i) fixed bed, (ii) fluidized bed, and (iii) moving bed [246,248].

5.1. Fixed Bed Reactor

Numerous research activities have focused on fixed bed reactor configuration due to its relatively simple operation and design [251–253] and the ability to test a variety of sorbents under different regeneration modes [248,254]. The fixed bed contactor is considered the more straightforward reactor configuration where the flue gas is passed through stationery millimeter-sized adsorbent particles or structured packing materials. Usually, structured packing materials are used to achieve a better adsorption rate and a lower pressure drop by optimizing the solid–gas contacting surface area and void spaces while allowing more effective gas flow rates [248,255]. Besides, fixed bed adsorption columns possess the plug-flow nature and are considered the main advantage since this arrangement can ensure the maximum CO_2 capture performance until the entire contactor bed gets almost saturated with CO_2 gas [256]. On the contrary, the CO_2 concentration in the feed gas stream, temperature of the feed, feed flow rate, and the amount of adsorbent injected are the critical parameters affecting the functionalization of a fixed bed adsorber [251]. Besides, due to the poor heat transfer properties of the fixed bed configuration, it makes the bed suitable for PSA operation when using physisorbents that possess lower reaction enthalpies and temperature sensitivity [256].

The significant limitations associated with fixed bed reactors are high pressure drops even at moderate gas flow rates, making it impossible to use high gas velocities during adsorption and regeneration steps [256,257] and poor heat transfer [256]. According to the literature, the maximum recommended pressure drop available across the fixed-bed reactor is around 0.21 atm [256]. Moreover, if low feed rates are used to reduce the pressure drop, the low feed gas flow rates result in decreased CO_2 gas capture capacities due to long residence times [257]. The fixed bed configuration can be classified into two main categories:

(i) Conventional fixed bed: In this configuration, large adsorbent pellets are used to minimize the pressure drop and achieve a better sorbent working capacity. However, this imposes mass transfer limitations [258] from large pellets and has a low heat transfer coefficient [259,260].

(ii) Structured fixed bed reactor: Structured fixed bed contactors are considered a better alternative to conventional fixed beds. In this arrangement, sophisticated packing materials are employed to maximize the surface area per volume of the adsorbent and heat transfer [248,261,262] while maintaining better temperature control [263,264]. Additionally, this reactor configuration is capable of lowering the pressure drop (50% reduction can be achieved compared to pellets) [264] and improves the gas throughput and productivity 3–10 times [265] while reducing the cycle time [247].

Activated carbon beads were used to recover CO_2 gas from flue gas in a fixed bed reactor under a two-stage VPSA process. This study stated that the two-stage VPSA process is viable since the CO_2 fixed concentration of 60%, a purity of 95.5%, and a CO_2 gas recovery of 83.4% could be obtained via the four-step cycles. Additionally, the total power consumption of the two-stage VPSA process was reported to be 723.6 KJ/kgCO_2 with a unit production of 0.85 molCO_2/kgh [266]. In a separate study using a fixed bed reactor, it was found that the CO_2 loading capacity of the carbon sorbent at 25 °C and 15% CO_2 reduced from 23 cc/g to 20.6 cc/g at 0 and 40% RH, respectively, and further reduced down to 19 cc/g at 80% RH [267]. In contrast, another study was carried out by Ren et al. [268] in order to investigate the CO_2 capture behavior of N-doped porous carbon in a fixed bed reactor with a sorbent dosage of 0.5 g. The inlet flow rate of the gas mixture containing 15% CO_2 and 85% N_2 was about 40 mL/min. This carbon sorbent exhibited high CO_2 uptake capacities under pure CO_2 gas flow and for the gas mixture of 15/85% CO_2/N_2 in the range of 4.59–6.73 mmol/g. The CO_2 selectivity value for the simulated flue gas was as high as 63 at 25 °C [268]. Nasri et al. [269] have measured the CO_2 capture performance of palm kernel shell-activated carbon in a fixed bed adsorption unit. The experimental results demonstrated that the time taken reach the equilibrium increased with the pressure valuing 50 min and 130 min at low and high pressures, respectively. Additionally, the CO_2 capture capacity dramatically increased with pressure (1.66 mmol/g at 1 bar and 7.32 mmol/g at 4 bar) [269].

5.2. Moving Bed

Moving bed contactor is another widely investigated reactor type for CO_2 gas adsorption as an alternative to fixed bed contactors [35]. In moving bed configuration, the sorbent particles are moved through different sections operated at the same operating conditions to reduce the pressure drop compared to an equivalent fixed bed [270]. The major drawback associated with this reactor type is the higher complexity. This complexity of the design arises with the necessity of moving the sorbent particles between different reactors while limiting the possibility for carrying out the PSA process. Besides, the moving bed contactor can overcome one of the significant shortcomings of the TSA process in a fixed bed reactor: the long cycle time related to heating/cooling steps, which eventually lowers the separation process efficiency [271].

Although the arrangement of the moving bed is similar to the multi-stage fluidized bed, during the enhancement of sorbent working capacity, at the same time, the heat transfer efficiency drops owing to poor mixing [35,272]. On the other hand, the major drawback in large-scale moving beds is that the feed gas velocity should be maintained as small enough to prevent the solids from being fluidized and simultaneously increase the footprint [271]. Moving bed configuration can be divided into two major categories as follows:

(i) Conventional moving bed: The conventional moving bed is similar to the fixed bed, benefiting from enabling the steady-state operation [248]. Additionally, the reactor is shorter than the conventional fixed bed and thus, reduces the pressure drop [270].
(ii) Rotary bed: The concept of a rotary bed has been innovated as an alternative to traditional moving beds [248]. This reactor configuration comprises a rotating reactor that can effectively separate CO_2 from industrial flue gas [248]. Even though the rotary bed enables steady-state operation, there might be sealing and leakage problems [248].

Hornbostel et al. [273] have prepared a carbon sorbent using commercial PVDC-methyl acrylate copolymer. The diameter of the prepared microbeads was in the range of 150–300 μm while the physical properties of the beads indicated that the heat capacity was constant in the temperature range of 25–100 °C, and it was also reported that the high thermal conductivity (0.82–0.90 W/mK) and low heat capacity (~1 J/gK) of the beads are capable of providing fast heat transfer rates. For the CO_2 adsorption measurements, the prepared sorbent was loaded into a moving bed. For a 100% CO_2 gas flow, the equilibrium CO_2 adsorption capacity was 4.5 mmol/g at standard temperature and pressure (STP).

Additionally, at 0.15 bar, the CO_2 partial pressure for a typical flue gas stream, and the CO_2 uptake was recorded as 1.76 mmol/g at 25 °C. Moreover, for a gas mixture containing 15% CO_2 and 85% N_2, the CO_2 adsorption capacity was reduced by around 5% as the temperature was increased from 25–30 °C. Most importantly, the experimental studies suggested maintaining the flue gas temperature as low as possible to reduce the sorbent amount in the bed. Thus, the capture capacity could be optimized. Besides, the heat required to raise the temperature of the sorbent material from 30–110 °C is estimated to be 80 J/g. Interestingly, this sorbent could exhibit higher selectivity values for CO_2 over other gases in a flue gas stream in the presence of N_2, O_2, SO_2, and Ar [273].

A separate study was conducted by Okumura et al. [274] to investigate the CO_2 capture performance of amine-functionalized sorbent materials using a Kawasaki CO_2 capacity moving bed system (KCC system). The results of this study indicated that the adsorber could remove over 90% of CO_2 contained in the exhaust gas and the sorption capacity of this bed was 1.6 T/day [274].

5.3. Fluidized Bed

In fluidized bed configuration, the adsorbent particles circulate as a fluid under a high mixing rate between the interconnected reactors, namely, adsorber and regenerator, which results in an excellent mass and heat transfer across the bed [248,275,276]. Fluidized beds act as potential candidates for TSA operation [277–279] due to better temperature control and the ability to recover or add heat into the bed depending on the need [275,280]. Fluidized bed reactors offer some inherent advantages over fixed bed configuration, including (i) excellent solid–gas contact due to continuous agitation of the adsorber particles, (ii) minimum resistance towards diffusion, (iii) faster kinetics, (iv) ability in managing the pressure drop limit, and (v) applicability of high flue gas velocities [246,281].

Though fluidized bed possesses the advantages mentioned above, it also presents a few disadvantages, such as complexity during scale-up [275]. The fluidized bed reactors were widely operated in the early stage using chemisorbents such as K_2CO_3 and Na_2CO_3 [282,283]. Interestingly, chemisorbents such as amine-functionalized carbons and silica materials have captured greater attention as potential candidates to be used in this bed configuration [211,284]. Fluidized bed reactors can be categorized into three significant configurations, as stated below.

(i) Single-stage fluidized bed: Single-stage fluidized bed operated at steady-state with a low-pressure drop while providing a high heat transfer coefficient in the range of 300–600 W/m^2 K [281]. On the contrary, this bed configuration possesses some disadvantageous properties, including attrition of sorbents and lower working capacity due to back mixing [275].

(ii) Multistage fluidized bed: Compared to the single-stage fluidized bed reactor, the multi-stage fluidized bed reduces the internal back mixing by introducing a plug flow behavior while enhancing the CO_2 capture performance as in packed beds just after 3–5 stages [285]. Moreover, the cost associated with the multi-stage fluidized bed is notably higher than that of the single-stage fluidized bed configuration. Even though high driving forces and improved CO_2 capture could be achieved in multi-stage fluidized beds, the complexity of this bed configuration hinders the industrial scale deployment [286].

(iii) Transient fluidized bed: The concept of transient fluidized bed reactor, which is also known as the swing adsorption reactor cluster (SARC), was initially proposed by Zaabat et al. [287]. In this bed configuration, there is no solid particle circulating, which enables the application of VSA during the regeneration step [287]. In this reactor, the back mixing is further reduced concerning the multi-stage fluidized bed [288], and a significant reduction of the energy penalty compared to other benchmarking technologies [289] improved CO_2 capture efficiencies, which meant adsorber working capacities [290] could be achieved. Interestingly, this contactor configuration

can be easily retrofitted into existing plants while applying both TSA and steam regeneration processes [291].

Das et al. [211] have developed a four-stage fluidized bed reactor to observe the sorption behavior of DEA-impregnated activated carbons prepared from green coconut shells at different operating conditions. According to their study, the maximum CO_2 gas removal efficiency of 80% was obtained under a high sorbent particle flow rate of 4.12 kg/h, a low gas flow rate of 0.188 m/s, and a considerable weir height of 50 mm [213]. Another separate study was conducted to observe the CO_2 removal ability of MEA-impregnated activated carbon in a four-staged fluidized bed reactor [284]. Most importantly, the study was able to reveal that the removal efficiency of CO_2 gas is a function of CO_2 concentration in the inlet gas stream, gas velocity, solid flow rate, and weir height [211,284]. The maximum CO_2% removal was obtained valuing 94.9% at a high solid flow rate of 4.12 kg/h, the low gas velocity of 0.188 m/s, and a significant weir height of 50 mm. Besides, a higher amine impregnation ratio has also led to better CO_2% removal efficiencies due to the availability of more functional groups [284]. Based on the optimization study carried out by Das et al. [292] using a multi-stage fluidized bed reactor, it was found that the optimum CO_2 gas removal efficiency of 95.17% was obtained with an initial CO_2 feed gas concentration of 7312 ppm, chemical impregnation ratio of 0.31, and a weir height of 48.65 mm.

On the contrary, Raganati et al. [293] have explored the CO_2 capture behavior of activated carbon using both common and sound-assisted fluidized bed reactor configuration. The results of this study showed that the acoustic field has a positive impact on the fluidization quality and CO_2 capture capacity, adsorption rate, and the fraction of the reactor bed utilized until the breakthrough occurred, while the optimum frequency range that provided the best capture performance was in the range of 50–120 Hz [293]. A laboratory-scale fluidized bed assisted by acoustic fields was used to examine the CO_2 removal of fine activated carbon using the TSA process. The experimental results demonstrated that the activated carbons were completely regenerated in the temperature range of 25–150 °C, and it was reported that the desorption temperatures larger than 70 °C were always favorable [294]. On the other hand, another study was carried out by Raganati et al. [295] using a lab-scale sound-assisted fluidized bed to investigate the CO_2 sorption performance of activated carbon under the TSA process. Activated carbon could be completely regenerated at 70 °C using both ordinary and sound-assisted fluidized bed reactors. Additionally, a longer desorption time duration was required for a more effective regeneration [295]. Apart from the studies mentioned above, Raganati et al. [296] have conducted adsorption and desorption tests using commercially available activated carbon using a lab-scale sound-assisted fluidized bed apparatus. An increase in the CO_2 recovery level with the increment of regeneration temperature was observed, whereas 80% CO_2 recovery could be obtained at 1 atm and a moderate desorption temperature of 130 °C [296].

However, much more research should be dedicated to process optimization due to the wide availability of different adsorbent materials, processing conditions and contactor configurations.

Even though numerous research studies are currently underway for discovering and synthesizing novel carbon-based materials for CO_2 capture, their practical applications on the commercial scale have been identified as a challenging task. As reported elsewhere, CCS or CCSU technologies face technical and economic challenges during large-scale deployment. Most importantly, these technologies require a considerable capital investment. Besides, sustainability issues associated with large-scale development should be carefully considered, and eco-friendliness should be maintained. Therefore, the environmental impacts should be accessed on a life cycle basis. Apart from the above, from an economic point of view, to assess whether a particular adsorbent is effective in contactor configuration, the experimental and theoretical studies that generate engineering data, including the heat of adsorption–desorption, stability over 1000 cycles, reusability, resistance against surface erosion, equilibrium CO_2 adsorption capacity over a range of temperatures, pressures

and CO_2 concentrations, breakthrough time, kinetic adsorption–desorption data, amine efficiency of amine-functionalized materials, the effect of moisture and flue gas contaminants/impurities on the CO_2 capture performance, thermal, chemical and mechanical stability, thermal and electrical conductivity should be investigated. However, due to the lack of such critical data, design and economic analysis are limited.

The effectiveness of the adsorbent is also highly dependent on the contactor bed configuration. Therefore, choosing an appropriate contactor that exhibits the highest adsorbent performance is vital in CO_2 capture. The available contactor types such as fixed bed, fluidized bed, and moving bed are matured, whereas circulating-bed, fast-fluidized bed, and transport bed are still in the developmental stage. Of these contactors, the fluidized bed is superior to fixed beds due to its advantageous properties, including minimal diffusion resistance, faster adsorption–desorption kinetics, better solid–gas contact, and uniform temperature throughout the bed [110]. It is reported that multistage-fluidized beds could notably reduce energy consumption while performing at high separation efficiencies. The combination of VSA and TSA is capable of reducing the regeneration cost. Moreover, it is crucial to determine the optimum adsorbent content to be inserted in a contactor, since a reduced adsorbent amount reduces operational cost due to lower temperature change and pressure drop within the gas stream [87]. On the other hand, a novel ESA is a cost-effective desorption strategy for amine-functionalized adsorbent materials. During industrial-scale carbon capture, adsorbents with longer breakthrough times should be synthesized to reduce the cost of the overall capture process. Research studies showed that the pH of the adsorbent could be increased to improve the capture capacity for shorter time intervals (<2 min), and, consequently, the breakthrough time decreases. Furthermore, an adsorbent should demonstrate stability over 1000 cycles and, henceforth, an appropriate regeneration strategy should be developed that may retain the adsorption capacity over multiple cycles.

During industrial-level applications, the cost of the adsorbent material should be reduced as much as possible, and the energy, time saving, and cheap synthesis routes should be adopted. The utilization of biomass as a carbon precursor can reduce the cost of raw materials due to their abundant availability and renewability. Having a local biomass resource can remarkably lower the costs associated with transportation of the feedstock while maintaining sustainability. Although the generation of narrow micropores is beneficial for a superior CO_2 capture capacity, designing such porous structures with marrow micropores is quite challenging via chemical activation. Thus, in recent years, nano-templating has garnered considerable attention, as it is capable of generating controlled pore size distribution. However, such processes are uneconomical. Interestingly, recent advances have witnessed that ultrasound technology reduces ash content during adsorbent synthesis. Apart from the above, it is desirable to design adsorbent materials that exhibit high CO_2 adsorption capacities at temperatures above 100 °C. It avoids cooling the flue gas before adsorption and can be beneficial from a cost and energy perspective. Most importantly, the adoption of single-stage carbonization and activation process is time, energy-saving, and cost-effective, as it reduces the overall cost associated with consumables and equipment wear and tear. Though many research activities aim for carbon capture by CO_2 gas streams containing high CO_2 concentrations, the removal of CO_2 in confined spaces such as underground parking and mines, space crafts, and cockpits is also of great importance. However, the challenge is at low CO_2 concentrations; the adsorbents demonstrate low adsorption capacities. Moreover, during carbon-based adsorbent synthesis, by-products might form, and hence, the collected by-products can be used for another product synthesis. For example, during carbon nano-flakes preparation, suberin is formed during the thermal pre-treatment of cork, and this collected suberin can be used for synthesizing polymer coatings and composites.

Since flue gas contains water vapor, the adsorbent material should demonstrate a higher CO_2 selectivity over H_2O since the presence of H_2O in the pores eventually results in higher regeneration costs. However, researchers stated that multi-layered adsorption

columns could eliminate the water vapor entering the adsorbent layer, as it contains a water desiccant [171]. The adsorbent shape also plays a vital role in cost and time during upscaling processes. Therefore, the adsorbents synthesized in powder form may require additional shaping before commercialization [153]. According to the published literature, amongst different macro-shaped solid adsorbents, the sphere is beneficial as it reduces the flow resistance and abrasion in the contactors. Additionally, monoliths demonstrate advantageous properties over the other adsorbent shapes owing to lower pressure drop in the flue gas streams, faster mass transport, and easy handling. However, monoliths exhibit shorter breakthrough times, reducing process effectiveness, increasing the overall cost, and reducing CO_2 capture performances during cyclic operations. Smaller amounts of polymer particles are often utilized to overcome the reduced cyclic stability of monoliths. However, such processes could lower CO_2 capture capacity [191]. Furthermore, even though carbon aerogels show superior CO_2 adsorption capacities, the synthesis process is expensive and lengthy since it comprises supercritical and freeze-drying. Interestingly, of the different carbon-based materials, CNTs have been proven as effective carbon capture candidates due to better chemical, thermal, and mechanical stability and high specific surface area [218].

When using amine-functionalized carbon adsorbents for CO_2 capture, some challenges have to be faced, including reduced CO_2 capture capacity due to pore blockage and poor stability due to amine degradation. Steric hindrance of bulky amine groups can also significantly reduce the interaction between amine group and CO_2 and thus lower CO_2 uptake. During temperature swing operations, using pure CO_2 purge gas stream at high temperatures may result in amine degradation through urea linkage formation. On the other hand, when choosing an amine, it is preferred to use high molecular weight amines such as PEI, which may provide better thermal and cyclic stability than TEPA. However, during impregnation of PEI into porous carbon supports, it is reported that the high molecular weight PEI does not quickly enter the pores of the carbon support. Though long-time stirring promotes PEI or the other amines to be coated on the support surface during evaporation of the solvent, long-time stirring destroys the shape of the adsorbent while not being suitable for large-scale applications. In recent approaches, polyethylene glycol (PEG) has been employed as an additive during synthesis to improve the lifetime of the adsorbent. PEG is also capable of increasing the diffusion kinetics and cyclic performance. On the other hand, oxidative degradation is also one of the significant stability issues aroused when using amine-based CO_2 adsorbents when the flue gas stream contains a significant amount of O_2 and uses air for cooling the adsorbent materials after desorption. Many efforts have been put towards converting primary amines into secondary or ternary amines to overcome oxidative degradation. Besides amine evaporation, leaching might occur during regeneration via TSA. Therefore, the thermal stability of the amine-functionalized carbon materials should be carefully examined in long-term implementations. Furthermore, the CO_2 adsorption capacity should be investigated under actual gas stream conditions, including elevated temperatures, gaseous streams with impurities and water, and low CO_2 partial pressures, since the CO_2 capture performance in actual conditions may be worse than the laboratory conditions. Another challenge that arises during the selective adsorption of CO_2 in the presence of other acidic gases is the irreversible adsorptive nature of NO_2 and SO_2 by amines under dry and humid conditions.

6. Future Research Directions

Even though extensive research studies have been conducted to discover numerous carbon-based CO_2 adsorbent materials for mitigating the negative impacts gained by the increase of atmospheric CO_2 concentration, the currently developed materials still exhibit several limitations, including high cost, energy, and time consumption owing to the adoption of lengthy and costly synthesis procedures, and the utilization of expensive raw materials. Limited research works have been carried out to investigate the CO_2 capture behavior of carbon-based materials synthesized via ultrasonic treatment and sonication methods. These treatment methods are time-saving and energy-efficient compared to

conventional thermal activation treatments. Moreover, the single-step carbonization and activation processes offer advantages such as reducing consumables and equipment wear and tear and providing high energy efficiency compared to the conventional two-step process of carbonization and activation, which notably increases the final cost of sorbent material. Additionally, it is reported that KOH, which is widely used as the chemical activator in numerous research activities, is not favorable from an economic and environmental point of view. In contrast, KOH requires higher temperatures over 600 °C to improve functionality. Therefore, it is necessary to discover chemical activators which function in low-temperature ranges of around 400–500 °C.

The researchers should be encouraged to adopt synthesis procedures containing lower activation temperatures since it avoids equipment corrosion, and is also favorable for energy savings and the development of microporosity. Another issue that arises during adsorbent synthesis is the destruction of the spherical morphology after activation processes. Thus, discovering synthesis routes that retain the physical structure of the final adsorbent material is highly important. Most importantly, most of the time, the heat treatment during adsorbent synthesis is conducted using tubular furnaces, which exhibits disadvantages such as high time and energy consumption, huge risk of ash formation, high-cost expenditure, non-uniform temperature profile, hindering the release of volatile gases which eventually affects the quality of the end material. On the other hand, it is said that the microwave treatment is a promising technology that can be used during the adsorbent synthesis process to offer several advantages over the conventional furnace heating, including cost-saving, reduced energy consumption and short operational time durations, better pore formation of porous carbon materials due to better release of volatile gases, and hence the future research activities should be focused on synthesis procedures, resulting in better pore formation, lower time and energy consumption, and cost-effectiveness.

Another crucial aspect is the selection of cheap raw materials for preparing cost-effective adsorbents. In this regard, the utilization of lignocellulosic waste materials can be considered a cost-effective approach. Additionally, the exploration of novel carbon precursors which possess basic sites such as nitrogen, sulfur, and metallic components is of great necessity since it avoids post-modification of the adsorbent surface while reducing energy, time, and cost. Besides, the researchers should adopt synthesis procedures and raw materials which might not harm either the environment or human health. Furthermore, the focus should be on the effective disposal of the used carbon adsorbents. The widely used resin type is resorcinol during carbon adsorbent preparation using synthetic resins, which is expensive. Hence, to reduce the cost associated with raw materials, resorcinol could be replaced with phenol or melamine. Furthermore, freeze and supercritical drying used for adsorbent synthesis should be replaced by discovering or developing cost-effective, energy-saving, and time-saving treatment methods.

Apart from the above, much effort should be devoted to preparing porous carbon materials with ultra-narrow micropores that serve as appropriate candidates in selective CO_2 adsorption, functionality enhancement, and stability against humid conditions. During carbon aerogel preparation, future research should emphasize reducing the number of steps associated with the synthesis process, reducing structural shrinkage and collapse, increasing mechanical strength, and enhancing the CO_2 selectivity. On the other hand, challenging work is needed during monolith synthesis, including enhancing mechanical strength and apparent density. Although the addition of polymer could enhance the mechanical stability of the monoliths during cyclic operation, the adsorption capacity decreases to some extent [191]. Therefore, many studies should be conducted to optimize the polymer content in the monoliths, which demonstrate better sorption capacities with higher cyclic stability.

Another issue associated with research work based on carbon-based adsorbent preparation is the lack of investigations on dynamic CO_2 adsorption behavior. Moreover, the development of porous carbons capable of adsorbing CO_2 under high gas flow conditions is highly imperative. Future research activities should be carried out under actual gas

conditions related to flue gas streams of power plants, oil refineries, and petrochemical industries, since the selectivity of CO_2 can be well defined in the presence of SO_X, NO_X, fly ash particles, and CO, using various contactor configurations, humid conditions, elevated temperatures (since the post-combustion capture is operated at high temperatures), high-pressure conditions (since the common working pressures of NG wells are around 300 bar), and low pressure (~0.1 bar) CO_2 capture conditions. For an adsorbent to be effective during practical operations, the adsorbent should be stable over 1000 cycles. However, the regeneration studies are only limited to 10–20 cyclic operations, while the adsorption capacity decreases with the increased cycle number. Therefore, it is imperative to develop a suitable regeneration strategy that retains the CO_2 sorption capacity nearly unchanged, and much dedication is required for a higher number of cyclic tests.

Another interesting aspect that needs more exploration is the design and optimization of the carbon capture process. Up to date, only a small number of articles have been published in the associated fields. Apart from the above, simulation work is also recommended for CO_2 diffusion rate as higher diffusion rates during the adsorption process can reduce the cycle time and for molecular-level influential factors. Moreover, CO_2 adsorption models can be generated when more influential factors are present. Additionally, an effort should be made to develop an interface software that can directly select the appropriate carbon-based adsorbent according to the relevant application. Furthermore, future research directions can be stated as the utilization of the synthesized carbon-based CO_2 adsorbent materials for measuring CO_2 levels in the breath, which provides a pain-free and cost-effective asthma diagnosis strategy. On the other hand, it would be an outstanding achievement if more focus is dedicated to the in-situ conversion of adsorbed CO_2 molecules on the adsorbent into cheap energy fuels since such a strategy might conserve the process sustainability and reduce the process harmful effects of CO_2 emissions.

7. Conclusions

The present review highlights the recent advances in the applicability of porous carbon materials synthesized using different carbon precursors and amine-functional groups for effective CO_2 capture. Usually, chemistry of precursors plays a vital role in determining the physicochemical characteristics of the prepared adsorbents. On the contrary, amine-functionalized carbons possess higher CO_2 selectivity over other gases and high CO_2 uptake in the presence of moisture, however, such adsorbents often suffer from being costly, structurally unstable, and requiring complicated preparation steps. Thus, CO_2 capture using amine-functionalized carbons is still less developed, and further research should be devoted towards using high molecular weight amine impregnation onto mesoporous carbon supports. Cosidering the cost and practical importance for industrial-scale production, biomass and industrial by-products play the major impact and make the porous carbons more economical. However, the performance of currently available carbon-based adsorbents should be further improved in many areas includingcyclic stability, adsorption capacity, gas selectivity, and resistivity against a range of temperatures and pressures. Interestingly, the capability of designing and tuning the porous carbon materials to achieve superior CO_2 capture performances from different gas streams make these materials more promising compared to other adsorbents. Accordingly, prompt measures should be taken to deploy CCS technologies that decrease atmospheric CO_2 concentration via converting the captured CO_2 into high-value products without harming the environment.

Author Contributions: Conceptualization, C.A.G., K.V. and O.H.P.G.; methodology, C.A.G. and O.H.P.G.; software, O.H.P.G.; validation, C.A.G., K.V., O.H.P.G. and S.M.A.; formal analysis, C.A.G., K.V., O.H.P.G. and S.M.A.; investigation, C.A.G. and O.H.P.G.; resources, data curation, writing—original draft preparation, C.A.G., S.M.A. and O.H.P.G.; writing—review and editing, C.A.G., K.V., O.H.P.G. and S.M.A.; visualization, supervision, project administration, C.A.G. and K.V.; funding acquisition, K.V. All authors have read and agreed to the published version of the manuscript.

Funding: This research received no external funding.

Institutional Review Board Statement: Not applicable.

Informed Consent Statement: Not applicable.

Data Availability Statement: Not applicable.

Conflicts of Interest: The authors declare no conflict of interest.

References

1. North, M. Chapter I-What is CO_2? Thermodynamics, basic reactions and physical chemistry. In *Carbon Dioxide Utilization*; Styring, P., Quadrelli, E.A., Armstrong, K., Eds.; Elsevier: Amsterdam, The Netherlands, 2015; pp. 3–17.
2. Salehi, S.; Anbia, M.; Hosseiny, A.H.; Sepehrian, M. Enhancement of CO_2 adsorption of polyethylenimine functionalized multiwalled carbon nanotubes/Cd-nanozeolite composites. *J. Mol. Struct.* **2018**, *1173*, 792–800. [CrossRef]
3. Kaur, B.; Singh, J.; Gupta, R.K.; Bhunia, H. Porous carbons derived from polyethylene terephthalate (PET) waste for CO_2 capture studies. *J. Environ. Manag.* **2019**, *242*, 68–80. [CrossRef] [PubMed]
4. Wang, X.; Zhou, J.; Xing, W.; Lui, B.; Zhang, J.; Lin, H.; Cui, H.; Zhou, S. Resorcinol-formaldehyde resin-based porous carbon spheres with high CO_2 capture capacities. *J. Energy Chem.* **2017**, *26*, 1007–1013. [CrossRef]
5. Qin, F.; Guo, Z.; Wang, J.; Qu, S.; Zuo, P.; Shen, W. Nitrogen-doped asphaltene-based porous carbon nanosheet for carbon dioxide capture. *Appl. Surf. Sci.* **2018**, *491*, 607–615. [CrossRef]
6. Wang, J.; Yuan, X.; Deng, S.; Zeng, X.; Yu, Z.; Li, S.; Lia, K. Waste polyethylene terephthalate (PET) plastics-derived activated carbon for CO_2 capture: A route to a closed carbon loop. *Green Chem.* **2020**, *22*, 6836–6845. [CrossRef]
7. Tehrani, N.H.M.H.; Alivand, M.S.; Maklarany, D.M.; Rashidi, A.; Samipoorgini, M.; Seif, A.; Yousefian, Z. Novel asphaltene-derived nanoporous carbon with N-S-rich-micro-mesoporous structure fro superior gas adsorption: Experimental and DFT study. *Chem. Eng. J.* **2018**, *358*, 1126–1138. [CrossRef]
8. Sepahvand, S.; Jonobi, M.; Ashori, A.; Gauvin, F.; Brouwers, H.J.H.; Oksman, K.; Yu, Q. A promising process to modify cellulose nanotubes for carbon dioxide (CO_2) adsorption. *Carbohydr. Polym.* **2019**, *230*, 115571. [CrossRef]
9. Rahimi, K.; Riahi, S.; Abbasi, M.; Fakhroueian, Z. Modification of multi-walled carbon nanotubes by 1,3-diaminepropane to increase CO_2 adsorption capacity. *J. Environ. Manag.* **2019**, *242*, 81–89. [CrossRef]
10. Jang, E.; Choi, S.W.; Hong, S.; Shin, S.; Lu, K.B. Development of a cost-effective CO_2 adsorbent from petroleum coke via KOH activation. *Appl. Surf. Sci.* **2017**, *429*, 62–71. [CrossRef]
11. Khuong, D.A.; Nguyen, H.N.; Tsubota, T. Activated carbon produced from bamboo and solid residue by CO_2 activation utilized as CO_2 adsorbents. *Biomass Energy* **2021**, *148*, 106039. [CrossRef]
12. Kaur, B.; Gupta, R.K.; Bhunia, H. CO_2 capture on activated carbon from PET (polyethylene terephthalate) waste: Kinetics and modelling studies. *Chem. Eng. Commun.* **2019**, *207*, 1031–1047. [CrossRef]
13. Tiwari, D.; Bhunia, H.; Bajpai, P.K. Development of chemically activated N-enriched carbon adsorbents from urea-formaldehyde resin for CO_2 adsorption: Kinetics, isotherm, and thermodynamics. *J. Environ. Manag.* **2018**, *218*, 579–592. [CrossRef] [PubMed]
14. Irani, M.; Jacobson, A.T.; Gasem, K.A.M.; Fan, M. Modified carbon nanotubes/tetraethylpentamine for CO_2 capture. *Fuel* **2017**, *206*, 10–18. [CrossRef]
15. Li, Y.; Wang, X.; Cao, M. Three-dimensional porous carbon frameworks derived from mangosteen peel waste as promising materials for CO_2 capture and supercapacitors. *J. CO_2 Util.* **2018**, *27*, 204–216. [CrossRef]
16. Liu, Z. National carbon emissions from the industry process: Production of glass, soda ash, ammonia, calcium carbide and alumina. *Appl. Energy* **2016**, *66*, 239–244. [CrossRef]
17. Sher, F.; Iqbal, S.Z.; Albazzaz, S.; Ali, U.; Mortari, D.A.; Rashidi, T. Development of biomass derived highly porous fast adsorbents for post-combustion CO_2 capture. *Fuel* **2020**, *282*, 118506. [CrossRef]
18. Lal, R. Acceleration soil erosion as a source of atmospheric CO_2 soil. *Soil Tillage Res.* **2019**, *199*, 35–40. [CrossRef]
19. Li, Y.; Liu, N.; Zhang, T.; Wang, B.; Wang, Y.; Wang, L.; Wei, J. Highly microporous nitrogen-doped carbons from anthracite for effective CO_2 capture and CO_2/CH_4 separation. *Energy* **2020**, *211*, 118561. [CrossRef]
20. Li, Y.; Xu, R.; Wang, B.; Wei, J.; Wang, L.; Shen, M.; Yang, J. Enhanced N-doped porous carbon derived from KOH-activated waste wool: A promising material for selective adsorption of CO_2/CH_4 and CH_4/N_2. *Nanomaterials* **2019**, *9*, 266. [CrossRef]
21. An, L.; Liu, S.; Wang, L.; Wu, J.; Wu, Z.; Ma, C.; Yu, Q.; Hu, X.C. Novel nitrogen-doped porous carbons derived from graphene for effective CO_2 capture. *Ind. Eng. Chem. Res.* **2019**, *58*, 3349–3358. [CrossRef]
22. Liu, Y.; Ghimie, P.; Jaroniec, M. Copper Benzene-1,3,5-Tricarboxylate (Cu-BTC) metal-organic framework (MOF) and porous carbon composites as effective carbon dioxide adsorbents. *J. Colloid Interface Sci.* **2018**, *535*, 122–132. [CrossRef] [PubMed]
23. Yuan, X.; Lee, J.G.; Yun, H.; Deng, S.; Kim, Y.J.; Lee, J.E.; Kwak, S.K.; Lee, K.B. Solving two environmental issues simultaneously: Waste polyethylene terephthalate plastic bottle-derived microporous carbons for capturing CO_2. *Chem. Eng. J.* **2020**, *397*, 125350. [CrossRef]
24. Tu, R.; Sun, Y.; Wu, Y.; Wang, J.; Chen, S.; Jia, Z.; Jiang, E.; Xu, X. Bio-tar derived porous carbon with high gas uptake capacities. *Renew. Energy* **2021**, *167*, 82–90. [CrossRef]
25. Benedetti, V.; Cordioli, E.; Patuzzi, F.; Baratieri, M. CO_2 adsorption study on pure and chemically activated chars derived from commercial biomass gasifiers. *J. CO_2 Util.* **2019**, *33*, 46–54. [CrossRef]

26. Patel, H.A.; Byun, J.; Yavez, C.T. Carbon dioxide capture adsorbents: Chemistry and Methods. *ChemSusChem* **2017**, *10*, 1303–1317. [CrossRef]
27. Kukulka, W.; Cendrowski, K.; Michalkiewicz, B.; Mkijowska, E. MOF-5 derived carbon as material for CO_2 adsorption. *R. Soc. Chem.* **2019**, *9*, 18527–18537. [CrossRef]
28. Dilokekunakul, W.; Teerachawanwong, P.; Klomkliang, N.; Supasitmouskol, S.; Chaemucheun, S. Effects of nitrogen and oxygen functional groups and pore width of activated carbon on carbon dioxide capture: Temperature dependence. *Chem. Eng. J.* **2020**, *389*, 124413. [CrossRef]
29. Arifin, N.P.T.A.; Zulkipils, N.A.N.; Yusof, N.; Ismail, A.F.; Azizi, F.; Salleh, W.N.W.; Jalefar, J.; Nordin, N.A.H.M.; Sazali, N. Preparation and characterization of APTES-functionalized graphene oxide for CO_2 adsorption. *J. Adv. Res. Fluid Mech. Therm. Sci.* **2019**, *61*, 297–305.
30. Dassanayake, R.S.; Acharya, S.; Abidi, N. Biopolymer-based material from polysaccharides: Properties, processing, characterization and sorption applications. *Adv. Sorpt. Process Appl.* **2018**, 1–24. [CrossRef]
31. Omidfar, N.; Mohamadalizadeh, A.; Mousavi, S.H. Carbon dioxide adsorption by modified carbon nanotubes. *Asia-Pac. J. Chem. Eng.* **2015**, *10*, 885–892. [CrossRef]
32. Idrees, M.; Rangari, V.; Jeelani, S. Sustainable packaging waste-derived activated carbon for carbon dioxide capture. *J. CO_2 Util.* **2018**, *26*, 380–387. [CrossRef]
33. Lee, S.; Park, S. A review on solid adsorbents for carbon dioxide capture. *J. Ind. Eng. Chem.* **2015**, *23*, 1–11. [CrossRef]
34. Kamran, U.; Choi, J.R.; Park, S. A role of activation for efficient CO_2 affinity on polyacronitrile based porous carbon materials. *Front. Chem.* **2020**, *8*, 710. [CrossRef] [PubMed]
35. Sreenivasalu, B.; Gayatri, D.V.; Sreedhar, I.; Ragharan, K.V. A journey into the process and engineering aspects of carbon capture technologies. *Renew. Sustain. Energy Rev.* **2015**, *41*, 1324–1350. [CrossRef]
36. Tiwari, D.; Bhunia, H.; Bajpai, P.K. Urea-formaldehyde derived porous carbons for adsorption of CO_2. *R. Soc. Chem.* **2016**, *6*, 111842–111855. [CrossRef]
37. Deng, M.; Park, H.G. Spacer-assisted amine-coiled carbon nanotubes for CO_2 capture. *Langmuir* **2019**, *35*, 4453–4459. [CrossRef]
38. Jena, K.K.; Panda, A.P.; Verma, S.; Mani, G.K.; Swain, S.K.; Alhassan, S.M. MWCNTs-ZnO-SiO_2 mesoporous nano-hybrid materials for CO_2 capture. *J. Alloy Compd.* **2019**, *800*, 279–285. [CrossRef]
39. Othman, F.E.C.; Yusof, N.; Ismail, A.F. Activated-carbon nanofibers/graphene nanocomposites and their adsorption performance towards carbon dioxide. *Chem. Engl. Technol.* **2020**, *43*, 2023, 2030. [CrossRef]
40. Shao, L.; Song, Y.; Huang, J.; Liu, Y. Triazine-based hyper-cross-linked polymers with inorganic-organic hybrid framework derived porous carbons for CO_2 capture. *Chem. Eng. J.* **2018**, *353*, 1–14. [CrossRef]
41. Salehi, S.; Anbia, M. Highly efficient CO_2 capture with a metal-organic framework-derived porous carbon impregnated with polyethylenimine. *Appl. Organomet. Chem.* **2018**, *32*, e4390. [CrossRef]
42. Tiwari, D.; Bhunia, H.; Bajpai, P.K. Adsorption of CO_2 on KOH activated N-enriched carbon derived from urea-formaldehyde resin: Kinetics, isotherm and thermodynamic studies. *Appl. Surf. Chem.* **2018**, *439*, 760–771. [CrossRef]
43. Ben-Mansour, R.; Habib, M.A.; Bamidek, O.E.; Basha, M.; Qasem, N.A.A.; Peedikakkal, A.; Laoui, T.; Ali, M. Carbon capture by physical adsorption: Materials, experimental investigations and numerical modelling and simulations-a review. *Appl. Energy* **2016**, *161*, 225–255. [CrossRef]
44. Han, J.; Zhang, L.; Zhao, B.; Qin, L.; Wang, Y.; Xing, F. The N-doped activated carbon derived from sugarcane bagasse for CO_2 adsorption. *Ind. Crops Prod.* **2019**, *128*, 290–297. [CrossRef]
45. Tiwari, D.; Kaur, S.; Bhunia, H.; Bajpai, P.K. CO_2 adsorption on oxygen enriched nanostructured carbon derived from silica templated resorcinol-formaldehyde. *J. Ind. Eng. Chem.* **2018**, *65*, 146–155. [CrossRef]
46. Nazir, G.; Rehman, A.; Park, S. Role of heteroatoms (nitrogen and sulfur)-dual doped corn-starch based porous carbons for selective CO_2 adsorption and separation. *J. CO_2 Util.* **2021**, *51*, 101641. [CrossRef]
47. Guo, Y.; Tan, C.; Sun, J.; Li, W.; Zhang, J.; Zhao, C. Porous activated carbon derived from waste sugarcane bagasse for CO_2 adsorption. *Chem. Eng. J.* **2020**, *381*, 122736. [CrossRef]
48. Gunathilake, C.; Dassanayake, R.S.; Abidi, N.; Jaroniec, M. Amidoxime-functionalized microcrystalline cellulose-mesoprous silica composites for carbon dioxide sorption at elevated temepratures. *J. Mater. Chem. A* **2016**, *4*, 4808–4819. [CrossRef]
49. Alabadi, A.; Razzaue, S.; Yang, Y.; Chen, S.; Tan, B. Highly porous activated carbon materials from carbonized biomass with high CO_2 capturing capacity. *Chem. Eng. J.* **2015**, *281*, 606–612. [CrossRef]
50. Liu, X.; Sun, C.; Liu, H.; Tan, W.H.; Wang, W.; Snape, C. Developing hierarchical ultra-micro mesoporous biocarbons for highly selective carbon dioxide adsorption. *Chem. Eng. J.* **2018**, *361*, 199–208. [CrossRef]
51. Dassanayake, R.S.; Gunathilake, C.; Dassanayake, A.C.; Abidi, N.; Jaroniec, M. Amidoxime-functionalized nanocrystalline cellulose-mesoporous silica composites for carbon dioxide sorption of ambient and elevated temperatures. *J. Mater. Chem. A* **2017**, *5*, 7462–7473. [CrossRef]
52. Dassanayake, R.; Gunathilake, C.; Abidi, N. Activated carbon derived from chitin aerogels: Preparation and CO_2 desorption. *Cellulose.* **2018**, *25*, 1911–1920. [CrossRef]
53. Lashake, M.J.; Khiavi, S.; Sayari, A. Stabilizing of amine-functionlaozed CO_2 adsorbents: A multifunctional puzzle. *Chem. Soc. Rev.* **2019**, *48*, 3320–3405. [CrossRef] [PubMed]

54. Igalavithana, A.D.; Choi, S.W.; Shang, J.; Hanif, A.; Dissanayake, P.D.; Tsang, D.C.W.; Kwon, J.; Lu, K.B.; Ok, Y.S. Carbon dioxide capture in biochar produced from pine sawdust and paper mill sludge: Effect of porous structure and surface chemistry. *Sci. Total Environ.* **2020**, *739*, 139845. [CrossRef] [PubMed]
55. Estevez, L.; Barpaga, D.; Zheng, J.; Sabale, S.R.; Patel, R.L.; Zhang, J.; McGrail, B.P.; Motkuri, B.K. Hierarchically porous carbon materials for CO_2 capture: The role of pore structure. *Ind. Eng. Chem. Res.* **2017**, *57*, 1262–1268. [CrossRef]
56. Mehrrarz, E.; Ghreyshi, A.A.; Jahanshaki, M. Adsorptive separation of CO_2 and CH_4 by the broom sorghum based activated carbon functionalized by diethanolamine. *Korean J. Chem. Eng.* **2016**, *34*, 413–424. [CrossRef]
57. Liu, K.; Jin, B.; Meng, L. Glucose/Graphene-based aerogels for gas adsorption and electric double layer capacitors. *Polymers* **2018**, *11*, 40. [CrossRef] [PubMed]
58. He, J.; To, J.W.F.; Psarras, P.C.; Yan, H.; Atkinson, T.; Holmes, R.T.; Norduland, D.; Bao, Z.; Wilcox, J. Tunable polyaniline-based porous carbon with ultrahigh surface area for CO_2 capture at elevated pressure. *Adv. Energy Mater.* **2016**, *6*, 1502491. [CrossRef]
59. Prasetyo, I.; Maukti, N.I.F.; Cahyono, R.B.; Prasetya, A.; Ariyanto, T. Nanoporous carbon prepared from palm kernel shell for CO_2/CH_4 separation. *Waste Biomass Volatilization* **2020**, *11*, 5599–5606. [CrossRef]
60. Shahrom, M.S.R.; Nordin, A.R.; Wilfred, C.D. The improvement of activated carbon as CO_2 adsorbent with supported amine functionalized ionic liquids. *J. Environ. Chem. Eng.* **2019**, *7*, 103319. [CrossRef]
61. Wang, J.; Zhang, P.; Liu, L.; Zhang, Y.; Yang, J.; Zeng, Z.; Deng, S. Controllable synthesis of bifunctional porous carbon for efficient gas-mixture separation and high-performance supercapacitor. *Chem. Eng. J.* **2018**, *348*, 57–66. [CrossRef]
62. Wang, J.; Huang, H.; Wang, M.; Yao, L.; Qiao, W.; Long, D.; Ling, L. Direct capture of low-concentration CO_2 on mesoporous carbon-supported solid amine adsorbents at ambient temperature. *Ind. Eng. Chem. Res.* **2015**, *54*, 5319–5327. [CrossRef]
63. Rashidi, N.A.; Yusup, S. An overview of activated carbon utilization of the post-combustion carbon dioxide capture. *J. CO_2 Util.* **2016**, *13*, 1–16. [CrossRef]
64. Zhu, X.; Tsang, D.C.W.; Wang, C.; Su, Z.; Hou, D.; Liangchun, L.; Shang, J. Machine learning exploration of the critical factors for CO_2 adsorption capacity on porous carbon materials at different pressures. *J. Clean. Prod.* **2020**, *263*, 122915. [CrossRef]
65. Chatterjee, R.; Sajjadi, B.; Chane, W.; Mattern, D.L.; Hamner, N.; Raman, V.; Dorris, A. Effect of pyrolysis temperature on physicochemical properties and acoustic-based amination of biochar for efficient CO_2 adsorption. *Front. Energy Res.* **2020**, *8*, 85. [CrossRef]
66. Singh, J.; Bhunia, H.; Basu, S. Development of sulfur-doped carbon monolith derived from phenol-formaldehyde resin for fixed bed CO_2 adsorption. *Environ. Innov.* **2020**, *20*, 101104. [CrossRef]
67. Cueller-Franca, R.M.; Azapagic, A. Carbon capture, storage and utilization technologies: A critical analysis and comparison of their life cycle environmental impacts. *J. CO_2 Util.* **2014**, *9*, 82–102. [CrossRef]
68. Rouzitalab, Z.; Maklavany, D.M.; Jafarinejad, S.; Rashidi, A. Lignocellulose-based adsorbents: A spotlight review of the effective parameters on carbon dioxide capture process. *Chemosphere* **2020**, *246*, 125746. [CrossRef]
69. Yu, J.; Xie, L.H.; Li, J.R.; Ma, Y.; Seminario, J.M.; Balbuena, P.B. CO_2 capture and separations using MOFs: Computational and experimental studies. *Chem. Rev.* **2017**, *117*, 9674–9754. [CrossRef]
70. Wang, P.; Guo, Y.; Zhao, C.; Yan, J.; Lu, P. Biomass derived wood ash with amine modification for post-combustion CO_2 capture. *Appl. Energy* **2017**, *201*, 34–44. [CrossRef]
71. Mukherjee, A.; Okolie, J.A.; Abdelrasoul, A.; Niu, C.; Dalai, A.K. Review of post-combustion carbon dioxide capture technologies using activated carbon. *J. Environ. Sci.* **2019**, *83*, 46–63. [CrossRef]
72. Najmi, B. *Operation of Power Cycles with Integrated CO_2 Capture Using Advances High-Temperature Technologies*; Department of Energy and Process Engineering, Norwegian University of Science and Technology: Trondheim, Norway, 2015; p. 77.
73. Zhang, Z.; Borhani, T.N.G.; El-Naas, M.H. Carbon Capture. In *Exegetic and Environmental Dimensions*; Academic Press, Elsevier: Amsterdam, The Netherlands, 2017.
74. Babu, P.; Linga, P.; Kumar, R.; Englezos, P. A review of the hydrate-based gas separation (HBGS) process for carbon dioxide pre-combustion capture. *Energy* **2015**, *85*, 261–279. [CrossRef]
75. Carrasco-Maldonado, F.; Sporl, R.; Fleiger, K.; Hoenia, V.; Maier, J.; Scheffknecht, G. Oxy-fuel combustion technology for cement production-state of the art research and technology development. *Int. J. Greenh. Gas Control* **2016**, *45*, 189–199. [CrossRef]
76. Zhang, X.; Elsayed, I.; Song, X.; Shmulsky, R.; Hasgan, E.B. Microporous carbon nanoflakes derived from biomass cork waste for CO_2 capture. *Sci. Total Environ.* **2020**, *748*, 142465. [CrossRef] [PubMed]
77. Henry, Z.; Rongwong, W.; Liu, H.; Fu, K.; Gao, H.; Cao, F.; Zhang, R.; Seira, T.; Henni, A.; Sumon, K.; et al. Recent progress and new developments in post-combustion carbon-capture technology with amine-based solvents. *Int. J. Greenh. Gas Control* **2015**, *40*, 26–54.
78. Singh, G.; Ismail, I.S.; Bilen, C.; Shanbhas, D.; Sathish, C.I.; Ramadass, K.; Vinu, A. A facile synthesis of activated porous carbon spheres from D-glucose using a non-corrosive activating agent for efficient carbon dioxide capture. *Appl. Energy* **2019**, *255*, 113831. [CrossRef]
79. Khalilis, S.; Khoshandam, B.; Jahanshahi, M. Synthesis of activated carbon/polyaniline nanocomposites for enhanced CO_2 adsorption. *RCS Adv.* **2016**, *6*, 35692–35704.
80. Hu, H.; Zhang, T.; Yuan, S.; Tang, S. Functionalization of multi-walled carbon nanotubes with phenylenediamine for enhanced CO_2 adsorption. *Adsorption* **2016**, *23*, 73–85. [CrossRef]

81. Yang, J.; Yue, L.; Hu, X.; Wang, L.; Zhao, Y.; Lin, Y.; Sun, Y.; DaCosta, H.; Guo, L. Efficient CO_2 capture by porous carbons derived from coconut shell. *Energy Fuels* **2017**, *31*, 4287–4293. [CrossRef]
82. Auta, M.; Umaru, M.; Yahya, M.D.; Adeniyi, O.D.; Aris, I.M.; Suleiman, B. Diethanolamine functionalized waste tea activated carbon for CO_2 adsorption. In Proceedings of the International Conference on Chemical, Environmental and Biological Sciences, Dubai, United Arab Emirates, 18–19 March 2015; pp. 96–99.
83. Bamdad, H.; Hawboldt, K.A.; MacQuarre, S.C. Nitrogen functionalized biochar as a renewable adsorbent for efficient CO_2 removal. *Energy Fuels.* **2018**, *32*, 11742–11748. [CrossRef]
84. Kim, H.R.; Yoon, T.; Kim, S.; An, J.; Bae, Y.; Lee, C.Y. Beyond pristine MOFs: Carbon dioxide capture by metal-organic frameworks (MOFs)-derived porous carbon materials. *R. Soc. Chem.* **2017**, *7*, 1266–1270. [CrossRef]
85. Yuan, X.; Li, S.; Jeon, S.; Deng, S.; Zhao, L.; Lee, K.B. Valorization of waste polyethylene terephthalate plastic into N-doped microporous carbon for CO_2 capture through a one-pot synthesis. *J. Hazard. Mater.* **2020**, *399*, 123010. [CrossRef]
86. Rashidi, N.A.; Yusup, S. Potential of pal, kernel shell as activated carbon precursors through single stage activated technique for carbon dioxide adsorption. *J. Clean. Prod.* **2017**, *168*, 474–486. [CrossRef]
87. Das, S.; Meikap, B.C. Comparison of adsorbent capacity of mono-ethanolamine and diethanolamine impregnated activated carbon in a multi-staged fluidized bed reactor for carbon-dioxide capture. *Fuel* **2018**, *224*, 47–56. [CrossRef]
88. Kamran, U.; Park, S. Tuning ratios of KOH and NaOH on acetic acid-mediated chitosan-based porous carbons for improving their textural features and CO_2 uptakes. *J. CO_2 Util.* **2020**, *40*, 101212. [CrossRef]
89. Jalilov, A.S.; Ruan, G.; Hwang, C.; Schipper, D.E.; Tour, J.J.; Li, Y.; Fei, H.; Samuel, E.L.G.; Tour, J.M. Asphalt-derived high surface area activated porous carbons for carbon dioxide capture. *ACS Appl. Mater. Interfaces* **2015**, *7*, 1376–1382. [CrossRef]
90. Tian, Y.; Lin, Y.; Hagio, T.; Hu, Y.H. Surface-microporous graphene for CO_2 adsorption. *Catal. Today* **2020**, *356*, 514–518. [CrossRef]
91. Li, M.; Xiao, R. Preparation of a dual pore structure activated carbon from rice husk char as an adsorbent for CO_2 capture. *Fuel Processing Technol.* **2019**, *186*, 35–39. [CrossRef]
92. Gadipelli, S.; Patel, A.A.; Guo, Z. An ultrahigh pore volume drives up the amine stability and cyclic CO_2 capacity of a solid-amine@carbon sorbent. *Adv. Mater.* **2015**, *27*, 4903–4909. [CrossRef]
93. Gunathilake, C.A.; Ranathunga, G.G.T.A.; Dassanayake, R.S.; Illesighne, S.D.; Mnchanda, A.S.; Kalpage, C.S.; Rajapakshe, R.M.G.; Karunaratne, D.G.G.P. Emerging investigator series: Synthesis of magnesium oxide nanoparticles fabricated on a graph oxide nanocomposite for CO_2 sequestration at elevated temperatures. *R. Soc. Chem.* **2020**, *7*, 1225–1239. [CrossRef]
94. Vinodh, R.; Babu, C.M.; Abidov, A.; Palanichainy, M.; Jang, H.T. Facile synthesis of amine modified silica reduced graphene oxide composite sorbent for CO_2 adsorption. *Mater. Lett.* **2019**, *247*, 44–47. [CrossRef]
95. Zhang, X.; Li, W.; Lu, A. Designed porous carbon materials for efficient CO_2 adsorption and separation. *New Carbon Mater.* **2015**, *30*, 481–501. [CrossRef]
96. Zhao, H.; Luo, X.; Zhang, H.; Sun, N.; Wei, W.; Suo, Y. Carbon-based adsorbents for post-combustion capture: A review. *Greenh. Gases Sci. Technol.* **2018**, *8*, 11–36. [CrossRef]
97. Xu, C.; Stromme, M. Sustainable porous carbon materials derived from wood-based biopolymers for CO_2 capture. *Nanomaterials* **2019**, *9*, 103. [CrossRef] [PubMed]
98. Singh, G.; Lakhi, K.S.; Sil, S.; Bhosale, S.V.; Kim, I.; Albahily, K.; Vinu, A. Biomass derived porous carbon for CO_2 capture. *Carbon* **2019**, *148*, 164–186. [CrossRef]
99. Berger, A.H.; Bhown, A.S. Comparing physisorption and chemisorption solid sorbents for use separating CO_2 from flue gas using temperature swing adsorption. *Energy Proc.* **2011**, *4*, 562–567. [CrossRef]
100. Nandi, M.; Uyama, H. Exceptional CO_2 adsorbents materials under different conditions. *Chem. Rec.* **2014**, *14*, 1134–1148. [CrossRef]
101. Chang, B.; Shi, W.; Yin, H.; Zhang, S.; Yang, B. Poplar catkin-derived self-templated synthesis of N-doped hierarchical porous carbon microtubes for efficient CO_2 capture. *Chem. Eng. J.* **2018**, *358*, 1507–1518. [CrossRef]
102. Kamran, U.; Park, S. Chemically modified carbonaceous adsorbents for enhanced CO_2 capture: A review. *J. Clean. Prod.* **2021**, *290*, 125776. [CrossRef]
103. Chen, Z.; Deng, S.; Wei, H.; Wang, B.; Huang, J.; Yu, G. Activated carbons and amine-modified materials for carbon dioxide capture—A review. *Front. Environ. Sci. Eng.* **2013**, *7*, 326–340. [CrossRef]
104. Tiwari, D.; Geol, C.; Bhunia, H.; Bajpai, P.K. Melamine-formaldehyde derived porous carbons for adsorption of CO_2 capture. *J. Environ. Manag.* **2017**, *197*, 415–427. [CrossRef]
105. Geol, C.; Bhunia, H.; Bajpai, P.K. Novel nitrogen enriched porous carbon adsorbents for CO_2 capture: Breakthrough adsorption study. *J. Environ. Chem. Eng.* **2016**, *4*, 346–356. [CrossRef]
106. Li, J.; Michalkiewicz, B.; Min, J.; Ma, C.; Chen, X.; Gong, J.; Mijowska, E.; Tang, T. Selective preparation of biomass-derived porous carbon with controllable pore sizes towards highly efficient CO_2 capture. *Chem. Eng. J.* **2018**, *360*, 250–259. [CrossRef]
107. Durante, L.A.; Walton, K.S.; Soll, D.S.; Jones, C.W. CO_2 capture via adsorption in amine-functionalized sorbents. *Curr. Opin. Chem. Eng.* **2016**, *12*, 82–90. [CrossRef]
108. Wang, M.; Yao, L.; Wang, J.; Zhang, Z.; Qiao, W.; Long, D.; Ling, L. Adsorption and regeneration study of polyethylenemine-impregnated millimeter-sized mesoporous carbon spheres for post-combustion CO_2 capture. *Appl. Energy* **2016**, *168*, 282–290. [CrossRef]

109. Shukrullah, S.; Naz, M.Y.; Mohamed, N.M.; Ibrahim, K.A.; Abdel-Salam, N.M.; Ghaffar, A. CVD synthesis, functionalization and CO_2 adsorption attribute of multiwalled carbon nanotubes. *Processes* **2019**, *7*, 634. [CrossRef]
110. Faisal, M.; Pamungkas, A.Z.; Krisnandi, Y.K. Study of Amine functionalized mesoporous carbon as CO_2 storage materials. *Processes* **2021**, *9*, 456. [CrossRef]
111. Cabriga, C.K.C.; Clarete, K.V.R.; Zhang, J.A.T.; Pacia, R.M.P.; Ko, Y.S.; Castro, J.C. Evaluation of biochar derived from the slow pyrolysis of rice straw as a potential adsorbent for carbon dioxide. *Biomass Convers. Biorefinery* **2021**. [CrossRef]
112. Shi, Y.; Liu, Q.; He, Y. CO_2 capture using solid sorbents. In *Handbook of Climate Change Mitigation and Adaptation*; Springer International Publishing: Cham, Switzerland, 2015.
113. Gunathilake, C.; Manchanda, A.S.; Chrimire, P.; Kruk, M.; Jaroniec, M. Amine-modified silica nanotubes and nanospheres: Synthesis and CO_2 sorption properties. *Environ. Sci. Nano* **2016**, *3*, 806–817. [CrossRef]
114. Yao, M.; Wang, L.; Hu, X.; Hu, G.; Luo, M.; Fan, M. Synthesis of nitrogen-doped carbon with three-dimensional mesostructures for CO_2 capture. *J. Mater. Sci.* **2015**, *50*, 1221–1227. [CrossRef]
115. Chen, C.; Kim, J.; Ahn, W. CO_2 capture by amine-functionalized nanoporous materials: A review. *Korean J. Chem. Eng.* **2014**, *311*, 1919–1934. [CrossRef]
116. Xu, C.; Ruan, C.; Li, Y.; Lindh, J.; Stromne, M. High performance activated carbons synthesized from nanocellulose for CO_2 capture and extremely selectivity removal of volatile organic compounds. *Adv. Sustain. Syst.* **2017**, *2*, 1700147. [CrossRef]
117. Shafeeyan, M.S.; Daud, W.M.A.W.; Shamiri, A.; Aghamohammadi, N. Adsorption equilibrium of carbon dioxide onammonia-modified activated carbon. *Chem. Eng. Res. Des.* **2015**, *104*, 42–54. [CrossRef]
118. Gomez-Pozuelo, G.; Sanz-Perez, E.S.; Arencibia, A.; Pizarro, P.; Sanz, R.; Serrano, D.P. CO_2 adsorption on amine-functionalized clays. *Microporous Mesoporous Mater.* **2019**, *282*, 38–47. [CrossRef]
119. Rasoulzadeh, H.; Zarandi, S.M.; Masoundinejad, M.; Amini, M.M. Modelling and optimization by response surface technique for adsorption of carbon dioxide by aminated basilica/alginate composite: Experiments characterization and regeneration studies. *Int. J. Environ. Anal. Chem.* **2021**. [CrossRef]
120. Sahequi, H.; Galvez, M.E.; Bacatirini, V.; Cheng, Y.; Steinfeld, A.; Zimmermann, T.; Tingant, P. Fast and reversible direct CO_2 capture from air onto all-polymer nanofibrillated cellulose-polyethylenimine foams. *Environ. Sci. Technol.* **2015**, *49*, 3167–3174. [CrossRef]
121. Gan, G.; Li, X.; Fan, S.; Wang, L.; Qin, M.; Yin, Z.; Chen, G. Carbon aerogels for environmental clean-up. *Eur. J. Inorg. Chem.* **2019**, *2019*, 3126–3141. [CrossRef]
122. Alveraz-Gutierrez, N.; Gil, M.V.; Rubiera, F.; Peviada, C. Kinetics of CO_2 adsorption on cherry stone-based carbons in CO_2/CH_4 separations. *Chem. Eng. J.* **2017**, *307*, 249–257. [CrossRef]
123. Chomiak, K.; Gryglewicz, S.; Kierzek, K.; Machnihowski, J. Optimizing the properties of granular walnut-shell based KOH activated carbons for carbon dioxide adsorption. *J. CO_2 Util.* **2017**, *21*, 436–443. [CrossRef]
124. Marin, L.; Dragoi, B.; Olaru, N.; Perju, E.; Coroaba, A.; Doraftei, F.; Scavia, G.; Destri, S.; Zappia, S.; Porzro, W. Nanoporous furfuryl-imine-chitosan fibers as a new pathway towards eco-materials for CO_2 adsorption. *Eur. Polym. J.* **2019**, *120*, 109214. [CrossRef]
125. Linga, Z.; Kun, C.; Feng, Z.; Qunfeng, Y. Adsorption of CO_2 and H_2 on nitrogen-doped porous carbon from Ionic Liquid precursor. *Chem. Res. Chin. Univ.* **2015**, *1*, 130–137.
126. Ma, X.; Li, L.; Wang, S.; Lu, M.; Li, H.; Ma, W.; Keener, T.C. Ammonia-treated porous carbon derived from ZIF-8 for enhanced CO_2 adsorption. *Appl. Surf. Sci.* **2016**, *369*, 390–397. [CrossRef]
127. Yang, M.; Guo, L.; Hu, G.; Hu, X.; Chen, J.; Shen, S.; Dai, W.; Fan, M. Adsorption of CO_2 by petroleum coke nitrogen-doped porous carbons synthesized by combining ammoxidation with KOH activation. *Am. Chem. Soc.* **2016**, *55*, 757–765. [CrossRef]
128. Jayaramulu, K.; Datta, K.K.R.; Shiva, K.; Bhattacharyya, A.J.; Eswaramoortrhy, M.; Maji, T.K. Controlled synthesis of tunable nanoporous carbons for gas storage and supercapacitor application. *Microporous Mesoporous Mater.* **2015**, *206*, 127–135. [CrossRef]
129. Psarras, P.; He, J.; Wilcox, J. Effect of water on the CO_2 adsorption capacity of amine-functionalized carbon sorbents. *Ind. Energy Chem. Res.* **2017**, *56*, 6317–6325. [CrossRef]
130. Jalilov, A.S.; Li, Y.; Tian, J.; Tour, J.M. Ultra-high surface area activated porous asphalt for CO_2 capture through competitive adsorption at high pressures. *Adv. Energy Mater.* **2016**, *7*, 1600693. [CrossRef]
131. Bai, B.C.; Kim, E.A.; Lee, C.W.; Lee, Y.; Im, J.S. Effects of surface chemical properties of activated carbon fibers modified by liquid oxidation for CO_2 adsorption. *Appl. Surf. Sci.* **2015**, *353*, 158–164. [CrossRef]
132. Laing, T.; Chen, C.; Li, X.; Zhang, J. Popcorn-derived porous carbon for energy storage and CO_2 capture. *Langmuir* **2016**, *32*, 8042–8049. [CrossRef]
133. Chen, S.; Li, Y.; Mi, L. Porous carbons derived from metal organic framework for gas storage and separation: The size effect. *Inorg. Chem. Commun.* **2020**, *118*, 107999. [CrossRef]
134. Ludwinowicz, J.; Jaroniec, M. Potassium salt-assisted synthesis of highly microporous carbon spheres for CO_2 adsorption. *Carbon* **2015**, *82*, 297–303. [CrossRef]
135. To, J.W.F.; He, J.; Mei, J.; Haghpanah, R.; Chen, Z.; Kurosuwa, T.; Chen, S.; Bae, W.; Pan, L.; Tok, J.B.H.; et al. Hierarchical N-doped carbon as CO_2 adsorbents with high CO_2 selectivity from rationally designed polypyrrole precursor. *J. Am. Chem. Soc.* **2015**, *138*, 1001–1009. [CrossRef]

136. Tiwari, D.; Bhunia, H.; Bajpai, P.K. Synthesis of nitrogen enriched porous carbons for urea formaldehyde resin and their carbon dioxide adsorption capacity. *J. CO_2 Util.* **2017**, *21*, 302–313. [CrossRef]
137. Qiao, Y.; Zhang, S.; Quan, C.; Gao, N.; Johnston, C.; Wu, C. One-pot synthesis of digestate-derived biochar for carbon dioxide capture. *Fuel* **2020**, *279*, 118525. [CrossRef]
138. Hong, S.; Yoon, H.J.; Choi, Y.; Cho, Y.; Mun, S.; Pol, U.S.; Lee, K.B. Solving two environmental problems simultaneously: Scalable production of carbon microsheets from structured packing peanuts with tailored microporosity for efficient CO_2 capture. *Chem. Eng. J.* **2020**, *379*, 122219. [CrossRef]
139. Wu, X.; Li, D.; Cheng, W.; Zhou, J.; Zhang, H. Progress in methods for preparation of monolith active carbons. *Nanosci. Nanotechnol. Lett.* **2017**, *9*, 839–848. [CrossRef]
140. Sun, Y.; Sui, Z.; Li, X.; Xiao, P.; Wei, Z.; Han, B. Nitrogen-doped porous carbons derived from polypyrrole-based aerogels for gas uptake and supercapacitors. *Appl. Nanomater.* **2018**, *1*, 609–616. [CrossRef]
141. Chen, W.; Wang, X.; Hashiso, Z.; Feizbakhshan, M.; Shariaty, P.; Wiknaddaf, S.; Zhou, X. Template-free and fast one-step synthesis from enzymatic hydrolysis lignin to hierarchical porous carbon for CO_2 capture. *Microporous Mesoporous Mater.* **2019**, *280*, 57–65. [CrossRef]
142. Tajer, M.; Anbia, M.; Salehi, S. Fabrication of polyacrylonitrile hybrid nanofiber scaffold containing activated carbon by electrospinning process as nanofilter media for SO_2, CO_2 and CH_4 adsorption. *Environ. Prog. Sustain. Energy* **2020**, *40*, e13498.
143. Li, L.; Wang, X.; Zhong, J.; Qian, X.; Song, S.; Zhang, Y.; Li, D. Nitrogen-enriched porous polyacrylonitrile-based carbon fibers for CO_2 capture. *Ind. Eng. Chem. Res.* **2018**, *57*, 11608–11616. [CrossRef]
144. Yun, S.; Lee, H.; Lee, W.; Park, H.S. Multiscale textured, ultralight graphene monoliths for enhanced CO_2 and SO_2 adsorption capacity. *Fuel* **2016**, *174*, 36–42. [CrossRef]
145. Li, Y.; Li, D.; Zhao, X.; Wu, M. Superior CO_2, CH_4 and H_2 uptakes over ultrahigh-surface-area carbon spheres prepared from sustainable biomass-derived char by CO_2 activation. *Carbon* **2016**, *105*, 454–462. [CrossRef]
146. Jang, E.; Choi, S.W.; Lee, K.B. Effect of carbonization temperature on the physical properties and CO_2 adsorption behavior of petroleum-coke derived porous carbon. *Fuel* **2019**, *248*, 85–92. [CrossRef]
147. Tobi, A.R.; Dennis, J.O.; Zid, H.M.; Adekoya, A.A.; Yar, A.; Usman, F. Comparative analysis of physicochemical properties of physically activated carbon from palm bio-waste. *J. Mater. Res. Technol.* **2019**, *8*, 3688–3695. [CrossRef]
148. Kuch, B.; Kapsi, M.; Veziri, C.; Athanasekou, C.; Pilatos, G.; Reddy, S.K.; Raj, A.; Karanikolas, G.N. Asphaltene-derived activated carbon and carbon nanotube membranes for CO_2 separation. *Energy Fuels* **2018**, *32*, 11718–11730.
149. Jalilov, A.S.; Li, Y.; Kittrell, C.; Tour, J.M. Increased CO_2 selectivity of asphalt-derived porous carbon through introduction of water into pore spaces. *Nat. Energy* **2017**, *2*, 932–938. [CrossRef]
150. Chowdhury, S.; Balasubramanian, R. Three-dimensional graphene-based porous adsorbents for post-combustion CO_2 capture. *Ind. Eng. Chem. Res.* **2016**, *55*, 7906–7916. [CrossRef]
151. Liu, Y.; Sjjadi, S.; Chen, W.; Chatterjee, R. Ultrasound assisted amine functionalized graphene oxide for enhanced CO_2 adsorption. *Fuel* **2019**, *247*, 10–18. [CrossRef]
152. Hsan, N.; Dutta, P.K.; Kumar, S.; Bera, R.; Das, N. Chitosan grafted graphene oxide aerogel—Synthesis, characterization and carbon dioxide capture study. *Int. J. Biol. Macromol.* **2019**, *125*, 300–306. [CrossRef] [PubMed]
153. Nan, D.; Liu, J.; Ma, W. Electrospun phenolic resin-based carbon-based ultrafine fibers with abundant ultra-small micropores for CO_2 adsorption. *Chem. Eng. J.* **2015**, *276*, 44–50. [CrossRef]
154. Choma, J.; Marsszewski, M.; Osuchowiski, L.; Jagiello, J.; Dziura, A.; Jaroniec, M. Adsorption properties of activated carbons prepared from waste CDs and DVDs. *Sustain. Chem. Eng.* **2015**, *3*, 733–742. [CrossRef]
155. Park, H.; Lee, C.H.; Cho, D.; Lee, C.; Park, J. Synthesis of porous carbon derived from poly (vinylidenefluoride) and its adsorption characteristics for CO_2 and CH_4. *Microporous Mesoporous Mater.* **2020**, *299*, 110121. [CrossRef]
156. Ge, C.; Song, J.; Qin, Z.; Wang, J.; Fan, W. Polyurethane foam-based ultra-microporous carbons for CO_2 capture. *Appl. Mater. Interfaces* **2016**, *8*, 18849–18859. [CrossRef]
157. Gong, J.; Lin, H.; Grygiel, K.; Yuan, J. Main-chain poly (ionic liquid)-derived nitrogen-doped micro-mesoporous carbons for CO_2 capture and selective aerobic oxidation of alcohols. *Appl. Mater. Today* **2017**, *7*, 159–168. [CrossRef]
158. Guo, Q.; Chen, C.; Xing, F.; Shi, W.; Meng, J.; Wan, H.; Guan, G. Constructing hierarchical porous N-doped carbon derived from poly (ionic liquids) with the multifunctional Fe-based template for CO_2 adsorption. American Chemical Society. *Omega* **2021**, *6*, 7186–7198. [CrossRef] [PubMed]
159. Gong, J.; Lin, H.; Antonietti, M.; Yuan, J. Nitrogen-doped porous carbon nanosheets derived from poly (ionic liquid): Hierarchical pore structures for efficient CO_2 capture and dye removal. *R. Soc. Chem.* **2013**, *4*, 7313–7321. [CrossRef]
160. Saha, D.; Bramer, S.E.V.; Orkoulas, G.; Ho, H.; Chen, J.; Henley, D.K. CO_2 capture in lignin-derived and nitrogen doped hierarchical porous carbons. *Carbon* **2017**, *121*, 257–266. [CrossRef]
161. Deneir, M.; Tessema, T.; Farghlay, A.A.; Nyankson, E.; Saraswat, S.K.; Aksoy, B.; Islamoglu, T.; Collinson, M.M.; El-Kaderi, H.M.; Gupta, R.B. Lignin-derived heteroatom-doped porous carbons for supercapacitor and CO_2 capture applications. *Int. J. Energy Res.* **2018**, *42*, 2686–2700. [CrossRef]
162. Leung, D.Y.C.; Caramanna, G.; Moroto-Vater, M.M. An overview of current status of carbon dioxide capture and storage technologies. *Renew. Sustain. Energy Rev.* **2014**, *39*, 426–443. [CrossRef]

163. Gao, A.; Guo, N.; Yan, M.; Li, M.; Wang, F.; Yang, R. Hierarchical porous carbon activated by $CaCO_3$ from pigskin collagen for CO_2 and H_2 adsorption. *Microporous Mesoporous Mater.* **2017**, *260*, 172–179. [CrossRef]
164. Li, Y.; Wnag, X.; Wnag, B.; Cao, J.; Yang, J.; Wei, J. Waste wool derived nitrogen-doped hierarchical porous carbon for selective CO_2 capture. *R. Soc. Chem.* **2018**, *8*, 19818–19826. [CrossRef]
165. Kwon, H.J.; Lee, C.; Kook, J.; Kim, J.H.; Hwang, K.; Lee, J. Amine functionalized wheat bran husk as bio-based organic adsorbent for low-density polyethylene composite of carbon dioxide capture. *Macromol. Res.* **2020**, *28*, 1289–1296. [CrossRef]
166. Diez, N.; Alveraz, P.; Granda, M.; Blanco, C.; Santamaria, R.; Menendez, R. CO_2 adsorption capacity and kinetics in nitrogen-enriched activated carbon fibers prepared by different methods. *Chem. Eng. J.* **2015**, *281*, 704–712. [CrossRef]
167. Liu, J.; Jin, B.; Meng, L.; Lee, K. Synthesis of polypyrrole-based nitrogen-containing porous carbon nanotubes for CO_2 adsorption. *Carbon Lett.* **2018**, *28*, 111–115.
168. Arami-Niya, A.; Rufford, T.E.; Zhu, Z. Activated carbon monoliths with hierarchical pore structure from tar pitch and coal powder for the adsorption of CO_2, CH_4 and N_2. *Carbon* **2016**, *103*, 115–124. [CrossRef]
169. Gao, S.; Ge, L.; Rufford, T.E.; Zhu, Z. The preparation of activated carbon discs from tar pitch and coal powder for adsorption of CO_2, CH_4 & N_2. *Microporous Mesoporous Mater.* **2016**, *238*, 19–26.
170. Ganesan, A.; Shaijumon, M.M. Activated graphene derived porous carbon with exceptional gas adsorption properties. *Microporous Mesoporous Mater.* **2015**, *220*, 21–27. [CrossRef]
171. Wang, Y.; Wang, H.; Zhang, T.C.; Yuan, S.; Liang, B. N-doped porous carbon derived from rGO-incorporated polyphenylenediamine composites for CO_2 adsorption and supercapacitors. *J. Power Sources* **2020**, *472*, 228610. [CrossRef]
172. Shao, L.; Wang, S.; Liu, M.; Huang, J.; Liu, Y. Triazine-based hyper-cross-linked polymers derived porous carbons for CO_2 capture. *Chem. Eng. J.* **2018**, *339*, 509–518. [CrossRef]
173. Liu, S.; Rao, L.; Yang, P.; Wang, X.; Wang, L.; Ma, R.; Yue, L.; Hu, X. Superior CO_2 uptake on nitrogen doped carbonaceous adsorbents from commercial phenolic resin. *J. Environ. Sci.* **2020**, *93*, 109–116. [CrossRef] [PubMed]
174. Ma, C.; Lu, T.; Shao, J.; Hung, J.; Hu, X.; Wang, L. Biomass derived nitrogen and sulfur co-doped porous carbons for efficient CO_2 adsorption. *Sep. Purif. Technol.* **2022**, *281*, 119899. [CrossRef]
175. Zhao, Z.; Ma, C.; Chen, F.; Xu, G.; Pang, R.; Qiao, X.; Shao, J.; Hu, X. Water caltrop shell-derived nitrogen-doped porous carbons with high CO_2 adsorption capacity. *Biomass Bioenergy* **2021**, *145*, 105969. [CrossRef]
176. Wang, H.; Wang, H.; Liu, G.; Yan, Q. In-situ pyrolysis of Taihu blue algae biomass as appealing porous carbon adsorbent for CO_2 capture: Role of the intrinsic N. *Sci. Total Environ.* **2021**, *771*, 145424. [CrossRef]
177. Liu, S.; Li, Q.; Wang, L.; Ma, R.; Zou, J.; Huang, L.; Hu, X. Facile single-step synthesis of porous carbons as efficient CO_2 adsorbents. *Energy Fuels* **2019**, *33*, 11544–11551. [CrossRef]
178. Kim, H.S.; Kang, M.S.; Yoo, W.C. Highly enhanced gas sorption capacities of N-doped porous carbon spheres by hot NH_3 and CO_2 treatments. *J. Phys. Chem.* **2015**, *119*, 28512–28522. [CrossRef]
179. Rao, L.; Liu, S.; Chen, J.; Wang, L.; An, L.; Yang, P.; Hu, X. Single step synthesis of nitrogen-doped porous carbons for CO_2 capture by low-temperature sodium amide activation of petroleum coke. *Energy Fuels* **2018**, *32*, 12787–12794. [CrossRef]
180. Zhuo, H.; Hu, Y.; Tong, X.; Zhong, L.; Peng, X.; Sun, R. Sustainable hierarchical porous carbon aerogel from cellulose for high-performance supercapacitors and CO_2 capture. *Ind. Crops Prod.* **2016**, *87*, 229–235. [CrossRef]
181. Liu, S.; Ma, R.; Hu, X.; Wang, L.; Wang, X.; Radosz, M.; Fan, M. CO_2 adsorption on hazelnut-shell derived nitrogen-doped porous carbons synthesized by single-step sodium amine activation. *Ind. Eng. Chem. Res.* **2019**, *59*, 7046–7053. [CrossRef]
182. Rao, L.; Yue, L.; Wang, L.; Wu, Z.; Ma, C.; An, L.; Hu, X. Low-temperature and single-step synthesis of N-doped porous carbons with a high CO_2 adsorption performance by sodium amide activation. *Energy Fuels* **2018**, *32*, 10830–10837. [CrossRef]
183. Liu, S.; Yang, P.; Wang, L.; Li, Y.; Wu, Z.; Ma, R.; Wu, J.; Hu, X. Nitrogen doped porous carbons from lotus leaf for CO_2 capture and supercapacitor electrodes. *Energy Fuels* **2019**, *33*, 6568–6576. [CrossRef]
184. Rao, L.; Liu, S.; Wang, L.; Ma, C.; Wu, J.; An, L.; Hu, X. N-doped porous carbons from low-temperature and single-step sodium amide activation of carbonized water chestnut-shell with excellent CO_2 capture performance. *Chem. Eng. J.* **2018**, *359*, 428–435. [CrossRef]
185. Wang, L.; Rao, L.; Xia, B.; Wang, L.; Yue, L.; Liang, Y.; DaCosta, H.; Hu, X. Highly efficient CO_2 adsorption bu nitrogen-doped porous carbons synthesized with low-temperature sodium amide activation. *Carbon* **2018**, *130*, 31–40. [CrossRef]
186. Yu, D.; Hu, J.; Zhou, L.; Li, J.; Tang, J.; Peng, C.; Liu, H. Nitrogen-doped coal tar pitch based microporous carbons with superior CO_2 capture performance. *Energy Fuels* **2018**, *32*, 3726–3732. [CrossRef]
187. Rehman, A.; Park, S. From chitosan to urea-modified carbons: Tailoring the ultra-microporosity for enhanced CO_2 adsorption. *Carbon* **2020**, *159*, 625–637. [CrossRef]
188. Fujiki, J.; Yogo, K. Increased CO_2 adsorption performance of chitosan derived activated carbon with nitrogen-doping. *Chem. Comm.* **2016**, *52*, 186–189. [CrossRef]
189. Singh, G.; Tiburcius, S.; Ruban, S.M.; Shanbhas, D.; Sathish, C.I.; Kamadass, K.; Vinu, A. Pure and strontium carbonate nanoparticles functionalized microporous carbons with high specific surface areas derived from chitosan for CO_2 adsorption. *Emergent Mater.* **2019**, *2*, 337–349. [CrossRef]
190. Wang, J.; Wang, F.; Duan, H.; Li, Y.; Xu, J.; Huang, Y.; Liu, B.; Zhang, T. Polyvinyl chloride-derived carbon spheres for CO_2 adsorption. *ChemSusChem* **2020**, *13*, 1–8.

191. Politakos, N.; Barbarn, I.; Cantador, L.S.; Cecilia, J.A.; Mehrarar, E.; Tamovska, R. Grpahene-based monolirhoc nanostructures for CO_2 capture. *Ind. Eng. Chem. Res.* **2020**, *58*, 3349–3358.
192. Li, P.; Zeng, H.C. Hierarchical nanocomposites by integrating reduced graphene oxide and amorphous carbon with ultrafine MgO nanocrystallites for enhanced CO_2 capture. *Environ. Sci. Technol.* **2017**, *51*, 12998–13007. [CrossRef]
193. Bai, R.; Yang, M.; Hu, G.; Xu, L.; Hu, X.; Li, Z.; Wang, S.; Dai, W.; Fan, M. A new nanoporous nitrogen-doped highly-efficient carbonaceous CO_2 sorbent synthesized with inexpensive urea and petroleum coke. *Carbon* **2015**, *81*, 465–473. [CrossRef]
194. Wang, W.; Motuzas, J.; Zhao, X.S.; Costa, J.C.D. 2D/3D assembles of amine-functionalized graphene silica (templated) aerogel for enhanced CO_2 sorption. *Appl. Mater. Interfaces* **2019**, *11*, 30391–30400. [CrossRef]
195. Plaza, M.G.; Duran, I.; Querejeta, N.; Rubiera, F.; Pevida, C. Experimental and Simulation Study of Adsorption in Post combustion Conditions using a Microporous Biochar.2.H_2O, CO_2 and N_2 Adsorption. *Ind. Eng. Chem. Res.* **2016**, *55*, 6854–6865. [CrossRef]
196. Yue, L.; Rao, L.; Wang, L.; Sun, Y.; Wu, Z.; DaCosta, H.; Hu, X. Enhanced CO_2 adsorption on nitrogen-doped porous carbons derived from commercial phenolic resin. *Energy Fuels* **2018**, *32*, 2081–2088. [CrossRef]
197. Gong, J.; Antonietti, M.; Yuan, J. Poly (ionic liquid)-derived carbon with site-specific N-doping and Biphasic Heterojunction for enhanced CO_2 capture and sensing. *Angewandate Chem.* **2017**, *129*, 7665–7671. [CrossRef]
198. Ma, X.; Li, L.; Ruofei, C.; Chunhao, W.; Li, H.; Shaobin, W. Heteroatom-doped nanoporous carbon derived from MOF-5 for CO_2 capture. *Appl. Surf. Sci.* **2017**, *435*, 494–502. [CrossRef]
199. Ma, X.; Li, L.; Chen, R.; Wang, C.; Li, H.; Li, H. Highly nitrogen-doped porous carbon derived from zeolitic imidazolate framework-8 for CO_2 capture. *Chem. Asian J.* **2018**, *13*, 2069–2076. [CrossRef] [PubMed]
200. Borchardts, L.; Zhu, Q.; Casco, M.E.; Berger, R.; Zhuang, X.; Kaskel, S.; Feng, X.; Xu, Q. Toward a molecular design of porous carbon materials. *Mater. Today* **2017**, *20*, 592–610. [CrossRef]
201. Li, Z.; Chen, T.; Wu, X.; Luo, L.; Zhang, Z.; Li, Z.; Fan, M.; Su, Z.; Zhao, W. Nitrogen-containing high surface area carbon cryogel from co-condensed phenol-urea-formaldehyde resin for CO_2 capture. *J. Porous Mater.* **2018**, *26*, 847–854. [CrossRef]
202. Zohdi, S.; Anbia, M.; Salehi, S. Improved CO_2 adsorption capacity and CO_2/CH_4 and CO_2/N_2 selectivity in novel hollow silica particles by modification with multi-walled carbon nanotubes containing amine groups. *Polyhedron* **2019**, *166*, 175–185. [CrossRef]
203. You, Y.Y.; Liu, X.J. Modelling of CO_2 Adsorption and Recovery from wet Flue Gas by Using Activated Carbon. *Chem. Eng. J.* **2019**, *369*, 672–685. [CrossRef]
204. Plaza, M.G.; Gonzalez, A.S.; Rubeira, F.; Pevida, C. Evaluation of Microporous biochars produced by single-step oxidation for post combustion CO_2 capture under humid conditions. *Energy Procedia* **2014**, *63*, 693–702. [CrossRef]
205. Lou, Y.; Qi, S.; Xue, D.; Gu, C.; Zhou, R.; Liu, X.; Sun, L. Solvent-free synthesis of N-containing polymers with high cross-linking degree to generate N-doped porous carbons for high-efficiency CO_2 capture. *Chem. Eng. J.* **2020**, *399*, 125845. [CrossRef]
206. Das, D.; Meikap, B.C. Role of amine-impregnated activated carbon in carbon dioxide capture. *Indian Chem. Eng.* **2020**, *63*, 425–447. [CrossRef]
207. Chai, S.; Liu, Z.; Huang, K.; Tan, S.; Dai, S. Amine-functionalization of microsized and nanosized mesoporous carbons for carbon dioxide capture. *Ind. Eng. Chem. Res.* **2016**, *55*, 7355–7361. [CrossRef]
208. Dutcher, B.; Fan, M.; Russell, A.G. Amine-based CO_2 capture technology development from the begening of 2013—A Review. *Appl. Mater. Interfaces* **2015**, *7*, 2137–2148. [CrossRef] [PubMed]
209. Ohs, B.; Krodel, M.; Kiessimg, M. Adsorption of carbon dioxide on solid amine-functionalized sorbents: A dual kinetic model. *Sep. Purif. Technol.* **2018**, *204*, 13–20. [CrossRef]
210. Peng, H.; Zhang, J.; Zhang, J.; Zhong, F.; Wu, P.; Huang, K.; Fan, J.; Liu, F. Chitosan-derived mesoporous carbon with ultrahigh pore volume for amine-impregnated and highly efficient CO_2 capture. *Chem. Eng. J.* **2018**, *359*, 1159–1165. [CrossRef]
211. Das, D.; Samal, D.P.; Meikap, B.C. Removal of CO_2 in a multistage fluidized bed reactor by diethanol amine impregnated activated carbon. *J. Environ. Sci. Health Part A* **2016**, *51*, 769–775. [CrossRef]
212. Sim, K.; Lee, N.; Kim, J.; Cho, E.; Gunathilake, C.; Jaroniec, M. CO_2 adsorption on amine-functionalized periodic mesoporous benzenesilicas. *Appl. Mater. Interfaces* **2015**, *7*, 6792–6802. [CrossRef]
213. Didas, S.A.; Kulkrani, A.R.; Sholl, D.S.; Jones, C.W. Role of amine structure on carbon dioxide adsorption from ultra dilute gas streams such as ambient air. *ChemSusChem.* **2012**, *5*, 2058–2064. [CrossRef]
214. Gholidoust, A.; Atkinson, J.D.; Hashisho, Z. Enhancing CO_2 adsorption via amine impregnated activated carbon from oil sands coke. *Energy Fuels* **2017**, *31*, 1756–1763. [CrossRef]
215. Chen, L.; Gong, M.; Cheng, Y.; Liu, Y.; Yin, S.; Luo, D. Effect of pore structure of supports on CO_2 adsorption of tetraethylene-pentamine/carbon aerogels prepared by incipient wetness impregnation method. *Pol. J. Environ. Stud.* **2019**, *28*, 4127–4137. [CrossRef]
216. Kongnoo, A.; Intharapat, P.; Worathanakul, P.; Phalakormkule, C. Diethanolamine impregnated palm shell activated carbon for CO_2 adsorption at elevated temperatures. *J. Environ. Chem. Eng.* **2015**, *4*, 73–81. [CrossRef]
217. Lee, M.; Lee, S.; Park, S. Preparation and characterization of multi-walled carbon nanotubes impregnated with polyethylenimine for carbon dioxide capture. *Int. J. Hydrogen Energy* **2015**, *40*, 3415–3421. [CrossRef]
218. Gibson, J.A.A.; Gromov, A.V.; Brandani, S.; Camphell, E.E.B. The effect of pore structure on the CO_2 adsorption efficiency of polyamine impregnated porous carbons. *Microporous Mesoporous Mater.* **2015**, *208*, 129–139. [CrossRef]
219. Numaguchi, R.; Fujiki, J.; Yamada, H.; Chowdhury, F.A.; Kida, K.; Goto, K.; Okumura, T.; Yoshizawa, K.; Yogo, K. Development of post-combustion CO_2 capture system using amine-impregnated solid sorbent. *Energy Procedia* **2017**, *114*, 2304–2312. [CrossRef]

220. Pen, H.; Zhong, F.; Zhang, J.; Zhang, J.; Wu, P.; Huang, K.; Fan, J.; Jiang, L. Graphitic carbon nitride functionalized with polyethylenimine for highly effective capture of carbon dioxide. *Ind. Eng. Chem. Res.* **2018**, *57*, 11031–11038.
221. Yaumi, A.L.; Bakar, M.Z.; Hameed, B.H. Melamine-nitrogenated mesoporous activated carbon derived from rice husk for carbon dioxide adsorption in fixed-based. *Energy* **2018**, *155*, 46–55. [CrossRef]
222. Lee, Y.; Lee, S.M.; Hong, W.G.; Huh, Y.S.; Park, S.Y.; Lee, S.C.; Lee, J.; Lee, J.B.; Lee, H.U.; Kim, H.J. Carbon dioxide capture on primary amine groups entrapped in activated carbon at low temperatures. *J. Ind. Eng. Chem.* **2014**, *23*, 16–20. [CrossRef]
223. Lee, M.; Park, S. Silica-coated multi-walled carbon nanotubes impregnated with polyethylenimine for carbon dioxide capture under the flue gas conditions. *J. Solid-State Chem.* **2015**, *226*, 17–23. [CrossRef]
224. Alhassan, M.; Auta, M.; Sabo, J.K.; Umaru, M.; Kovo, A.S. CO_2 capture using amine-impregnated activated carbon from Jatropha curas shell. *Br. J. Appl. Sci. Technol.* **2016**, *14*, 1. [CrossRef]
225. Luo, S.; Chen, S.; Chen, S.; Zhuang, L.; Ma, N.; Xu, T.; Li, Q.; Hou, X. Preparation and characterization of amine-functionalized sugarcane bagasse for CO_2 capture. *J. Environ. Manag.* **2016**, *168*, 142–148. [CrossRef]
226. Ali, U.F.M.; Azmi, N.H.; Isa, K.M.; Aroua, M.K.; Shien, T.R.; Khamidun, M.H. Optimization study on preparation of amine functionalized sea mango (*Cerbia Odollam*) activated carbon for carbon dioxide (CO_2) adsorption. *Combust. Sci. Technol.* **2018**, *190*, 1259–1282. [CrossRef]
227. Sreedhar, I.; Aniruddha, R.; Malik, S. Carbon capture using amine modified porous carbons derived from starch (starbons). *SN Appl. Sci.* **2019**, *1*, 463. [CrossRef]
228. Wang, X.; Wang, D.; Song, M.; Xin, C.; Zeng, W. Tetraethylenepentamine-modified activated semi coke for CO_2 capture from the flue gas. *Energy Fuels* **2017**, *31*, 3055–3061. [CrossRef]
229. Shin, G.; Rhee, K.; Park, S. Improvement of CO_2 capture by graphite oxide in presence of polyethylenimine. *Int. J. Hydrog. Energy* **2016**, *41*, 14351–14359. [CrossRef]
230. Ardhyarini, N.; Krisnandi, Y.K. Carbon dioxide capture by activated methyl diethanol amine impregnated mesoporous carbon. *Int. Symp. Curr. Prog. Math. Sci.* **2017**, *1862*, 0300090.
231. Pruna, A.; Carcel, A.C.; Benedito, A.; Gimenez, E. Effect of synthesis conditions on CO_2 capture of ethylenediamine-modified graphene aerogels. *Appl. Surf. Sci.* **2019**, *487*, 228–235. [CrossRef]
232. Chi, Y.Z.Y.; Liu, C.Z.Y.; Zhao, Y.; Jiang, L.; Song, Y. CO_2 adsorption behaviour of graphite oxide modified with Tetraethylenepentamine. *J. Chem. Eng.* **2018**, *63*, 202–207.
233. Iqbal, N.; Wang, X.; Yu, J.; Ding, B. Robust and flexible carbon nanofibers doped with amine functionalized carbon nanotubes for efficient CO_2 capture. *Adv. Sustain. Syst.* **2017**, *1*, 1600028. [CrossRef]
234. Lourenco, M.A.O.; Fontana, M.; Jagdale, P.; Pirris, C.F.; Bocchini, S. Improved CO_2 adsorption properties through amine functionalization of multi-walled carbon nanotubes. *Chem. Eng. J.* **2021**, *414*, 128763. [CrossRef]
235. Park, J.M.; Woo, H.C.; Jhung, S.H. Effective CO_2 adsorption of low pressure over nitrogen-enriched porous carbons derived from melamine-loaded polyaniline. *Chem. Eng. J.* **2021**, *412*, 128641. [CrossRef]
236. Peng, A.; Qi, S.; Liu, X.; Xue, D.; Peng, S.; Yu, G.; Liu, X.; Sun, L. Fabrication of N-doped porous carbons for enhanced CO_2 capture: Rational design of an ammoniated polymer precursor. *Chem. Eng. J.* **2019**, *369*, 170–179. [CrossRef]
237. Li, D.; Chen, Y.; Zheng, M.; Zhao, H.; Zhao, Y.; Sun, Z. Hierarchical structured porous nitrogen-doped carbon for highly selective CO_2 capture. *Sustain. Chem. Eng.* **2015**, *4*, 298–304. [CrossRef]
238. Zhang, W.; Bao, Y.; Bao, A. Preparation of nitrogen-doped hierarchical porous carbon materials by a template-free method and its application to CO_2 capture. *J. Environ. Chem. Eng.* **2020**, *8*, 103732. [CrossRef]
239. Adio, S.O.; Ganiyu, S.A.; Usman, M.; Abdulazeez, I.; Alhooshani, K. Facile and efficient nitrogen modifies porous carbon derived from sugarcane bagasse for CO_2 capture: Experimental and DFT investigations of nitrogen atoms on carbon frameworks. *Chem. Eng. J.* **2019**, *382*, 122964.
240. Keller, L.; Chs, B.; Lenhart, J.; Abduly, L.; Blanke, F.; Wessling, M. High capacity polyethylenimine impregnated microtubes made of carbon nanotubes for CO_2 capture. *Carbon* **2017**, *126*, 338–345. [CrossRef]
241. Liu, Q.; Xiong, B.; Shi, J.; Tao, M.; He, Y.; Shi, Y. Enhanced Tolerance to Flue Gas Contaminants on Carbon Dioxide Capture Using Amine-Functionalized Multiwalled Carbon Nanotubes. *Energy Fuels* **2014**, *28*, 6494–6501. [CrossRef]
242. Ning, H.; Yang, Z.; Wang, D.; Meng, Z.; Li, Y.; Ju, X.; Wang, C. Graphene-based semi-coke porous carbon with N-rich hierarchical sandwich-like structure for efficient separation of CO_2/N_2. *Microporous Mesoporous Mater.* **2021**, *311*, 110700. [CrossRef]
243. Du, N.; Ma, R.; Liu, Z.; Yang, G.; Chen, J. Study on the adsorption properties of graphene oxide/Laponite RD/chitosan composites. *Materials* **2021**, *14*, 3224. [CrossRef]
244. Andreoli, E.; Cullum, L.; Barron, A.R. Carbon dioxide adsorption by polyethylenimine-functionalized nanocarbons: A kinetic study. *Ind. Eng. Chem. Res.* **2014**, *54*, 878–889. [CrossRef]
245. Ye, Q.; Jiang, J.; WANG, c.; Liu, Y.; Pan, H.; Shi, Y. Adsorption of Low-Concentration Carbon Dioxide on Amine-Modified Carbon Nanotubes at Ambient Temperature. *Energy Fuels* **2012**, *26*, 2497–2504. [CrossRef]
246. Zhang, J.; Webley, P.A.; Xiao, P. Effect of process parameters on power requirements of vacuum swing adsorption technology for CO_2 capture from flue gas. *Energy Convers Manag.* **2018**, *49*, 346–356. [CrossRef]
247. Abanades, J.C.; Arias, B.; Lyngfelt, A.; Mattison, T.; Wiley, D.E.; Li, H.; Ho, M.T.; Mangano, E.; Barandani, S. Emerging CO_2 capture systems. *Int. J. Greenh. Gas Control* **2015**, *40*, 126. [CrossRef]

248. Dhoke, C.; Zaabout, A.; Cloete, S.; Amini, S. Review on reactor Configurations for Adsorption-Based CO_2 capture. *Ind. Eng. Chem. Res.* **2021**, *60*, 3779–3798. [CrossRef]
249. Chalmers, H.; Leach, M.; Lucquiaud, M.; Gibbins, J. Valuing flexible operation of power plants with CO_2 capture. *Energy Procedia* **2009**, *1*, 4289–4296. [CrossRef]
250. Normann, F.; Gardarsdottir, S.O.; Skagestad, R.; Mathisen, A.; Johnsson, F. Partial capture of Carbon Dioxide from Industrial Sources-A discussion on Cost optimization and the CO_2 Capture Rate. *Energy Procedia* **2017**, *114*, 113–121. [CrossRef]
251. Auta, M.; Darbis, N.D.A.; Din, A.T.M.; Hamed, B.H. Fixed-bed column adsorption of carbon dioxide by sodium hydroxide modifies activated alumina. *Chem. Eng. J.* **2013**, *233*, 80–87. [CrossRef]
252. Webley, P.A.; Zhang, J. Microwave assisted vacuum regeneration for CO_2 capture from wet flue gas. *Adsorption* **2014**, *20*, 201–210. [CrossRef]
253. Luberti, M.; Oreggion, G.D.; Ahn, H. Design of rapid vacuum pressure swing adsorption (RVPSA) process for post-combustion CO_2 capture from a biomass-filled CHP plant. *J. Environ. Chem. Eng.* **2017**, *5*, 3973–3982. [CrossRef]
254. Grande, C.A.; Ribeiro, R.P.L.; Olivera, E.G.L.; Rodrigues, A.E. Electric swing adsorption as emerging CO_2 capture technology. *Energy Procedia* **2009**, *1*, 1219–1225. [CrossRef]
255. Raganati, F.; Miccio, F.; Ammendola, P. Adsorption of Carbon Dioxide for Post-combustion Capture: A Review. *Energy Fuels* **2021**, *35*, 12845–12868. [CrossRef]
256. Riboldi, L.; Bolland, O. Evaluating pressure swing adsorption as a CO_2 separation technique in coal-fired power plants. *Int. J. Greenh. Gas Control* **2015**, *39*, 1–16. [CrossRef]
257. Babu, P.; Kumar, R.; Linga, P. Pre-combustion captuire of carbon dioxide in a fixed bed reactor using the clathrate hydrate process. *Energy* **2013**, *50*, 364–373. [CrossRef]
258. Dantas, T.L.P.; Luna, I.M.T.; Sivar, J.I.J.; Tores, A.E.B.; de-Azevedo, D.C.S.; Rodrigues, A.E.; Moreira, R.F.P.M. Modeling of the fixed-bed adsorption of carbon dioxide and a carbon-dioxide-nitrogen mixture on zeolite 13X. *Braz. J. Chem. Eng.* **2011**, *28*, 533–544. [CrossRef]
259. Liu, Z.; Wang, L.; Kong, X.; Li, P.; Yu, J.; Rodrigues, A.E. Onsite CO_2 capture from flue gas by an adsorption process in a coal-fired power plant. *Ind. Eng. Chem. Res.* **2012**, *51*, 7355–7363. [CrossRef]
260. Joss, L.; Gazzani, M.; Mazzotti, M. Rational design of temperature swing adsorption cycles for post-combustion CO_2 capture. *Chem. Eng. Sci.* **2017**, *158*, 381–394. [CrossRef]
261. Razaei, F.; Webley, P. Structured adsorbents in gas separation process. *Sep. Purif. Technol.* **2010**, *70*, 243–256. [CrossRef]
262. Ruthven, D.M.; Thaeron, C. Performance of a parallel passage adsorbent contactor. *Gas. Sep. Purif.* **1996**, *10*, 63–73. [CrossRef]
263. Razaei, F.; Grahn, M. Thermal management of structured adsorption in CO_2 capture process. *Ind. Eng. Chem. Res.* **2012**, *51*, 4025–4034. [CrossRef]
264. Lively, R.P.; Chance, R.R.; Kelley, B.T.; Deckman, H.W.; Drese, J.H.; Jones, C.W.; Koros, W.J. Hollow fiber adsorbents for CO_2 removal from flue gas. *Ind. Eng. Chem. Res.* **2009**, *48*, 7314–7324. [CrossRef]
265. Plaza, M.G.; Rubiera, F.; Penda, C. Evaluating the feasibility of a TSA process based on steam stripping in combination with structured carbon adsorbent to capture CO_2 from a coal power plant. *Energy Fuels* **2017**, *31*, 9760–9775. [CrossRef]
266. Shen, C.; Liu, Z.; Li, P.; Yu, J. Two-stage VPSA process for CO_2 capture from flue gas using Activated carbon beads. *Ind. Eng. Chem. Res.* **2012**, *51*, 5011–5021. [CrossRef]
267. Choi, S.; Drese, J.H.; Jones, C.W. Adsorbent materials for carbon dioxide caoture from large anthropogenic point sources. *ChemSusChem* **2009**, *2*, 796–854. [CrossRef]
268. Ren, X.; Li, H.; Chen, J.; Wei, L.; Modak, A.; Yang, H.; Yang, Q. N-doped porous carbons with exceptionally high CO_2 selectivity for CO_2 Capture. *Carbon* **2017**, *114*, 473–481. [CrossRef]
269. Nasri, N.S.; Hamza, Y.D.; Ismail, S.N.; Ahmed, M.M.; Mohsin, R. Assessment of porous carbons derived from sustainable palm solid waste for carbon dioxide capture. *J. Clean. Prod.* **2014**, *71*, 148–157. [CrossRef]
270. Kim, K.; Son, Y.; Lee, K.S. Moving bed adsorption process with internal heat integration for carbon dioxide capture. *Int. J. Greenh. Gas Control* **2013**, *17*, 13–24. [CrossRef]
271. Mondino, G.; Grande, C.A.; Blom, R.; Nord, L.O. Moving bed temperature swing adsorption for CO_2 capture from a natural gas combined cycle power plant. *Int. J. Greenh. Gas Control* **2019**, *85*, 58–70. [CrossRef]
272. Zhang, W.; Liu, H.; Sun, C.; Drage, T.C.; Snape, C.E. Performance of polyethylenimine-silica adsorbents for post-combustion CO_2 capture in a bubbling fluidized bed. *Chem. Eng. J.* **2014**, *251*, 293–303. [CrossRef]
273. Hornbostel, M.C.; Bao, J.; Krishnan, G.; Nagar, A.; Jyaweera, I.; Kobayashi, T.; Sanjurjo, A.; Sweeney, J.; Carruttler, D.; Petruska, M.; et al. Characterizatiom of an advanced carbon sorbent for CO_2 capture. *Carbon* **2013**, *56*, 77–85. [CrossRef]
274. Okummura, T.; Ogino, T.; Nishihe, S.; Nonaka, Y.; Shoji, T.; Higashi, T. CO_2 Capture test for a moving bed system utilizaing low-temperature steam. *Energy Procedia* **2014**, *63*, 2249–2254. [CrossRef]
275. Dhoke, C.; Zaoubout, A.; Cloete, S.; Seo, H.; Park, Y.K.; Demoulin, L.; Amini, S. Demonstration of the novel swing adsorption reactor cluster concept in multistage fluidized bed with heat transfer surface for post-combustion CO_2 capture. *Ind. Eng. Chem. Res.* **2020**, *59*, 22281–22291. [CrossRef]
276. MCDonogh, J.R.; Law, R.; Reany, D.A.; Zivkovic, V. Intensified carbon capture using adsorption. *Heat Prog.* **2018**, *8*, 17–30.
277. Monazam, E.R.; Spenk, J.; Shadi, L.J. Fluid bed adsorption of carbon dioxide on immobilized polyethyleneimine (PEI): Kinetic analysis and breakthrough behaviour. *Chem. Eng. J.* **2013**, *223*, 795–805. [CrossRef]

278. Yashoobi-Khankhanej, S.; Alizadeh, R.; Zarghami, R. Adsorption modeling of CO_2 in fluidized bed reactor. *Chem. Eng. Res. Des.* **2018**, *129*, 111–121.
279. Raganati, F.; Chirone, R.; Ammmendola, P. Calcium-looping for thermomechanical energy storage in concentrating solar power applications: Evaluation of the effect of acoustic perturbation on the fluidized bed carbonation. *Chem. Eng. J.* **2020**, *392*, 123658. [CrossRef]
280. Hofer, G.; Schony, G.; Fuchi, J.; Proli, T. Investigating wall-to-bed heat transfer in view of a continuous temperature swing adsorption process. *Fuel Process Technol.* **2018**, *169*, 157–159. [CrossRef]
281. Yang, W.C.; Hoffman, J. Exploration Design Study on Reactor Configurations for Carbon Dioxide Capture from Conventional Power Plants Employing Regenerable Solid Sorbents. *Ind. Eng. Chem. Res.* **2009**, *48*, 341–356. [CrossRef]
282. Seo, Y.; Jo, S.H.; Ryu, H.J.; DalBae, H.; Ryu, C.K.Y. Effect of water pre-treatment on CO_2 capture using a potassium-based solid sorbent in a bubbling fluidized bed reactor. *Korean J. Chem. Eng.* **2007**, *24*, 457–460. [CrossRef]
283. Yi, C.K.; Jo, S.H.; Ryu, H.J.; Yoo, Y.W.; Lee, J.B.; Ryu, C.K.; Rubin, E.S.; Keith, D.W.; Gilboy, C.F.; Wilson, M.; et al. CO_2 reaction characteristics of dry sorbents in fluidized reactors. *Greenh. Gas Control Technol.* **2005**, *7*, 1765–1769.
284. Das, D.; Meikap, B.C. Removal of CO_2 in a multistage fluidized bed reactor by monoethanolamine impregnated activated carbon. *Miner. Processing Extr. Metall.* **2019**. [CrossRef]
285. Varma, Y.B.G. Pressure drop of the fluid and the flow patterns of the phases in multistage fluidization. *Power Technol.* **1975**, *12*, 167–174. [CrossRef]
286. Schony, G.; Zehetner, E.; Fuchi, J.; Proll, T.; Sprachmann, G.; Hofbauer, H. Design of a bench scale unit for continuous CO_2 capture via temperature swing adsorption-Fluid Dynamic feasibility study. *Chem. Eng. Res. Des.* **2016**, *106*, 155–167. [CrossRef]
287. Zaabout, A.; Romano, M.C.; Cloete, S.; Guiffrida, A.; Morud, J.; Chiesa, P.; Amini, S. Thermodynamic assessment of the swing adsorption reactor cluster (SARC) concept for post-combustion CO_2 capture. *Int. J. Greenh. Gas Control* **2017**, *60*, 74–92. [CrossRef]
288. Cloete, S.; Guiffrida, A.; Romano, M.C.; Zaabout, A. The swing adsorption reactor cluster for post-combustion CO_2 capture from cement plants. *J. Clean. Prod.* **2019**, *223*, 692–703. [CrossRef]
289. Cloete, S.; Guiffrida, A.; Romano, M.C.; Zaabout, A. The effect of sorbent regeneration enthalpy on the performance of the novel swing adsorption reactor cluster (SARC) for post-combustion CO_2 capture. *Chem. Eng. J.* **2018**, *377*, 119810. [CrossRef]
290. Zaabout, A.; Romano, M.C.; Cloete, S.; Guiffrida, A.; Morud, J.; Chiesa, P.; Amini, S.A. Novel swing adsorption reactor cluster (SARC) for cost effective post combustion CO_2 capture: A Thermodynamic Assessment. *Energy Procedia* **2017**, *114*, 2488. [CrossRef]
291. Cloete, S.; Guiffrida, A.; Romano, M.C.; Zaabout, A. Economic assessment of the swing adsorption reactor cluster for CO_2 capture from cement production. *J. Clean. Prod.* **2020**, *275*, 123024. [CrossRef]
292. Das, D.; Behran, K.B.; Meikap, B.C. Removal of CO_2 in a multistage fluidized bed reactor by amine impregnated activated carbon: Optimization using response surface methodology. *Int. J. Coal. Sci. Technol.* **2019**, *6*, 445–458. [CrossRef]
293. Raganati, F.; Ammendola, P.; Chirone, R. CO_2 adsorption on fine activated carbon in a sound assisted fluidized bed: Effect of sound intensity and frequency, CO_2 partial pressure and fluidization velocity. *Appl. Energy* **2014**, *113*, 1269–1282. [CrossRef]
294. Ammendola, P.; Raganati, F.; Chirone, R. Effect of operating conditions on the CO_2 recovery from a fine activated carbon by means of TSA in a fluidized bed assisted by acoustic fields. *Fuel Processing Technol.* **2015**, *134*, 494–501. [CrossRef]
295. Raganati, F.; Ammendola, P.; Chirone, R. Effect of acoustic field on CO_2 desorption in a fluidized bed on fine activated carbon. *Particuology* **2015**, *23*, 8–15. [CrossRef]
296. Raganati, F.; Ammendola, P.; Chirone, R. On improving the CO_2 recovery efficiency of a conventional TSA process in a sound assisted fluidized bed by separating heating and purging. *Sep. Purif. Technol.* **2016**, *167*, 24–31. [CrossRef]